FLUCTUATIONS IN A TOKAMAK PLASMA

Thesis by

R. L. Kubena

In Partial Fulfillment of the Requirements

for the Degree of

Doctor of Philosophy

California Institute of Technology

Pasadena, California

1978

(Submitted February 17, 1978)

ACKNOWLEDGMENTS

ABSTRACT

An experimental investigation of low frequency floating potential fluctuations ($f \leq 200$ kHz) in a research tokamak plasma using two spatially separated electrostatic probes has been performed. The spectra, correlation length, and the phase velocity of the fluctuations in both the radial and azimuthal direction have been determined. The propagation velocity in the toroidal direction was also measured and was found to be in the direction of electron current flow. The waves traveled azimuthally in the ion diamagnetic drift direction, even after the usual $\vec{E} \times \vec{B}$ rotation was taken into account. The electron density fluctuations associated with these oscillations were large, $\delta n/n \simeq 0.35 - 0.50$.

The spectra were found to have regularly spaced peaks which seemed to be related to specific azimuthal modes ($m = 1,2,3,\cdots,$etc.) A parametric study was made to determine what effect plasma parameters had on these peaks. During periods of high electron density in the first 2 msec of the plasma lifetime, strong sawtooth type oscillations were observed. These oscillations typically had frequencies of approximately 10 kHz and were also present when large amounts of neutral gas were added during the discharge by a process called "gas puffing."

The results are compared with experimental observations made on other plasma devices with electric and magnetic probes and with microwave and CO_2 laser scattering techniques. (The scattering measurements are complimentary to the probe measurements since, in the former case, the wavelength is fixed by the scattering angle, but the oscillations could not be spatially localized.) The oscillations in the Caltech torus were

probably related to a drift-tearing type instability which is thought to play a major role in the anomalous particle and energy flux observed in tokamaks. Comparisons are made between current theory and the experimental results. However, the theory for the observed oscillations is still in a rudimentary stage of development, and it is hoped that the present investigation will stimulate future analytical work.

TABLE OF CONTENTS

I. INTRODUCTION

Confinement of thermonuclear plasmas in tokamak toroidal magnetic containers is believed to be a promising approach for the development of fusion reactors. In a tokamak a plasma is confined in a strong toroidal magnetic field B_t which is generated by an external magnetic coil. The magnetic field lines are given a helical twist by the poloidal magnetic field B_p generated by the plasma current. This current, which is produced by external "ohmic heating" coils, also serves to heat the plasma resistively. The basic magnetic field configuration in a tokamak is shown in Figure 1.

PLASMA CURRENT I — — INSULATED SLIT

POLOIDAL MAGNETIC FIELD B_p — COPPER STABILIZING SHELL

INSULATED SLIT— TOROIDAL MAGNETIC FIELD B_t

PLASMA AXIAL DIRECTION

AZIMUTHAL DIRECTION
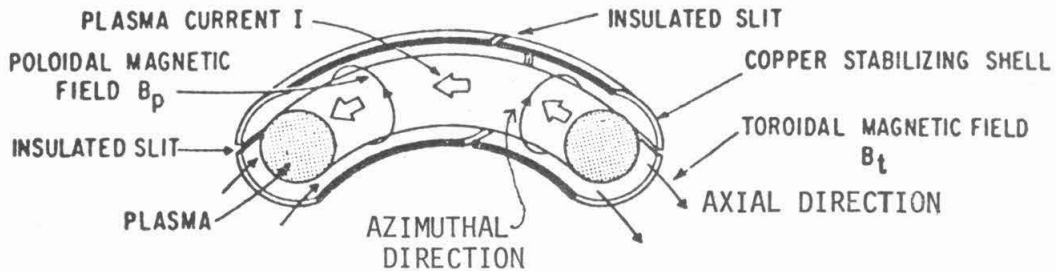
Fig. 1. The principal magnetic fields in a tokamak. (From Status and Objectives of Tokamak Systems for Fusion Research, S. D. Dean, et al.)

The degree to which the poloidal magnetic field twists the magnetic lines of force is measured by the rotational transform angle i[1], which equals the angle a line of force rotates in the poloidal direction after one complete rotation in the toroidal direction. With a little geometry one can show that

$$\frac{B_t}{B_p} = \frac{2\pi R}{ai} \qquad , \qquad (1.1)$$

or

$$\frac{2\pi}{i} = \frac{a}{R}\frac{B_t}{B_p} \equiv q \quad , \tag{1.2}$$

where R is the major radius of the torus and a is the minor radius. Thus, a magnetic field line makes q transits in the toroidal direction in making a single transit in the poloidal direction. The parameter q is important in many aspects of tokamak research and generally must be larger than 2.5-3.0 at the edge of the plasma if stability is to be achieved.

The beneficial effect of the helicity of the lines of force can be seen by the following argument. In a simple torus in which the lines of force are closed circles, the magnetic field varies as $1/r$. The resulting curvature and gradient drifts cause a vertical charge separation, which in turn causes the plasma to drift outward due to the $\vec{E} \times \vec{B}$ drift (to be derived later). A helical line of force connects regions of positive charge to regions of negative charge and therefore short-circuits the vertical electric field. If collisions are included (i.e., if the plasma resistivity is finite), the rotational transform must be sufficiently large before stability is established.

One of the major problems that confronts fusion researchers is how to minimize the rate of leakage of the plasma from a tokamak magnetic bottle. The observed particle and energy diffusion rates cannot be explained by classical diffusion theory and are therefore termed "anomalous". Classical theory predicts that, for a fully ionized gas, a fluid element should move across straight magnetic field lines with a diffusion coefficient[2]

$$D_\perp = \frac{\eta_\perp n \sum KT}{B^2} \quad , \tag{1.3}$$

where $\eta_\perp$ is the perpendicular resistivity, n is the particle density, and the sum is over all particle species. $D_\perp$ is the coefficient for the entire fluid; no ambipolar electric field arises because both the ions and electrons diffuse at the same rate.

In toroidal geometry the diffusion coefficient becomes $D'_\perp = D_\perp(1 + q^2)$, where $(1 + q^2)$ is called the Pfirsch-Schluter factor[3]; and since $q \simeq$ 5-6 in most tokamaks, the geometrical effect is fairly large. The situation in tokamaks, however, is made even more complicated by the twist in the magnetic field needed to eliminate the unidirectional grad-B and curvature drifts and the magnetic field's radial dependence.

As a particle travels along a line of force, it passes through a larger B_t field near the inside wall of the torus than it does near the outside wall. Thus, if the particle's mean free path is larger than the distance between maximum field regions, it may be trapped by the magnetic mirror effect. When trapping occurs, the particle will trace out banana-shaped orbits[4] as it makes successive passes through a given cross section. If the particle collides with other particles, it can move from one banana orbit to another, and its random-walk step length becomes the banana orbit width rather than its Larmor radius. Since banana orbit widths in tokamaks are typically much larger than the ion Larmor radius, the classical diffusion coefficient is increased.

The combined effect of toroidal geometry and trapped particles is described by the neoclassical diffusion coefficient[5] as seen in Figure 2.
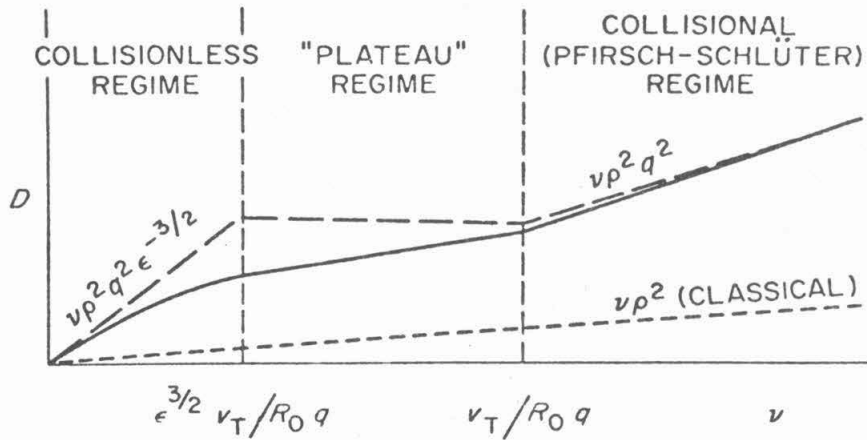
Fig. 2. The neoclassical diffusion coefficient as a function of the
electron-ion collision frequency. $\epsilon = r/R_0$, r is minor radius,
R_0 is major radius, ρ is the electron Larmor radius, and V_T is
the electron thermal speed. (From F. L. Hinton and M. N.
Rosenbluth, Phys. Fluids $\underline{16}$, 836 (1973)).

For low electron-ion collision frequencies, banana diffusion is predomi-
nant, while for high collision frequencies, collisional Pfirsch-Schluter
diffusion is most important. The "plateau" region aptly describes the
diffusion between the two extremes. For the Caltech tokamak the collision
frequencies were such that all experiments were performed in the transi-
tion region between the plateau and Pfirsch-Schluter regimes.

If Coulomb collisions were the only significant processes that led
to plasma transport in tokamaks, the plasma confinement times would be
ample by several orders of magnitude for fusion reactor requirements. Un-
fortunately, while the Coulomb collisional transport theory for equili-
brium plasmas is reasonably well developed, its predictions have been
verified experimentally only for toroidal plasmas that do not carry a
toroidal current.[6,7] In current-carrying tokamak plasmas, the particle
transport and electron heat conduction processes typically exceed the

neoclassical values by several orders of magnitude. However, it has been found in several experiments[8,9] that the ion heat transport agrees reasonably well with the neoclassical prediction for the ion heat conductivity. It is generally assumed that the discrepancy between the theoretical values for particle transport and the observed values is due to plasma instability.

Since a plasma must be spatially uniform and must have a Maxwellian velocity distribution to be in thermodynamic equilibrium, any confined plasma is necessarily out of equilibrium. A plasma that is not in equilibrium can relax by either Coulomb collisions or by various types of collective plasma instabilities. These instabilities are customarily divided into two classes: macroinstabilities (derivable from a fluid description) and microinstabilities (derivable from a kinetic description, or in some cases two-fluid theory). Macroinstabilities include the kink, flute, sausage, tearing, and disruptive instabilities, while the important microinstabilities in tokamaks involve the drift-type fluctuations. Since the transport caused by various types of these instabilities is in general in excess of, and relatively unrelated to, classical transport, it is usually referred to as "anomalous" transport.

In particular, when collisions are sufficiently rapid so that particles collide before they bounce, drift dissipative modes[10] may develop. The theoretical particle diffusion coefficient due to these modes is roughly $D_\perp \simeq C_1 \nu_{ei} \rho_{\theta e}^2$.[11] The particular empirical constant C_1 used in this "pseudoclassical" theory is somewhat different for various tokamaks. At present, it is commonly assumed that $C_1 \simeq 1.0$. It is important to

understand that pseudoclassical diffusion, although yielding diffusion rates close to those observed experimentally, has been derived from a phenomenological picture and not from first principles. Thus, its scaling and validity for tokamak diffusion is a subject for considerable debate.

During the past decade many experiments have been performed on various plasma devices in an attempt to identify which instabilities (i.e., kink, tearing, drift, etc.) were present and which contributed most strongly to the "anomalous" transport. In Q-machines and stellarators these experiments usually involved the use of electrostatic and magnetic probes. However, in tokamaks the electron temperature is generally much higher than in other plasma devices, and this has prevented the direct insertion of probes into the plasma for diagnostic measurements. Other techniques, such as laser and microwave scattering, have therefore been employed to study the fluctuation characteristics in tokamak plasmas. However, scattering techniques have suffered from several disadvantages. First, the scattering volume comprised a fairly large region of the plasma in which the magnetic field, temperature, and density all varied. In some experiments the variations in temperature and density in the scattering volume may have been as much as a factor of ten. Thus, in past investigations many of the important physical parameters which might affect the fluctuations have been poorly determined. Second, the propagation direction and the radial and azimuthal correlation length of the oscillations were difficult to measure by scattering techniques.

For this thesis, fluctuations were studied in a tokamak plasma with electrostatic probes. This was possible since, in the Caltech tokamak, the electron temperature and plasma current

were lower than in most other tokamaks. Thus, direct probe measurements were possible in the outer region of the plasma. This allowed for very localized measurements of the plasma fluctuations.

In Chapter II a brief explanation of drift and tearing modes is presented, and a summary is given of experimental results from other machines which indicates that both modes may play a major role in the anomalous transport of plasma to the walls. In Chapter III the Caltech experimental equipment is discussed, and in Chapter IV the plasma characteristics are described. Chapter V is devoted to the numerical methods which were used to analyze the rather noisy probe signals, which were digitally recorded during plasma shots, and the experimental results are described in Chapters VI and VII. Finally, in Chapter VIII an attempt is made both to summarize the large quantity of data which was accumulated and to indicate how the results compare with the predictions of current theories of drift and tearing instabilities.

II. BACKGROUND ON DRIFT AND TEARING MODES

2.1 The Diamagnetic Drift Velocity and a Simple Derivation of the Drift Wave Dispersion Relation

In the fluid approximation one considers the plasma to be composed of two or more fluids, one for each species. In the simplest case, when there is only one species of ions, there are two equations of motion, one for the positively charged ion fluid and one for the negatively charged electron fluid. The fluid equation of motion for electrons is[12]

$$mn \frac{d\vec{V}_e}{dt} = -en(\vec{E} + \vec{V}_e \times \vec{B}) - \vec{\nabla}P_e - \vec{\nabla}\cdot\vec{\vec{\pi}}_e + \vec{P}_{ei} \quad . \tag{2.1}$$

The term $\vec{P}_{ei}$ represents the momentum gain of the electron fluid due to electron-ion collisions; and the stress tensor $\vec{\vec{P}}_e$ has been split into the isotropic part P_e and the anisotropic viscosity tensor $\vec{\vec{\pi}}_e$.

Now if we neglect electron-ion collisions, viscosity, and assume that $\vec{V}_e$ is uniform, then in the steady state

$$0 = -en(\vec{E} + \vec{V}_e \times \vec{B}) - \vec{\nabla}P_e \quad . \tag{2.2}$$

Taking the cross product with $\vec{B}$ and considering only $\vec{V}_{e\perp}$ we get

$$0 = -en(\vec{E} \times \vec{B} + (\vec{V}_{e\perp} \times \vec{B}) \times \vec{B}) - \vec{\nabla}P_e \times \vec{B} \quad , \tag{2.3}$$

or

$$0 = -en(\vec{E} \times \vec{B} + \vec{B}(\vec{V}_{e\perp}\cdot\vec{B}) - \vec{V}_{e\perp}B^2) - \vec{\nabla}P_e \times \vec{B} \quad , \tag{2.4}$$

so

$$\vec{V}_{e\perp} = \frac{\vec{E} \times \vec{B}}{B^2} + \frac{\vec{\nabla}P_e \times \vec{B}}{enB^2} \quad . \tag{2.5}$$

Thus, the perpendicular electron velocity has two terms: the first term which is independent of particle charge and mass is called the $\vec{E} \times \vec{B}$ drift velocity, and the second term which does depend on the particle charge is called the diamagnetic drift velocity. Note that

$$\vec{V}_{De} = \frac{\vec{\nabla P}_e \times \vec{B}}{enB^2} = -\frac{KT_e}{eB_0} \frac{1}{n_0} \frac{\partial n_0}{\partial x} \hat{e}_y \quad , \tag{2.6}$$

when $\vec{B} = B_0 \hat{e}_z$ and $n = n_0(x)$.

The physical reason for the diamagnetic drift can be seen from the following diagram:
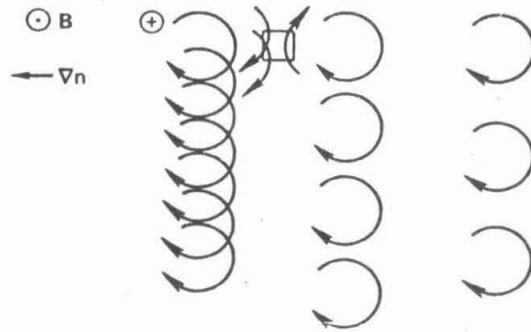
(From F. Chen, <u>Introduction to Plasma Physics</u>, Ref. 2)

In the preceding diagram the orbits of ions gyrating in a magnetic field are drawn. Since there is a density gradient to the left, more ions will pass through the fixed volume element traveling downward than traveling upward. Hence, there is an ion fluid drift perpendicular to $\vec{\nabla}n$ and $\vec{B}$ even though the guiding centers are stationary.

For drift waves,[13] which are a type of universal instability (caused by the lack of perfect thermodynamic equilibrium for confined plasmas), $k_z \neq 0$, and electrons can flow along B_0 to establish a thermodynamic

equilibrium among themselves. Therefore, they will obey the Boltzmann relation along B_0

$$n_e = \bar{n}_e \ e^{e\phi/kT_e} \quad , \tag{2.7}$$

where ϕ is the plasma potential. For the unperturbed plasma case $n_e = n_{oe}$ and $\phi = \phi_0$, so

$$n_{oe} = \bar{n}_e \ e^{e\phi_0/kT_e} \quad . \tag{2.8}$$

For the perturbed plasma case $n_e = n_{oe} + n_{1e}$ and $\phi = \phi_0 + \phi_1$, where $|\phi_1| \ll |\phi_0|$ and $e|\phi_1| \ll kT_e$, hence

$$n_{oe} + n_{1e} = n_e = \bar{n}_e \ e^{e\phi_0/kT_e} \ e^{e\phi_1/kT_e} \quad , \tag{2.9}$$

or

$$n_{oe} + n_{1e} \simeq \bar{n}_e \ e^{e\phi_0/kT_e} \ (1 + \frac{e\phi_1}{kT_e})$$

$$= n_{oe} + n_{oe} \frac{e\phi_1}{kT_e} \quad , \tag{2.10}$$

so

$$\frac{n_{1e}}{n_{oe}} \simeq \frac{e\phi_1}{kT_e} \quad . \tag{2.11}$$

The behavior of the ions is governed by the continuity equation

$$\frac{\partial n_i}{\partial t} = - \vec{\nabla} \cdot (n_i \vec{V}_i) \tag{2.12}$$

and the equation of motion

$$\frac{\partial \vec{V}_i}{\partial t} = - \frac{e}{m_i} \vec{\nabla}\phi + \Omega_i (\vec{V}_i \times \hat{e}_z) \quad . \tag{2.13}$$

For directions perpendicular to $\hat{e}_z$ ($\vec{B} = B_0 \hat{e}_z$), one can show, with a little algebra, that the linearized solution to equation (2.13) is

$$V_{i\perp} \simeq -i\,k_y \frac{\phi_1}{B_o}\,\hat{e}_x \qquad , \qquad (2.14)$$

assuming $|\omega| \ll \Omega_i$. The perturbed continuity equation for the ions then gives (again for directions perpendicular to $\hat{e}_z$)

$$\frac{\partial n_{1i}}{\partial t} = -n_{oi}\nabla_x(V_{ix}) - V_{ix}\nabla_x n_{oi} \simeq -V_{ix}\frac{\partial n_{oi}}{\partial x} \qquad (2.15)$$

where it is assumed that the term $n_{oi}\nabla_x(V_{ix})$ is small compared with $V_{ix}\nabla_x n_{oi}$; that is, the fluid oscillates incompressibly. Also, n_{oi} is assumed to vary gradually in the $\hat{e}_x$ direction. Therefore,

$$-i\omega n_{1i} = ik_y \frac{\phi_1}{B_o}\frac{\partial n_{oi}}{\partial x} \qquad (2.16)$$

or

$$\frac{n_{1i}}{n_{oi}} = -k_y \frac{\phi_1}{\omega B_o}\frac{1}{n_{oi}}\frac{\partial n_{oi}}{\partial x} \qquad . \qquad (2.17)$$

Hence, assuming quasineutrality ($n_{1i}/n_{oi} = n_{1e}/n_{oe}$),

$$-k_y \frac{\phi_1}{\omega B_o}\frac{1}{n_{oi}}\frac{\partial n_{oi}}{\partial x} = \frac{e\phi_1}{KT_e} \qquad (2.18)$$

so

$$\omega/k_y = -\frac{KT_e}{eB_o}\frac{1}{n_o}\frac{\partial n_o}{\partial x} = V_{De} \qquad . \qquad (2.19)$$

Thus, the azimuthal phase velocity of these waves is equal to the electron diamagnetic drift velocity.

It should be noted that in the previous derivation no instability is predicted. A more complete analysis[14] shows that if some process exists that can retard the motion of either the electrons or the ions, then this retardation will cause the species to get out of phase. The

result of this phase difference can be shown to make the perturbed potential ϕ_1 lag behind the perturbed density n_1 and, under certain conditions, to cause the perturbed fluid velocity to be outward when the plasma has already shifted outward. The perturbation then grows.

2.2 The Ellis and Motley Two-Fluid Drift Wave Theory[14]

A complete two-fluid theory for current driven collisional drift waves has been derived by Ellis and Motley (1974), and their results were shown to agree well with observations in a Q-machine. Their theory was modified by the author to include the effect of different electron and ion temperatures. The dispersion relation which was solved numerically on the IBM-370 using typical Caltech tokamak parameters is of the form

$$a_3\omega^3 + a_2\omega^2 + a_1\omega + a_0 = 0 \quad , \tag{2.20}$$

where a_3, a_2, a_1, and a_0 are complicated algebraic functions of the plasma parameters (see Appendix B). The results of the numerical calculation, using the Caltech computer library program cpoly which finds the zeros of any complex polynomial, give three roots: the first two roots are heavily damped for all physically interesting values of $k_\perp$, but the third root has a positive growth rate for specific values of $k_\perp$.

The two heavily damped roots can have phase velocities either in the electron or ion diamagnetic drift direction, depending on the magnitude of $k_\perp$; however, the third root always has a phase velocity in the electron diamagnetic direction. Both the real and imaginary parts of the frequency for the third root are plotted vs. reciprocal wavelength, $1/\lambda_y$, in Figures 3a,b. When the imaginary part of the frequency was negative (corresponding

Figure 3a. The frequency for drift waves versus $1/\lambda_y$ (for $\lambda_v = \lambda_\chi$) based on the two-fluid theory of Ellis and Motley[14]. Curves calculated from measured plasma parameters at several radial positions in the Caltech tokamak.
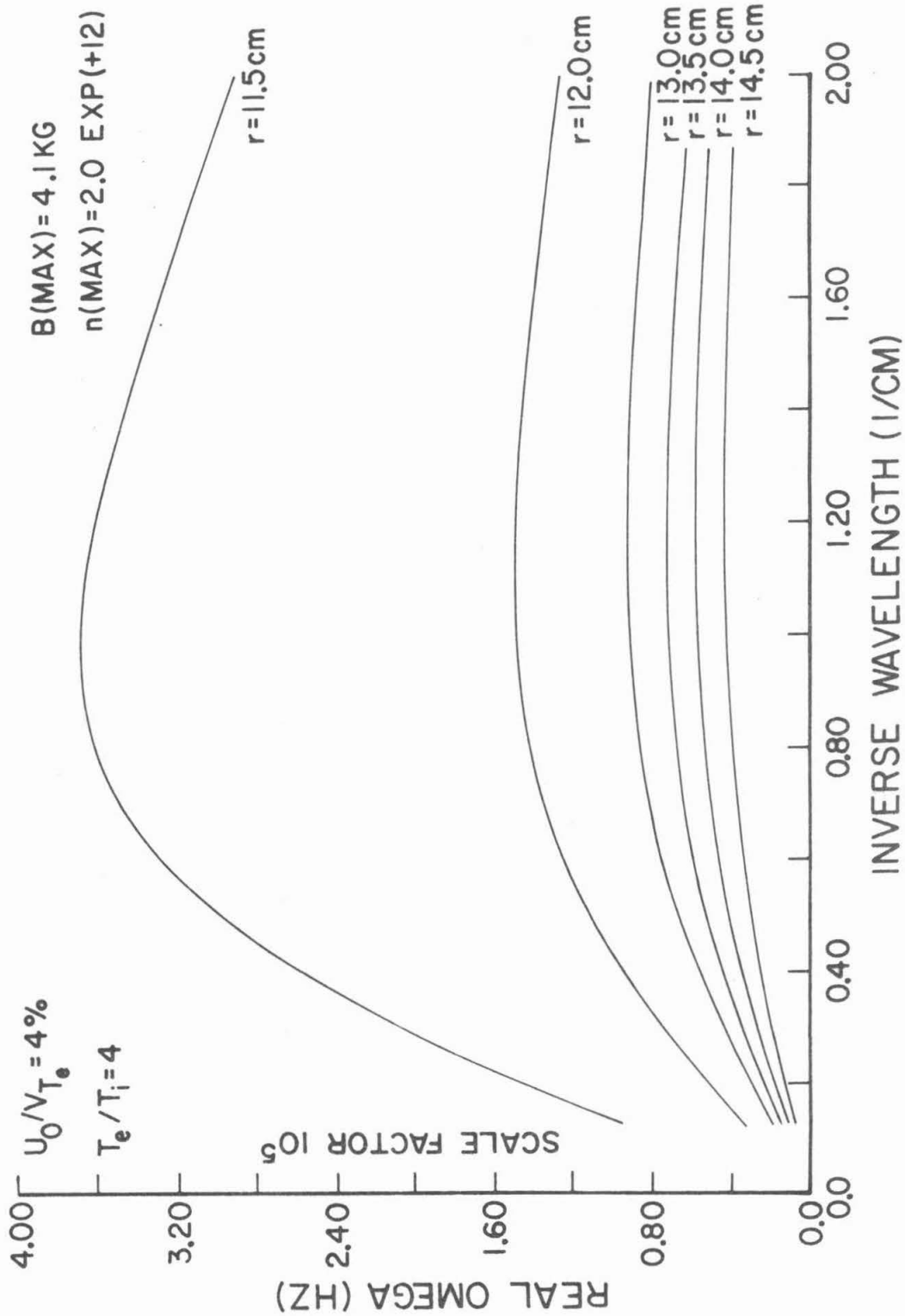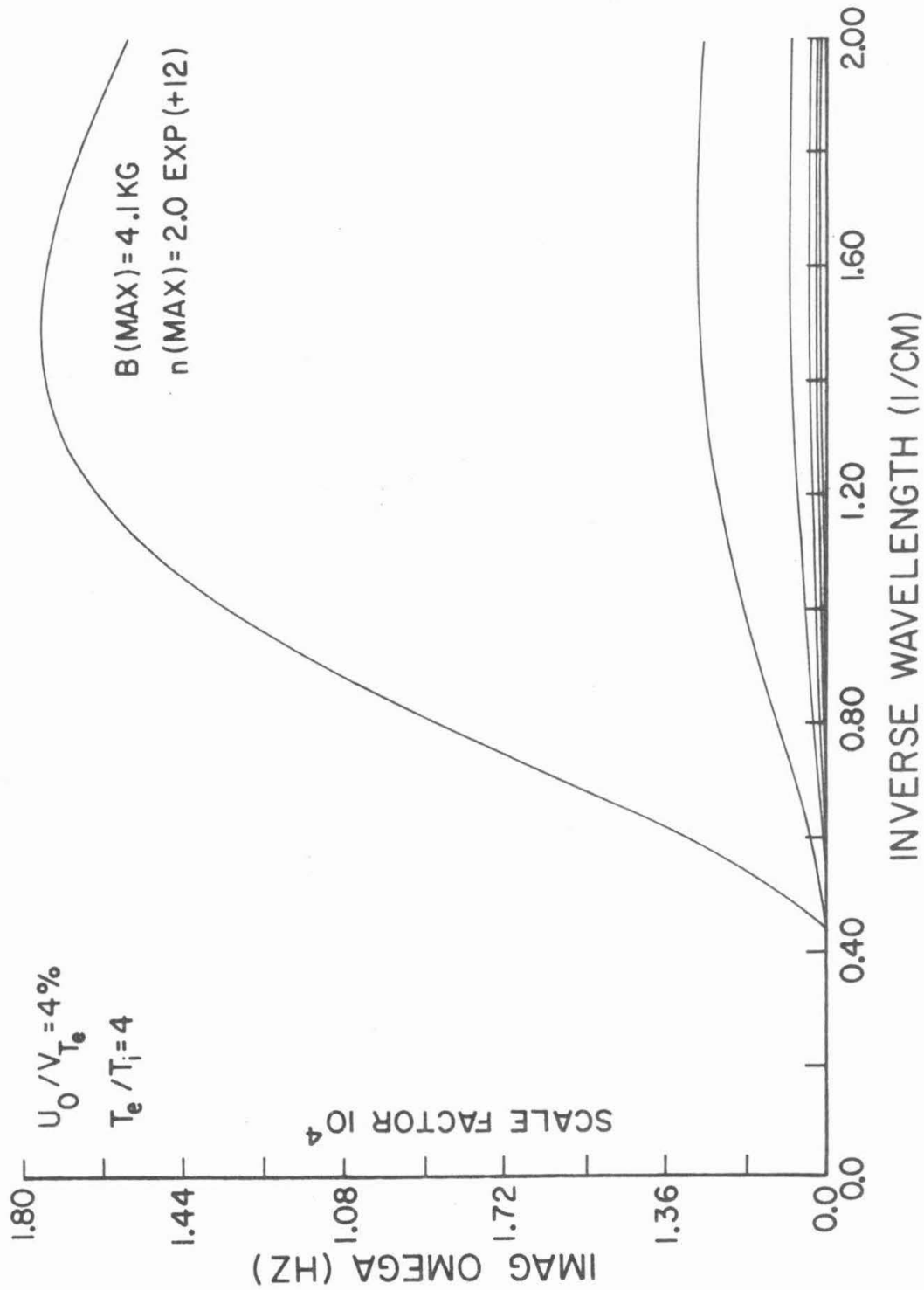
Figure 3b. The growth rates for drift waves versus $1/\lambda_y$ (for $\lambda_y = \lambda_x$) based on the two-fluid theory of Ellis and Motley[14]. The curves correspond from top to bottom to those in Figure 3a.

to damped waves), its value was set equal to zero in the plots.

The phase velocity of the third root is constant for λ_y larger than approximately 1.6 cm, but the oscillations are damped for λ_y much larger than 2 cm. Hence, the modified Ellis and Motley two-fluid theory predicts growing drift waves for the Caltech tokamak parameters only for azimuthal wavelengths shorter than about 2 cm. In the present experiment, azimuthal wavelengths between 6 and 70 cm were observed.

It should be noted, however, that for a plasma in a strong magnetic field ($\lambda_{mfp} \gg \rho$) a necessary prerequisite for a fluid description is $\lambda_\perp \gg \rho_i$. Since in the Caltech tokamak, $\rho_i \approx 0.17$ cm, any fluid theory is strictly valid only for $\lambda_\perp \gg 0.17$ cm. This condition was well satisfied for the observed fluctuations.

2.3 Kink and Tearing Modes

We now consider a different type of oscillation which is classified as a macroscopic instability, since the gross motion of the plasma column is affected. The following diagram shows a current flowing in a plasma column in the direction of a magnetic field B_0.
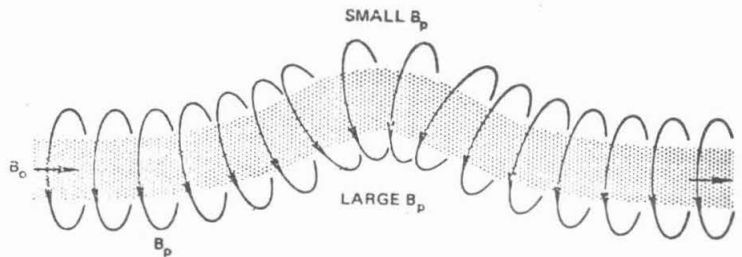
(From F. Chen, Introduction to Plasma Physics, Ref. 2)

If a kink develops, the poloidal magnetic field lines B_p which are produced by the current have a higher density on the inside of the kink than

on the outside. The magnetic pressure $B_p^2/8\pi$ therefore acts to in-
crease the size of the kink, and the plasma is pushed to the walls.

Kink modes have been observed in linear plasma devices for many
years, and hence when toroidal devices were first built it was assumed
that some form of kink might develop in tokamak plasmas. The standard
MHD model for kink instabilities[15] assumes that a perfectly conducting
plasma exists in the radial direction between r = 0 and the plasma edge
at r = a. Outside this region the plasma is assumed to be surrounded
by a vacuum with a perfectly conducting boundary located at r = b (b>a).
An analysis has been performed by Kruskal[16] for the stability
of a stellarator plasma against perturbations of the general form
Re $e^{i(\pm m\theta + kz)}$. On the basis of such analysis, the onset of instabil-
ity of the mth kink mode is predicted to coincide with a rotational
transform of $2\pi/m$ at the outer edge of the plasma column.

Since the rotational transform angle i equals $2\pi/q$, theory
predicts that in a torus the onset of the mth kink mode should
occur when q(a) = m. Moreover, since q(a) = a/R B_t/B_p, one would expect
that as B_t decreases, or as B_p increases, the predominant mode number
should decrease. Furthermore, in most tokamaks q(a) $\simeq$ 4-6 and is a mono-
tonically increasing function of radial position; so it is of interest
to determine what modes, if any, are unstable when q(r_s) = m, where r_s
is a point in the interior of the plasma. It is found that in this case,
the standard kink mode models do not predict strongly unstable modes.

However, the description of the plasma as an infinite-conductivity
fluid surrounded by a vacuum region is not entirely satisfactory. In

experiments, it is clear that the points r_s corresponding to integral values of q fall well within the region of conductive, and usually current-carrying plasma. Therefore, it is appropriate to treat the medium at r_s as a finite-resistivity plasma rather than as a vacuum. This is the basis of tearing mode analysis.

To understand tearing modes[18] in a qualitative manner, consider a slab of current J_z of width a which is uniform in the y-z plane moving along a large B_z field.
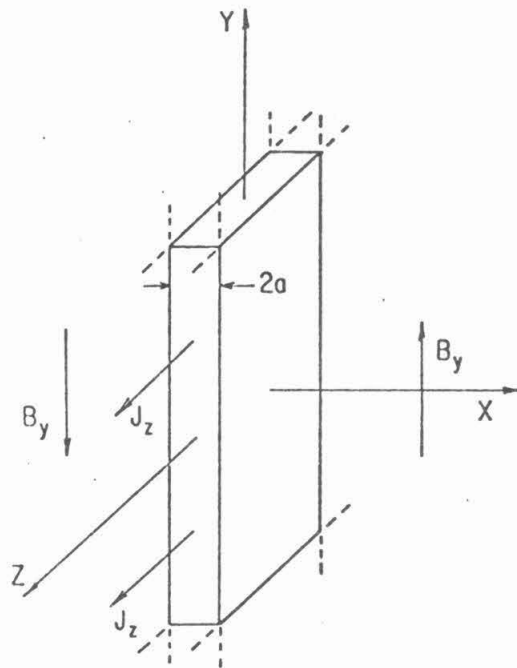
(From J. F. Drake and Y. C. Lee, Ref. 18)

A self-consistent $B_y(x)$ field is produced which changes direction across the current sheet, hence $B_y = 0$ at $x = 0$. Finite resistivity allows the tearing instability to relax the system to a lower magnetic energy state. Specifically, the tearing mode results in a bunching of the

current into filaments along the y direction. The magnetic field in the x-y plane is also deformed and is seen in the following diagram.
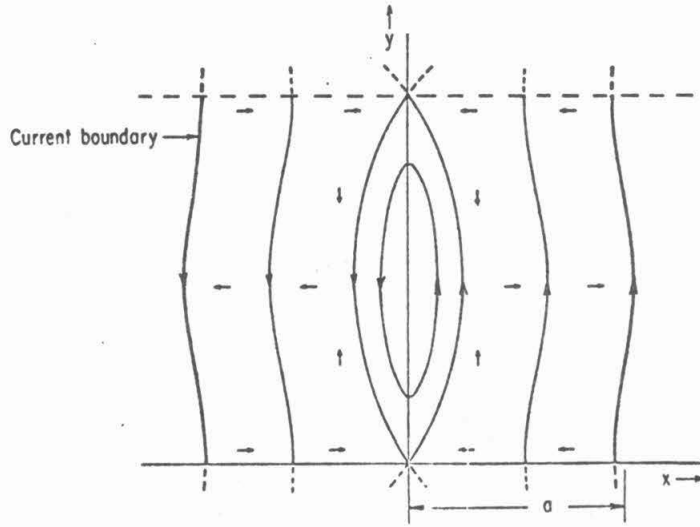
(From J. F. Drake and Y. C. Lee, Ref. 18)

The nonlinear evolution of such a mode is characterized by the B_y field lines tearing and reconnecting near $\vec{k} \cdot \vec{B} = 0$ surfaces. (This is equivalent to the region around $q(r) = m$ when the toroidal wavelength of the mode equals $2\pi R$.) Within this narrow layer, the field lines move without carrying the plasma with them, and this slippage produces an induced electric field E_{z_1} which accelerates the electrons along the local magnetic field.[18] The perturbed current J_{z_1} which results is localized, and, along with the current in the other regions of the plasma, self-consistently produces the magnetic field shown in the previous diagram. Thus, the tearing mode is a mechanism in which magnetic energy is converted to particle energy by the acceleration of electrons in the narrow layers around $\vec{k} \cdot \vec{B} = 0$. The kink mode, however, transfers magnetic energy to the gross plasma column motion.

Recently, the effects of electron temperature and density gradients have been included in tearing mode analysis[18,19], and the modified instabilities are termed drift-tearing modes. Although the theory is still very new and nonlinear, and toroidal effects have not been completely derived, some general remarks can be made concerning the latest results. First, the instabilities are still predicted to be localized around the $\vec{k} \cdot \vec{B} = 0$ singular layers, but the disturbance widths are broadened due to the electron temperature and density gradients. Second, depending on the electron-ion collision frequency, the modes can be classified in three groups: collisionless, semi-collisional, and collisional. Most present generation tokamak plasmas lie in the semi-collisional regime. Finally, for the Caltech tokamak plasma parameters, the predicted oscillation frequency is roughly equal to the electron diamagnetic frequency $\omega^* = k_y V_{De}$.

2.4 Fluctuation Characteristics in Past Experiments

Many experiments have been performed during the past decade on numerous machines in the hope of determining which instability mechanisms are responsible for anomalous transport. In this section a summary will be given of the various experimental techniques and observations that have preceded the current investigation on the Caltech tokamak. It should become apparent in this summary that there exist large discrepancies in past results, both between different experiments and between experiment and theory, and this confusion has served to motivate the present research.

Many of the machines used in previous studies and their plasma parameters are summarized in Figure 4. As one can see, the observed fluctuations were thought to be due either to MHD kink-tearing modes or to drift-type waves. Moreover, the direction of the azimuthal propagation varied between experiments.

In the Etude stellarator experiments[20] (1964), Bol used two electrostatic probes and a wide variety of filters to measure the fluctuation spectrum and correlation between the probes. He observed a broadband frequency spectrum which extended to 2 MHz and which had a slight peak at 60 kHz for a particular plasma parameter range. This peak was attributed to a 2.0×10^4 cycle/sec rotation rate of the plasma column, combined with a m = 3 kink-type distortion. Distinct peaks in the correlation function existed for various plasma currents, and these peaks were related to m = 2,3,4,5 instabilities. The azimuthal correlation length for most frequencies was found to be roughly a tenth of the circumference of the plasma at the probe tips, and the azimuthal velocity was observed to be a linear function of the frequency for $f \leq 100$ kHz. Since the $\vec{E} \times \vec{B}$ velocity was roughly 1.88×10^5 cm/sec at r = 1.5 cm, while the azimuthal phase velocity extended to 5.65×10^5 cm/sec at the same radius, no explanation could be given for the measured phase velocity.

In more recent experiments, R. F. Ellis and R. W. Motley[14] found good agreement between their two-fluid theory of drift waves and their measurements on a Q-machine. The observed frequency spectra were fairly narrow (f ≃ 10 kHz), and the perpendicular wavelengths were of the order of 1 cm. The waves were found to travel in the electron diamagnetic drift direction, in agreement with drift wave theory, and long axial

AUTHOR	MACHINE	PLASMA CHARACTERISTICS	TYPE OF FLUCTUATION "THOUGHT" TO BE PRESENT	METHODS OF MEASUREMENT	PROPAGATION DIRECTION
A. Bol[20]	Etude Stellarator	T_e = 20 eV, B_T = 6.7 KG, $\bar{n}_e$ = 1.0×10^{13}cm^{-3}, I_p = 500A	Kink	Electrostatic Probes	Ion diamagnetic drift direction
K. M. Young[21]	C Stellarator	T_e = 20 eV, B_T = 35 KG, $\bar{n}_e$ = 1.0×10^{13}cm^{-3}, I_p = 1.0 kA	1) Current-driven universal 2) Tearing 3) Rippling	Electrostatic Probes	Ion and electron diamagnetic drift direction depending on V_D/V_i
R. F. Ellis & R. W. Motley[14]	Q-Machine	T_e =2500°K, B_T = 5-15 KG, $\bar{n}_e$ = 1.0×10^{11}cm^{-3}, I_p = 100 MA	current-driven collisional drift	Electrostatic Probes	Electron diamagnetic drift direction
K. Wakishima, et al.[22]	Minimak	T_e = 6 eV, B_T = 1.0 KG, n_e ≈ 5×10^{12}cm^{-3}, I_p = 5 kA	MHD-tearing	Magnetic Loop Probes	Ion diamagnetic drift direction
S. V. Mirnov, et al.[23]	T-3	B_T = 20 KG, n_e =1.0×10^{13}cm^{-3}, I_p = 50-150 kA	MHD	Magnetic loop probes outside limiter	Ion diamagnetic drift directions
R. Prater, et al.[24]	DC octupole	B_T = 0-1000G, B_p = 114G, n_e = 10^8-10^{9}cm^{-3}, T_e = 1 eV	Dissipative trapped electron instability	Electrostatic Probes	Electron diamagnetic drift direction
Hosea, et al.[25]	ST	T_e = 800 eV, B_T = 34 KG, $\bar{n}_e$ = 3.0×10^{13}cm^{-3}, I_p = 40 kA	drift or tearing	Magnetic loop probes outside limiter	Electron diamagnetic drift direction
S. M. Harberger, et al.[26]	Torso Torsatron	T_e = 100 eV, B_T = 4-10 KG, $\bar{n}_e$ = 1.0×10^{13}cm^{-3}, I_p = 1-10 kA	drift	Microwave Beams	Electron diamagnetic drift direction
Surko & Slusher[27]	ATC	T_e = 800 eV, B_T = 16 KG, n_e = 1.0×10^{13}cm^{-3}, I_p = 70 kA	drift	CO_2 laser scattering	Undetermined
Mazzucato[28]	ATC	T_e = 400 eV, B_T = 20 KG, n_e = 2.0×10^{13}cm^{-3}, I_p = 70 kA	drift	Microwave scattering	Undetermined

Figure 4. A summary of the devices used in previous fluctuation studies and their plasma parameters. Also listed are the methods of measurement and the types of instabilities which were thought to have been present.

wavelengths were observed, $\lambda_z \simeq 250$ cm. Other experimental results such as the frequency dependence on magnetic field strength and plasma current and the variation of the critical current for mode onset agreed favorably with their two-fluid theory.

In the Minimak tokamak,[22] K. Makishimi, et al. used magnetic loop probes to observe magnetic fluctuations which were found to travel in the ion diamagnetic drift direction; similar results were obtained at higher temperatures and densities on T-3 by Mirnov and Semenov.[23] From both the Minimak and T-3 results, it was concluded that long wavelength ($\lambda_\perp \sim 10$ cm) MHD tearing modes were present and were carried azimuthally around the torus by the $\vec{E} \times \vec{B}$ drift.

However, a great deal of confusion was created when Hosea, et al.[25] reported that in the ST tokamak the fluctuations had an azimuthal velocity in the electron diamagnetic drift direction. Both the methods of measurement and the plasma parameters were very similar for the T-3 and ST tokamaks, and thus similar results were expected. In ST, therefore, drift waves were thought to play some role in producing the observed fluctuations. The principal results of the study of the signals observed on magnetic loop probes placed outside the limiter on ST were the following. First, the frequency spectra were narrow with $f \simeq 100-140$ kHz. Second, the density fluctuations ($\delta n/n$) were approximately four percent; and third, the azimuthal mode number decreased with time, with cooling of the plasma surface by pulsing in gas, with an increase in the initial gas pressure, with a decrease in toroidal field, and with an increase in plasma current.

The most recent group of experiments performed since 1975 have involved various scattering techniques in which large regions of the plasma have been examined at one time. S. M. Hamberger, et al.[26] reported observing electrostatic drift-type waves in a plasma with temperatures, magnetic fields, and currents similar to those in the Caltech tokamak. Several microwave beams perpendicular to the toroidal magnetic field were passed through the plasma, and correlation studies were performed on the microwave signal fluctuations. The fluctuations were observed to travel in the electron diamagnetic drift direction and to have perpendicular wavelengths of the order of 1 cm. A wide frequency spectrum extending to 200 kHz was measured, and the density fluctuations ($\delta n/n$) were estimated to be approximately ten percent.

In the ATC experiments CO_2 laser[27] and microwave scattering[28] were employed to study the instabilities, and results which, in some respects, resemble those reported by S. M. Hamberger were obtained. The perpendicular propagation direction was not determined in these experiments, but the frequency spectrum was broad and extended to 400 kHz. The perpendicular wavelengths ranged between 0.1-2.0 cm, and the fluctuations were attributed to electrostatic drift-type waves with density fluctuations ($\delta n/n$) of one percent. However, no systematic study was undertaken to determine the effects of different plasma conditions on the oscillations.

Thus, at the time the present research was begun, there were many discrepancies in the experimental results. The earlier work on tokamaks which involved magnetic loop probes seemed to indicate that the tearing

instability was the most important source of turbulence, while the fluctuations observed several years later using scattering techniques were attributed to electrostatic drift-type waves. It should be pointed out, however, that in the scattering experiments plasma oscillations in only a limited wavelength range could be resolved. Since the plasma wavelength observed in these experiments is determined by the scattering angle and since detectors and beam dumps have finite solid angles, the previous scattering experiments were limited to observing wavelengths shorter than about 2 cm. Since the predominant tearing modes generally have low azimuthal mode numbers (m=1,2,3,4, etc.) and the minor circumference of most present tokamaks is of the order of 100 cm, these modes could not be adequately studied by scattering techniques.

The purpose of this thesis, therefore, was to determine by electrostatic probe techniques, which afforded very localized measurements of the plasma conditions, which instability was most predominant in the Caltech tokamak. The results of this study indicate that both the drift and tearing modes may be responsible for the observed fluctuations. Unfortunately, a complete nonlinear kinetic theory in toroidal geometry which includes both types of instability does not exist at present. The linear kinetic theory for tearing modes[18] in cylindrical geometry is only several months old, and although the results look favorable, a more complete theory is badly needed. Thus, it is hoped that the present work will serve as motivation for theorists who are interested in plasma instabilities.

III.   EXPERIMENTAL APPARATUS

3.1   The Tokamak: Machine Parameters, Power Supplies, and Discharge Cleaning

The experiments in this thesis were performed on the Caltech tokamak which was constructed between June 1975 and June 1976.   The vacuum liner was made from four 0.25-inch thick stainless steel 90° elbows which, when joined together, formed a torus with a major radius R = 46 cm and a minor radius a = 15 cm.   The toroidal magnetic field coils were wound directly on the vacuum liner, and ohmic heating and vertical field coils were attached to the torus by wooden brackets.   The ohmic heating coils were wound in such a manner as to produce a changing magnetic flux through the center of the torus and thereby induce an ohmic heating electric field around the tokamak.   The vertical field coils produced a small vertical magnetic field inside the torus to stabilize the plasma against its natural tendency to reduce its free energy and expand.   (That is, the poloidal magnetic pressure $B_p^2/8\pi$, being larger on the inside, would tend to increase the major radius of the plasma.)   Stabilization was accomplished, since the plasma current I_p coupled to the vertical field to produce a $\vec{J} \times \vec{B}$ force.   By orienting the vertical field in the proper direction relative to the plasma current, an inward directed force on the plasma could be produced.

The toroidal magnetic field was produced by a 50 Kjoule capacitor bank and was kept from ringing during the course of a plasma shot by a crowbar circuit.   The crowbar ignitron shorted the toroidal field windings when the current in them reached a maximum value.   Thus, the only

time variation of the magnetic field was a slow decay due to the finite resistance in the windings. However, during the plasma lifetime, the toroidal magnetic field was practically constant and could be varied from 2.6 kG to 4.7 kG.

The ohmic heating electric field and the vertical magnetic field were each generated by two sets of capacitors, the fast and slow banks. The fast banks had lower capacity than the slow banks and, therefore, had shorter rise times $\tau = \sqrt{LC}$, where L is the inductance of the ohmic heating or vertical field windings and C is the capacity of the respective fast or slow bank. This short rise time enabled the ohmic heating coils to produce an initially large electric field in the torus to promote breakdown of the plasma and allowed the vertical magnetic field to rise to an acceptable level quickly. When the voltages on the fast banks decreased and became equal to the slow bank voltages, two "zero crossing" networks added the slow bank capacitors in parallel with the fast banks and hence increased the rise time of each LC circuit. This allowed the ohmic heating electric field to be maintained for approximately 6 msec. A single horizontal wire loop around the top of the torus was used to monitor this electric field, and the signal from the loop was aptly called the "one-turn voltage".

In order to facilitate the initial breakdown of the plasma, a 1.5 MFD preionization capacitor charged to 4 kV was discharged into the ohmic heating coil for roughly 1 msec. This initial discharge, which rang at roughly 13 kHz, preceded the main ohmic heating pulse by 0.9 msec and was the source of considerable electrical noise in the laboratory.

The inside wall of the tokamak was cleaned by a procedure called discharge cleaning[47] in which hydrogen gas was broken down in a weak ($\leq$ 200G) toroidal magnetic field. The plasma was not well contained by this field and hence bombarded the wall. Impurities were thereby knocked off the surface and into the vacuum chamber where they were pumped out of the torus. The plasma was produced by pulsing 3-5 kW at 20 kHz into the ohmic heating coils for a period of 0.2 sec. The repetition rate for these pulses could be varied, but it was generally set at about 1.0 sec.

A steady D.C. toroidal magnetic field of 180 gauss was normally used during the cleaning process. This field was produced by passing 70 amperes through the toroidal field windings from a Hewlett-Packard power supply, Model 6453A. A filling pressure of 0.2-0.5 millitorr of hydrogen was used for discharge cleaning, and the impurities in the torus were monitored as a function of time with a Varian quadrupole gas analyzer, Model 978-1000 and with a Hewlett-Packard chart recorder, Model 7155B.

It was found that the general impurity conditions in the tokamak could be estimated by observing the levels of CH_3, CH_4, and H_2O for a period of several hours during discharge cleaning. The levels for these impurities decreased rapidly during the first few hours of cleaning, but once the wall conditions became favorable for tokamak operations, the impurity levels decreased more slowly with time. Generally, the tokamak was discharge cleaned every morning for approximately five hours before data were taken.

Using this procedure for eliminating wall contamination, it was possible to obtain a considerably cleaner plasma than in tokamaks which

were not discharge cleaned by this process. Although we had no direct
confirmation, it was estimated that our $Z_{eff} \simeq 1.5$-3.0. The results of
no cleaning were most noticeable after the tokamak had been open to at-
mospheric pressure for several hours. Even with the ohmic heating capa-
citor bank charged to its full voltage, only very short low current plasma
pulses (5 kA for approximately 2 msec) could be obtained before discharge
cleaning. After several hours of cleaning, however, much longer and
higher current plasmas (15 kA for approximately 12 msec) were easily ob-
tainable. Thus, the impurity content drastically affected the value of
both the plasma current and the plasma duration which could be obtained
for a given amount of ohmic heating energy.

3.2 Diagnostics

Several diagnostic signals were available for determining the
general characteristics of the plasma. These included the one-turn
voltage, plasma current, in-out and up-down signals, Langmuir traces,
and microwave interferometer fringes. The one-turn voltage was measured
by a single loop of wire placed on top of the torus in which the ohmic
heating magnetic flux passed. This voltage fell to zero approximately six
msec after the plasma was formed, and thus no plasma heating occurred
during the last few milliseconds of the plasma lifetime ($\tau_d \simeq 12$ msec).

The plasma current was measured by a Rogowski coil[29], and vertical
and horizontal plasma movements were detected by up-down and in-out
coils,[29] respectively. These latter coils were similar to the usual
Rogowski coil with the following exceptions. First, for the in-out coil,
the windings were more closely spaced on the sides of the torus than on

the top and bottom of the vacuum chamber. For the up-down coil the opposite was true. Second, the turns were wound in opposing directions on opposite sides of the torus so that the polarity of the signals from the coils (for a constant I_p) indicated the direction of motion of the plasma column. When the plasma moved outward, toward the side of the vacuum liner, the in-out coil produced a positive signal, and conversely, inward motion produced a negative signal. Likewise, the up-down coil was used to detect vertical plasma movement.

The up-down coil was useful after the tokamak's initial construction when magnetic field errors prevented the plasma current from lasting longer than 2 msec. However, once these problems were corrected, the in-out signal became an important diagnostic in determining the correct vertical field to be used for different plasma conditions. It was found, for instance, that as the ohmic heating was increased and the plasma current rose, the vertical field had to be increased to prevent the plasma from moving outward.

Langmuir probe measurements were taken for the outer 6 cm of the plasma, and from the resulting current versus voltage curves the electron temperature, density, and floating potential were calculated. Also, the line averaged electron density was measured by a 4 mm microwave interferometer.[30] The interference fringes which were produced by the phase shift created by the presence of the plasma in one path of the microwave signal were recorded on a 16 channel digital transient recorder. The number of fringes produced when the plasma conditions varied was directly calibrated to the electron density; and thus by some judicious counting, the line averaged electron density was

determined for the entire plasma lifetime. The results of these measurements and other plasma characteristics are the subject of Chapter IV.

3. Probes and Data Acquisition

Two electrostatic probes were used in this thesis to study the spectra and correlation of fluctuations in the Caltech tokamak plasma. The basic construction of the probes and the precision port aligner (described below) in which one probe was mounted are shown in Figure 5. The probes were approximately 40 cm long and were constructed from 0.317 cm stainless steel tubing. Tungsten wire 0.076 cm in diameter was used as the center conductor, and glass insulation was employed to prevent the tungsten and stainless steel from shorting. The length of the exposed tungsten wire was 0.8 cm, and glass sleeves covered the stainless steel near the probe tips. The insulating sleeves prevented the steel from electrically shorting the plasma. The tungsten wire was connected internally to copper wire near the R.F. connectors at the ends of the probes.

Two 8-inch RG-174 semi-rigid coaxial cables connected the probes either to 1.0 MΩ input impedance common mode rejection circuits, or to a Hewlett-Packard dual DC power supply, Model 6205B, which was used to bias the probes. Since common mode voltage problems were prevalent in the tokamak laboratory, it was found by experimentation that operational amplifier (LM-318 op amps were used) common mode rejection circuits were needed to eliminate extraneous probe signals. Thus, most of the data in this thesis were collected with the probes connected to 1.0 MΩ loads.
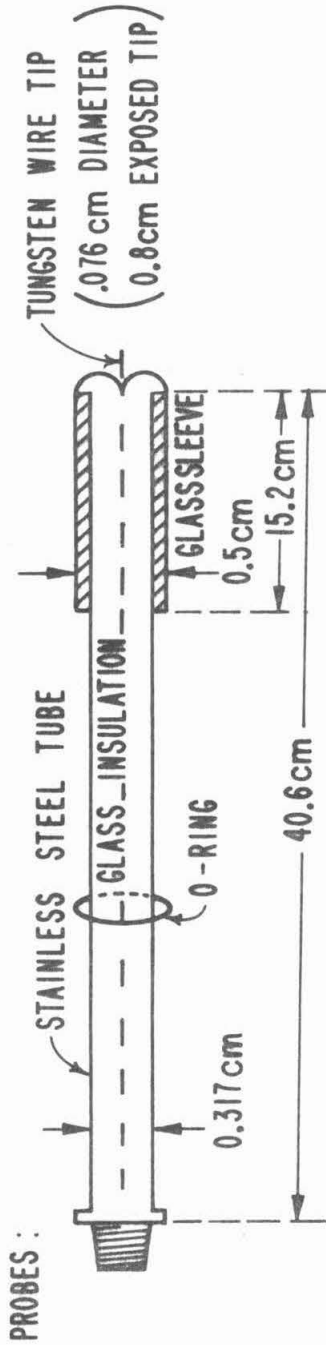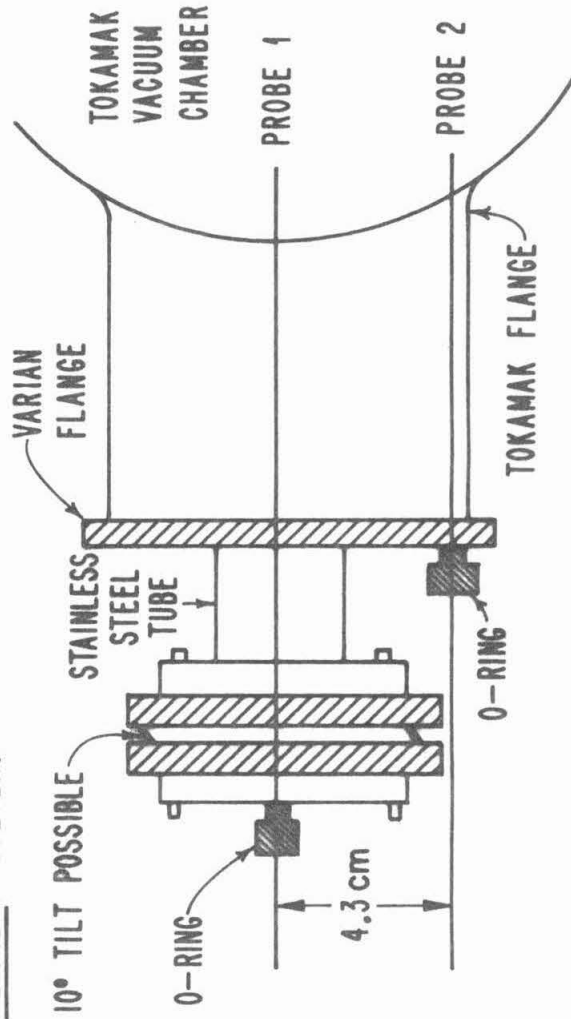
Figure 5. The electrostatic probes used to study the plasma fluctuations, and the port aligner which allowed the top probe to be positioned anywhere within a 20° cone

As will be shown later, the floating potential was between 0 and +10 volts for the regions of the plasma in which most of the data were taken. Moreover, a 1.0 MΩ load line for the probes lay extremely close to the voltage axis of the Langmuir trace and intersected the Langmuir curve near the floating potential. Hence, in most cases, when the probes were not biased to measure ion saturation current (which was used to calculate $\delta n/n$), the probe signals were equal to the floating potential fluctuations.

The probe's resistance near the floating potential was determined from the Langmuir curves and was approximately 500Ω. Since the 8-inch RG-174 coaxial cables and the probes themselves had a combined capacitance of around 40 $\mu\mu$f, the RC time constant due to these elements of the system was roughly 2.0×10^{-8}sec. In addition, the common mode rejection circuits had output impedances of about 50Ω, and approximately 20 feet of RG-58/u cable with a capacitance of 30 $\mu\mu$f/ft connected the rejection circuits to the transient recorders. Thus, the RC time constant due to this longer coaxial cable was $\tau \simeq 3.0 \times 10^{-8}$sec. Therefore, the frequency response of the system was limited by the transient recorder's sampling time of 1.0 μsec, and not by the cable capacitance.

One probe was mounted in a Perkin-Elmer Ultek precision port aligner which allowed the probe to be positioned anywhere within a 20° cone. The second probe was mounted 4.3 cm directly below the port aligner. Thus, a simple tilt of the first probe could be used to vary the azimuthal distance between the probe tips. Both probes could be moved radially; and if the probe in the port aligner was moved radially

inward and tilted downward relative to the bottom probe, radial fluctuation characteristics of the plasma could be studied.

The probe signals were recorded on a 16-channel digital transient recorder with a 1.0 μsec analog-to-digital conversion rate. A 1024 word memory was available for each channel, which allowed 1.0 msec of data to be recorded for each plasma shot. Between shots the digital data were transferred to paper or magnetic tape for numerical processing on the IBM-370. A block diagram of the data acquisition units is shown in Figure 6.
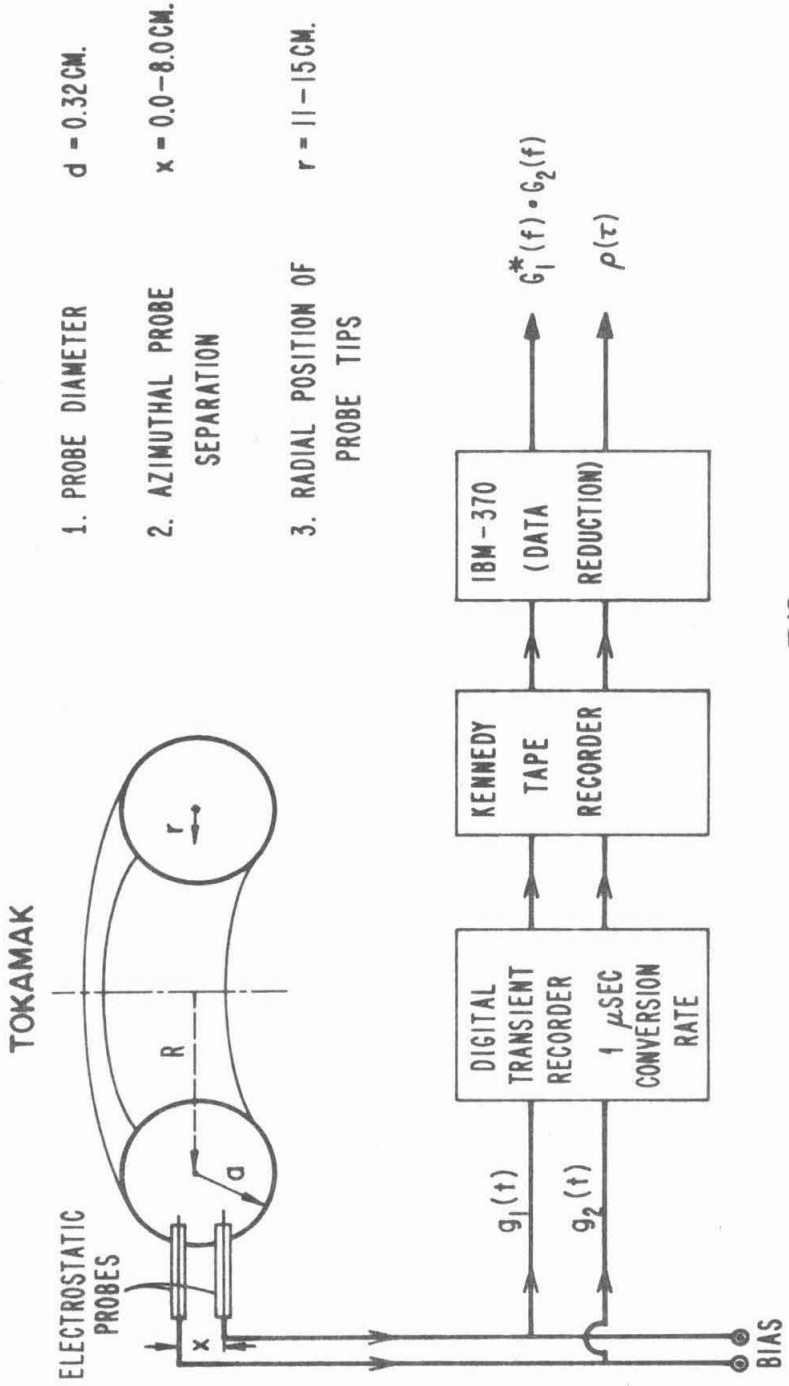
Figure 6. A block diagram of the data acquisition units

IV. PLASMA CHARACTERISTICS

In this chapter the general properties of the tokamak plasma will be described. As noted previously, by changing the ohmic heating electric field the plasma current could be varied. The minimum plasma current which could be obtained was about 6 kA, and the maximum current was approximately 18 kA. The one-turn voltage fell to zero 6 msec after the plasma was formed, and the length of the plasma pulse $\tau_d \simeq$ 10-12 msec. As the plasma current was increased, the conductivity and Langmuir probe temperatures were found to increase as shown in Figure 7. (In the conductivity temperature calculations the inductance of the plasma L was computed for a circular loop current with a parabolic current distribution.[29] L was assumed to be constant as a function of time; and thus, the one-turn voltage $V = RI_p + L \frac{dI_p}{dt}$, where R is the plasma resistance.) For a completely pure hydrogen discharge Z_{eff} = 1.0, but due to impurities, Z_{eff} usually lies between about 1.5 and 6.0 in most tokamaks.

From the 4 mm microwave interferometer it was found that the line averaged electron density rose to a peak value of about $1.0 \times 10^{13} cm^{-3}$ approximately 1.0 msec after the plasma was formed, and then dropped to $1.0 \times 10^{12} cm^{-3}$ 1.0 msec later. The density was then fairly constant for the remainder of the plasma lifetime. By taking Langmuir probe traces at several radial positions (see Fig. 8a), electron density, electron temperature, space potential and floating potential profiles were obtained for the outer half of the plasma. These results are shown in Figure 8b. By varying the time in the discharge t in which these traces were taken, the electron temperature and density variations during the plasma lifetime were ascertained.
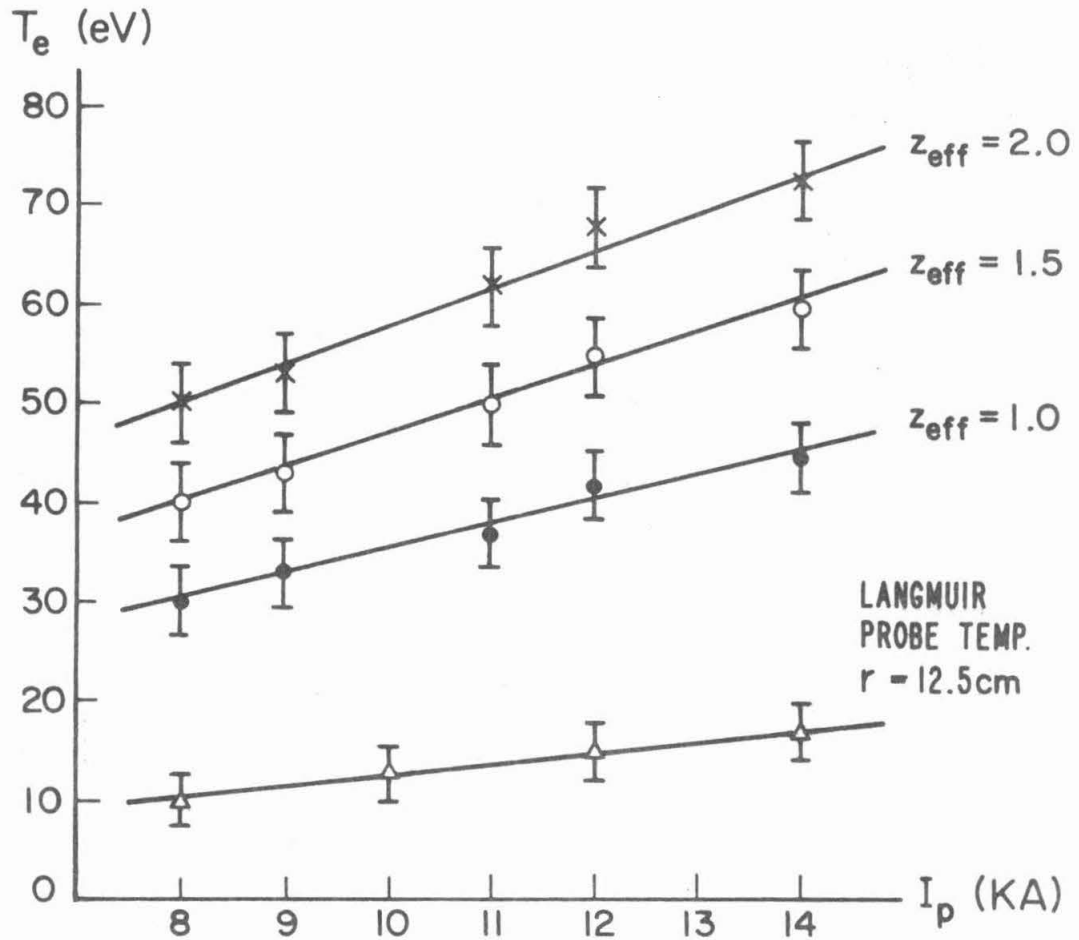
Figure 7. Variations of plasma temperature as a function of I_p, 2.0 msec into the discharge. Top three curves show the conductivity temperature using three values for Z_{eff}. Bottom curve is the electron temperature from a Langmuir probe at r = 12.5 cm. H_2 filling pressure = 1.05×10^{-4} Torr.
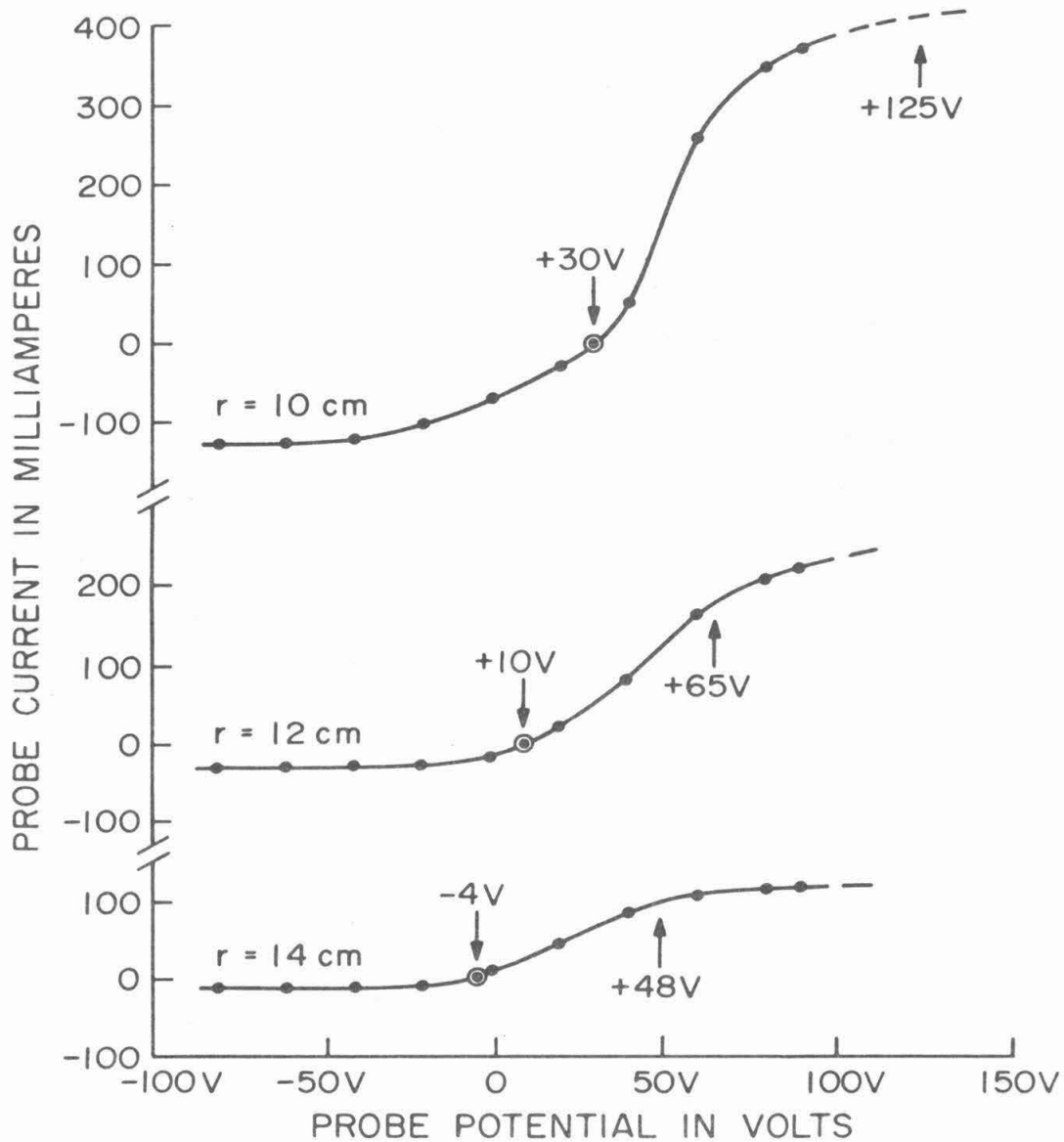
Figure 8a. Langmuir curves for three radial positions. Arrows represent floating potential and inferred space potential (see Appendix A).
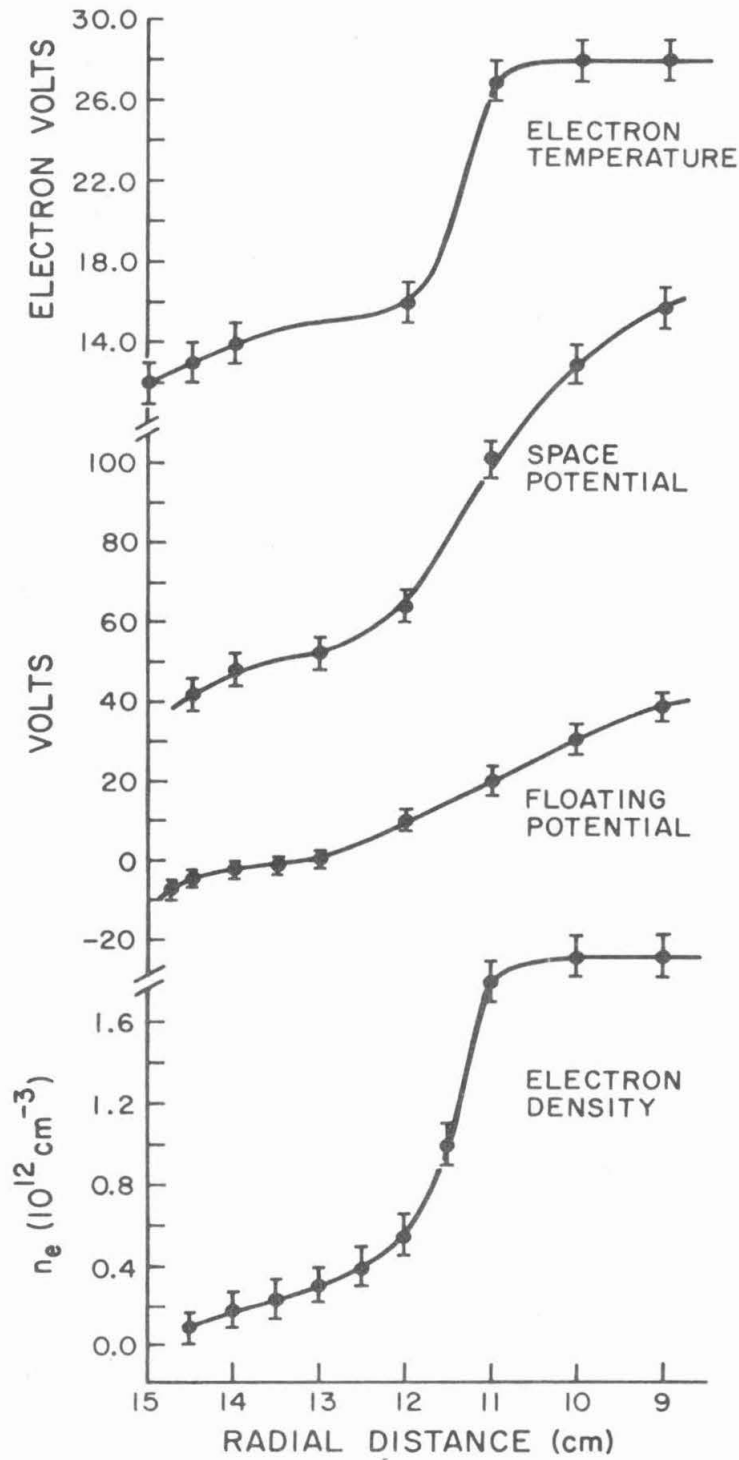
Figure 8b. Radial profiles of electron temperature, electron density, space potential, and floating potential at t (time in discharge) = 2.0 - 4.0 msec; I_p= 14 kA, B_t = 4.2 kG. H_2 filling pressure = 1.05 x 10^-4 Torr

The values calculated from probe measurements for the electron density were in good agreement with the results obtained from the microwave interferometer.

The time evolution of the plasma current, line averaged electron density, one-turn voltage, conductivity temperature, and Langmuir probe temperature at r = 12.5 cm are shown in Figure 9. Both the conductivity and the Langmuir probe temperatures reached a maximum about 4 msec after the formation of the plasma when the current reached its peak. From the floating potential and electron temperature profiles (see Appendix A) the radial electric field E_r between r = 11 and 13 cm was calculated. The $\vec{E} \times \vec{B}$ velocity was then determined and was found to be in the ion diamagnetic drift direction. The time evolution of the radial electric field is shown in Figure 10.

Finally, in order to compare experimental results with drift wave theory, a knowledge of the density and temperature gradients is necessary. In Figure 11 the density gradient 1/n dn/dr, as measured by a Langmuir probe, is plotted as a function of time during the plasma shot. As can be seen, the density gradient was fairly constant in the outer regions of the plasma during most of the discharge. The density and temperature gradient profiles are also shown in Figure 12. Since the Caltech tokamak did not have a limiter, the large gradients which were present at r ≃ 11.5 cm may be indicative of some form of magnetic confinement. If magnetic field errors near the walls contributed to particle loss, the observed radial profiles could be produced.
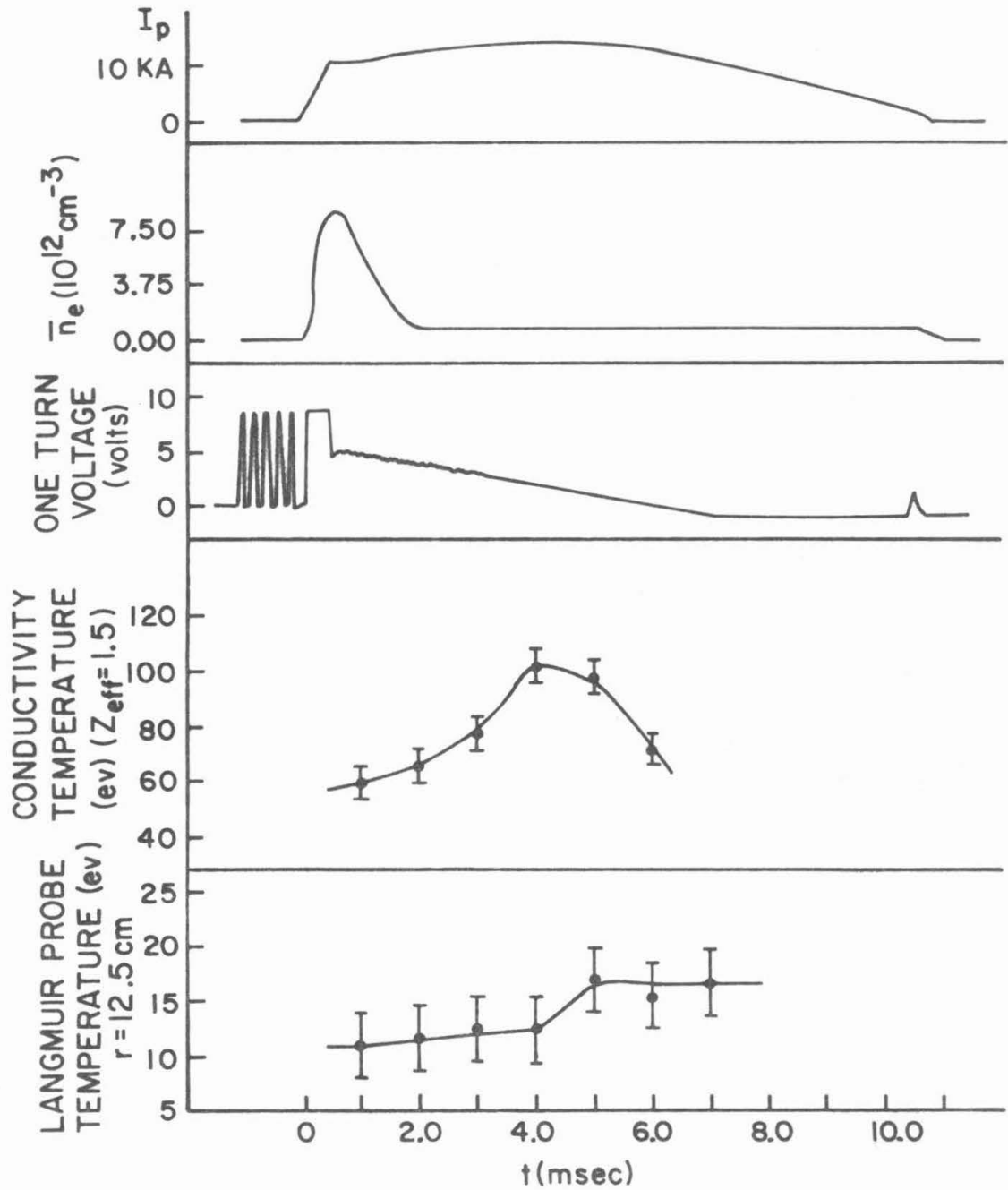
Figure 9. Time evolution of the line averaged electron density, one-turn voltage, conductivity temperature (assuming Z_{eff} = 1.5), and Langmuir probe temperature at r = 12.5 cm, H_2 filling pressure = 1.05 x 10^{-4} Torr.
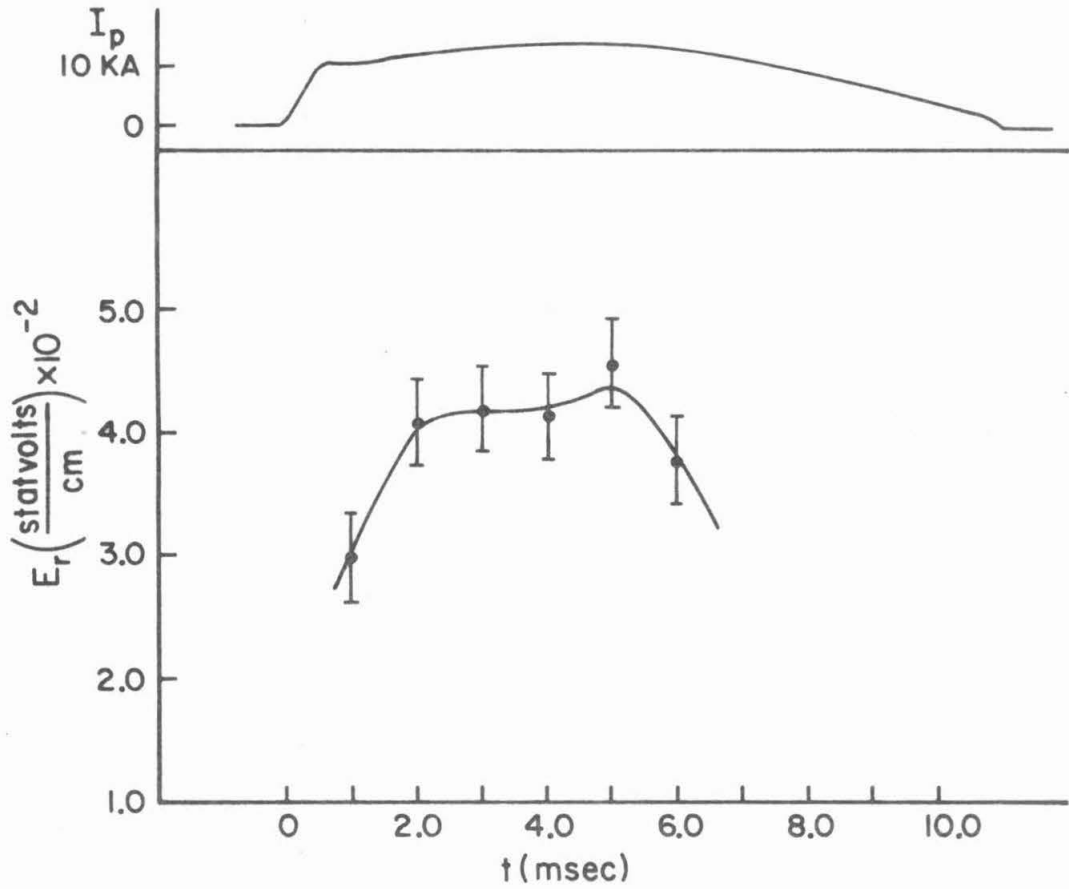
Figure 10. Time evolution of the radial electric field E_r for radial distances r = 11-13 cm; B_t = 4.2 kG, H_2 filling pressure = 1.05 x 10^{-4} Torr.
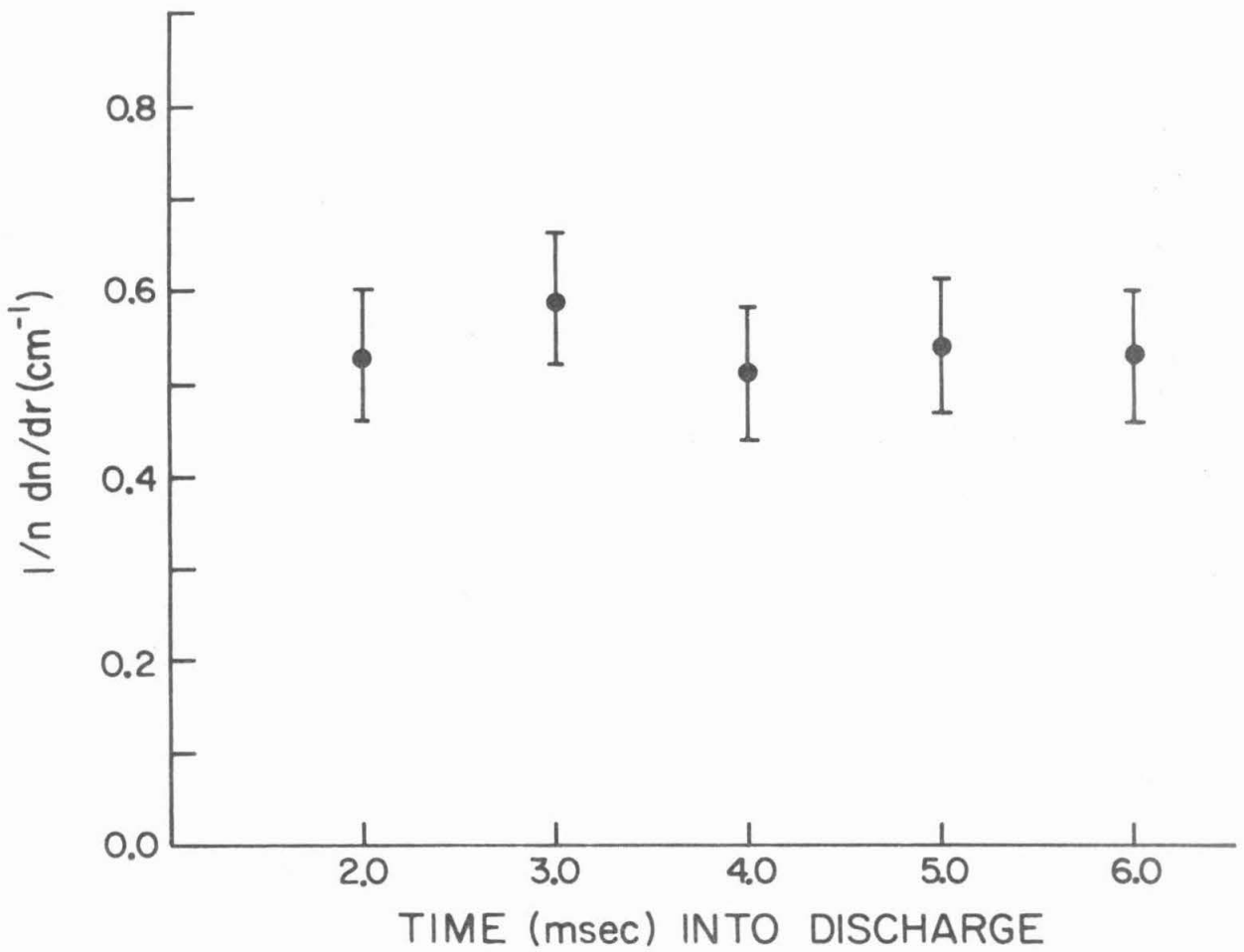
Figure 11. Time evolution during a discharge of the density gradient, $1/n \, dn/dr$, at $r = 12.5$ cm, $I_p = 14$ kA, $B_t = 4.2$ kG, H_2 filling pressure = 1.05×10^{-4} Torr.
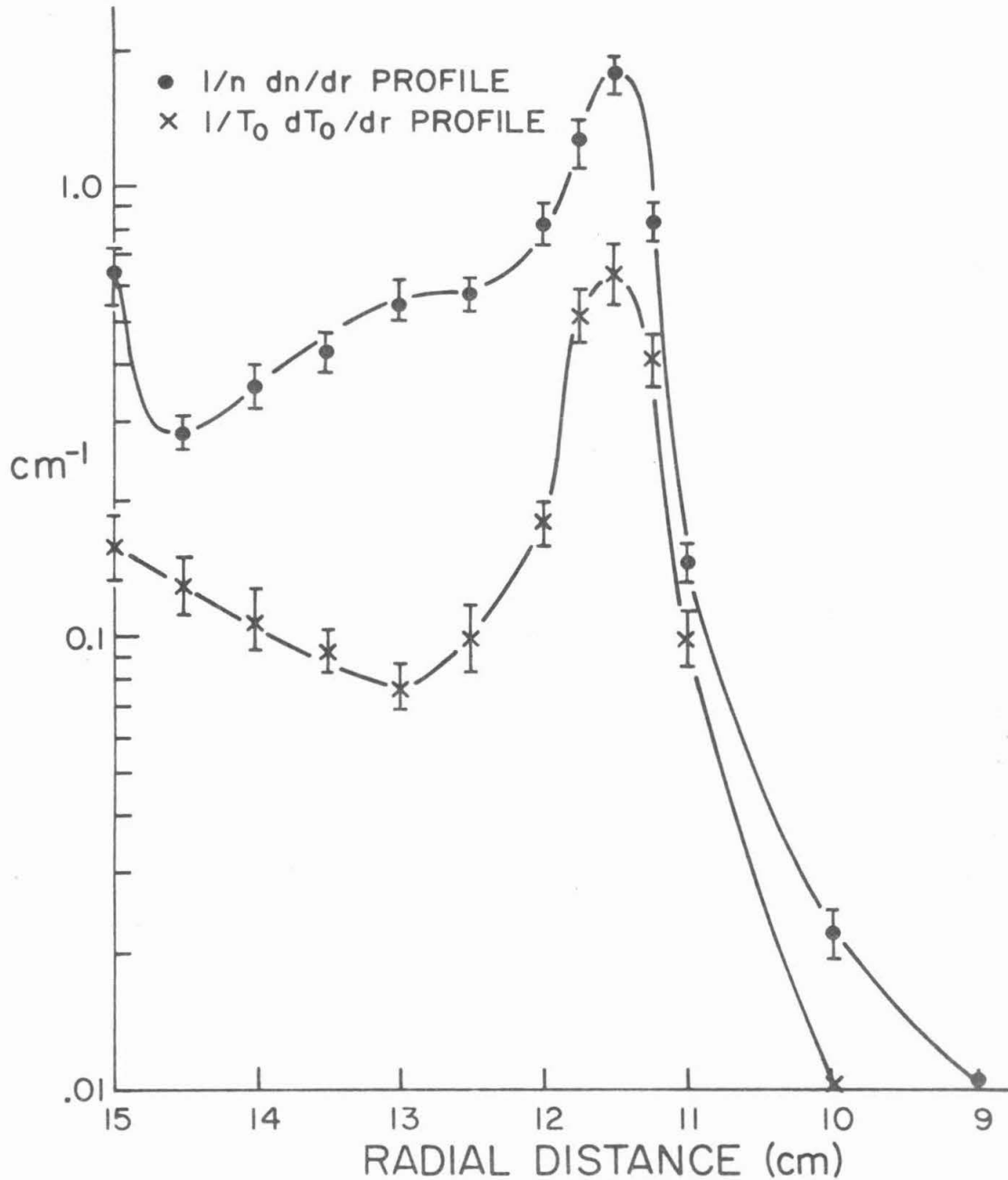
Figure 12. Electron density and temperature gradient profiles as measured by a Langmuir probe at t = 2.0-4.0 msec; I_p = 14 kA, B_t = 4.2 kG, H_2 filling pressure = 1.05 x 10^{-4} Torr. Unless otherwise stated, all subsequent results are for the same pressure.

V. COMPUTATIONAL TECHNIQUES

In order to study the fluctuations systematically, the spectra and correlation function were calculated from the digitized probe signals on the IBM-370. In this chapter a description is given of the analytical techniques used for these computations.

Let the two probe signals be denoted by $f_1(t)$ and $f_2(t)$, each of which is known at 2N equispaced points. (In the present experiment 2N = 1024 and data were taken at equispaced time intervals T = 1.0 μsec.) If the values of $f_1(t)$ are denoted by $X_{1,\nu} = x_1(\nu T)$ where $\nu = 0,1,2,\cdots$, 2N-1, then the Fourier series of $X_{1,\nu}$ is[31]

$$X_{1,\nu} = \frac{a_1(0)}{2} + \sum_{k=1}^{N-1} \left(a_1(k) \cos \frac{\pi \nu k}{N} + b_1(k) \sin \frac{\pi \nu k}{N} \right) + \frac{a_1(N)}{2} (-1)^\nu,$$

(5.1)

with

$$F_1(k) \equiv a_1(k) + ib_1(k) = 1/NT \int_0^{2NT} x_1(t)\, e^{-i\pi kt/NT}\, dt ,$$

$$k = 0,1,\cdots,N .$$

(5.2)

Similarly, $F_2(k)$ is defined as

$$F_2(k) \equiv a_2(k) + ib_2(k) = 1/NT \int_0^{2NT} x_2(t)\, e^{-i\pi kt/NT}\, dt ,$$

$$k = 0,1,\cdots,N .$$

(5.3)

The amplitude of the Fourier spectrum of each probe signal is therefore,

$$AMP[F_1(k)] = [a_1^2(k) + b_1^2(k)]^{1/2} , \qquad (5.4)$$

$$AMP[F_2(k)] = [a_2^2(k) + b_2^2(k)]^{1/2} , \qquad (5.5)$$

and the phase angle between the two series is

$$\theta(k) = ATAN[\frac{b_1(k)}{a_1(k)}] - ATAN[\frac{b_2(k)}{a_2(k)}] \quad , \quad k = 0,1,\cdots,N \quad . \quad (5.6)$$

Unfortunately, the computer calculates the arctan for angles between π and $-\pi$, and therefore θ can lie between 2π and -2π. Since the phase angle has meaning only in a 2π interval, points which lie outside the range $[-\pi,\pi]$ can be transformed so as to lie in this interval by adding or subtracting 2π. However, if one wishes to average adjacent data points over a small frequency interval when the points lie close to $\pm\pi$, points which originally had absolute magnitudes slightly larger than π will be averaged incorrectly with points of absolute magnitude slightly smaller than π. This problem can, however, be circumvented by averaging in the complex plane rather than averaging the phase angle alone. To implement this procedure, the cross power spectral density function was explicitly computed.

Letting the Fourier series of each probe signal be denoted as ($k = 0,1,2,\cdots512$ in all the following expressions),

$$F_1(k) = A_1(k) e^{i\theta_1(k)} \quad , \quad (5.7)$$

$$F_2(k) = A_2(k) e^{i\theta_2(k)} \quad , \quad (5.8)$$

where $A_1(k)$ and $A_2(k)$ are real variables; the cross power spectral density function[32] is defined as

$$P_{12}(k) = F_1^*(k) F_2(k) = A_1^*(k) A_2(k) e^{i(\theta_2(k) - \theta_1(k))} \equiv A(k) + iB(k).$$

$$(5.9)$$

But

$$F_1^*(k) \; F_2(k) = [a_1(k) - ib_1(k)][a_2(k) + ib_2(k)]$$

$$= a_1(k) \; a_2(k) + ia_1(k) \; b_2(k) - ib_1(k) \; a_2(k) + b_1(k) \; b_2(k)$$

$$\equiv A(k) + iB(k) \tag{5.10}$$

Hence,

$$A(k) = a_1(k) \; a_2(k) + b_1(k) \; b_2(k) \quad , \tag{5.11}$$

$$B(k) = a_1(k) \; b_2(k) - b_1(k) \; a_2(k) \quad . \tag{5.12}$$

However, since the amplitude and phase of the cross power spectral density function were not smooth functions of k, the running averaged amplitude and phase were computed for a range of k' using the following expressions:

$$AMPLITUDE(k') \;\; = \;\; (\overline{A}(k')^2 + \overline{B}(k')^2)^{1/2} \quad , \tag{5.13}$$

$$PHASE(k') \;\; = \;\; ATAN(\overline{B}(k')/\overline{A}(k')) \quad , \tag{5.14}$$

where $\overline{A}(k')$ and $\overline{B}(k')$ represent, respectively, the averages of $A(k)$ and $B(k)$ over the points $k'-i$, $k'-i+1$, $\cdots$, k', $\cdots k'+i-1$, $k'+i$, where i is an integer, $k' \geq i$, and $k'+i \leq 512$. Both step and Gaussian weighting functions were used to calculate $\overline{A}(k)$ and $\overline{B}(k)$ from a set of $A(k)$'s and $B(k)$'s. Thus, for example,

$$\overline{A}(k') = \frac{\omega(-i)A(k'-i) + \omega(-i+1)A(k'-i+1) + \cdots \omega(+i) \; A(k'+i)}{NF} \; , \tag{5.15}$$

where ω is a weighting function, and

$$NF = \sum_{I=-i}^{+i} \omega(I) \quad . \tag{5.16}$$

In the case of a Gaussian weight, both the number of points included in the average and the width of the Gaussian can be selected.

One can also compute the cross correlation function or convolution $\rho(\tau)$ of $f_1(t)$ and $f_2(t)$. For arbitrary real functions of t, g(t) and k(t), the cross correlation function is defined as

$$\rho(\tau) = \int_{-\infty}^{+\infty} g(t)\, k(t+\tau)\, dt \quad . \tag{5.17}$$

However, from the convolution theorem,[32] $\int_{-\infty}^{+\infty} g(t)\, k(t+\tau)\, dt$ has the Fourier transform $G^*(f)\, K(f)$, where

$$G(f) = \int_{-\infty}^{+\infty} g(t)\, e^{i2\pi ft}\, dt \quad , \tag{5.18}$$

and

$$K(f) = \int_{-\infty}^{+\infty} k(t)\, e^{i2\pi ft}\, dt \quad . \tag{5.19}$$

Thus, one would expect that the phase velocities of the fluctuations computed from the correlation function would agree with those computed from the cross power spectral density function. This was experimentally verified.

The algorithm used to numerically compute the normalized correlation function from the two probe signals, each defined at 1024 data points, was

$$\rho_1(IA) = \frac{\frac{1}{1025-IA}\sum_{m=1}^{1025-IA} \underline{x}_1[(m-1)T]\,\underline{x}_2[((m-2)+IA)T]}{\frac{1}{1024}[(\sum_{m=1}^{1024} \underline{x}_1^2[(m-1)T])(\sum_{m=1}^{1024} \underline{x}_2^2[m-1)T])]^{1/2}} \quad , \tag{5.20}$$

and

$$\rho_2(IA) = \frac{\frac{1}{1025-IA}\sum_{m=1}^{1025-IA} \underline{x}_2[(m-1)T]\underline{x}_1[((m-2)+IA)T]}{\frac{1}{1024}[(\sum_{m=1}^{1024} \underline{x}_1^2[(m-1)T])(\sum_{m=1}^{1024} \underline{x}_2^2[(m-1)T])]^{1/2}} \quad , IA = 1,2,\cdots 1024 \tag{5.21}$$

where

$$\underline{x}_1(mT) = x_1(mT) - \overline{x}_1 \quad , \tag{5.22}$$

and

$$\underline{x}_2(mT) = x_2(mT) - \overline{x}_2 \quad , \quad m = 0,1,2,\cdots,1023. \tag{5.23}$$

$\overline{x}_1$ and $\overline{x}_2$ are the averages of $x_1(mT)$ and $x_2(mT)$ over the range $m = 0,1,2,\cdots,1023$, respectively.

The averages were subtracted from x_1 and x_2, since their digital values ranged from 0 to 255 and hence were not symmetrical around zero. $\rho_1(IA)$ is the correlation function when $\underline{x}_2$ is evaluated at progressively later times relative to $\underline{x}_1$ in the product defining ρ; and conversely, $\rho_2(IA)$ defines the correlation function when $\underline{x}_1$ is evaluated at progressively later times relative to $\underline{x}_2$.

It should be noted that Gaussian averaging the cross power spectral density function in the frequency domain is equivalent to multiplying the cross correlation function by a Gaussian in the time domain. To show this, consider the Gaussian averaged cross spectral density function $F'(\omega)$,

$$F'(\omega) = \int_{-\infty}^{+\infty} F(\omega') \, G(\omega - \omega') \, d\omega' \quad , \tag{5.24}$$

where $F(\omega') = F_1^*(\omega') \, F_2(\omega')$ and $G(\omega)$ is a Gaussian weighting function. Then by the convolution theorem, the Fourier transform of $F'(\omega)$ is

$$\mathcal{F}(F'(\omega)) \equiv f'(t) = \frac{1}{\sqrt{2\pi}} G'(t) \int_{-\infty}^{+\infty} F_1^*(\omega') \, F_2(\omega') e^{-i\omega' t} \, d\omega' \quad , \tag{5.25}$$

and $G'(t)$ is another Gaussian function. Therefore,

$$f'(t) = G'(t) \int\limits_{-\infty}^{+\infty} f_1(\tau) \ f_2(t+\tau) \ d\tau \quad , \tag{5.26}$$

so

$$f'(t) = G'(t) \ \rho(t) \quad . \tag{5.27}$$

Finally, by normalizing the amplitude of the cross power spectral density function by the auto-power spectra

$$P_{11}(k) = F_1^*(k) \ F_1(k) \quad , \tag{5.28}$$

and

$$P_{22}(k) = F_2^*(k) \ F_2(k) \quad , \tag{5.29}$$

one obtains the "coherence spectrum"[33]

$$\gamma_{12}(k) = \frac{| \ F_1^*(k) \ F_2(k)|}{[F_1^*(k) \ F_1(k)]^{1/2} \ [F_2^*(k) \ F_2(k)]^{1/2}} \quad . \tag{5.30}$$

$\gamma_{12}(k)$ is a measure of the degree of cross-correlation between $f_1(t)$ and $f_2(t)$ at each frequency. If $\gamma_{12}(k)$ is zero at a particular frequency, then $f_1(t)$ and $f_2(t)$ are "incoherent", whereas if $\gamma_{12}(k) = 1$, $f_1(t)$ and $f_2(t)$ are "coherent" at that frequency.

The plasma characteristics which were studied by the use of the preceding analysis will be described in the following two chapters.

VI. EXPERIMENTAL RESULTS FOR FIXED MACHINE PARAMETERS

6.1 The Spectra and Phase Relations

Data were recorded for 1.0 msec intervals during a plasma shot on two channels of a digital transient recorder. Typical probe signals are shown in Figure 13. The Fourier series of these probe signals was computed, and a spectrum as seen in Figure 14 was obtained. The spectrum extends to roughly 250 kHz and resembles the results obtained from microwave and CO_2 laser scattering experiments on ATC.[27,28] In these latter experiments, the wavelengths of the fluctuations which could be resolved were limited by the scattering angle to roughly 0.1-2.0 cm. Drift instabilities were thought to be the cause of the oscillations in ATC.

However, when the running averaged amplitude and phase of the cross spectral density function, as defined in equations (5.13) and (5.14), were computed, the spectra became more structured. The amplitude exhibited distinct peaks at certain frequencies, and the phase difference between the probes displayed a linear functional dependence on the frequency. Again, using the same plasma shot as in Figure 14, the running averaged amplitude and phase of the cross spectral density function are shown in Figure 15 when eleven adjacent A(k)'s and B(k)'s were averaged with equal weight in the calculations for $\overline{A}$ and $\overline{B}$. A similar spectrum was observed for the poloidal magnetic field fluctuations using magnetic loop probes.[34] The linear dependence of the phase on frequency for a fixed azimuthal probe separation implies that the azimuthal fluctuations propagated with a single average phase velocity.
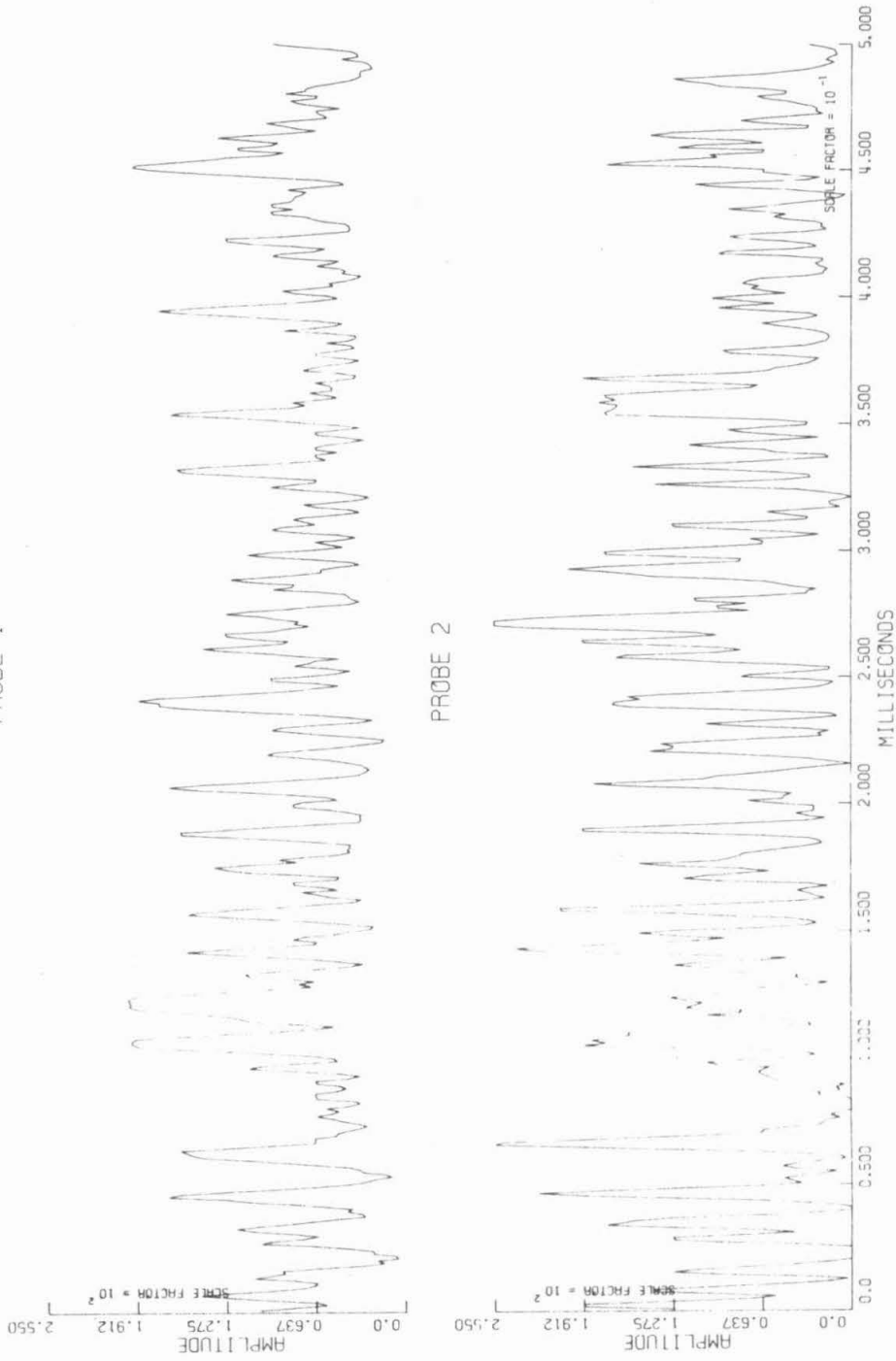
Figure 13. Typical probe signals for t = 2.0 - 2.5 msec, r = 12.5 cm, azimuthal probe separation, x = 2.0 cm, I_p = 12 kA, B_t = 4.2 kG.
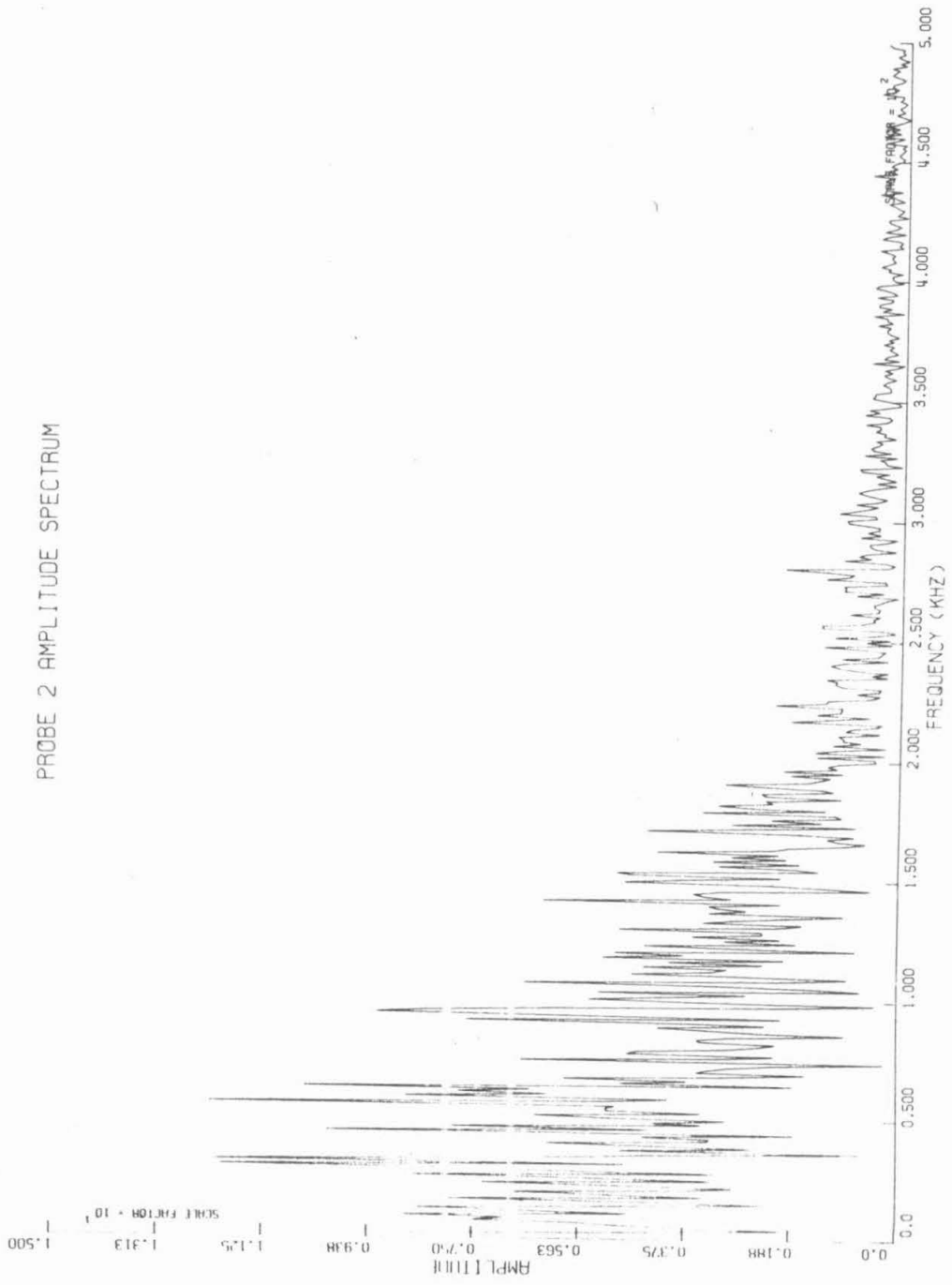
Figure 14. The Fourier series of the signal from the second probe as shown in Figure 13.
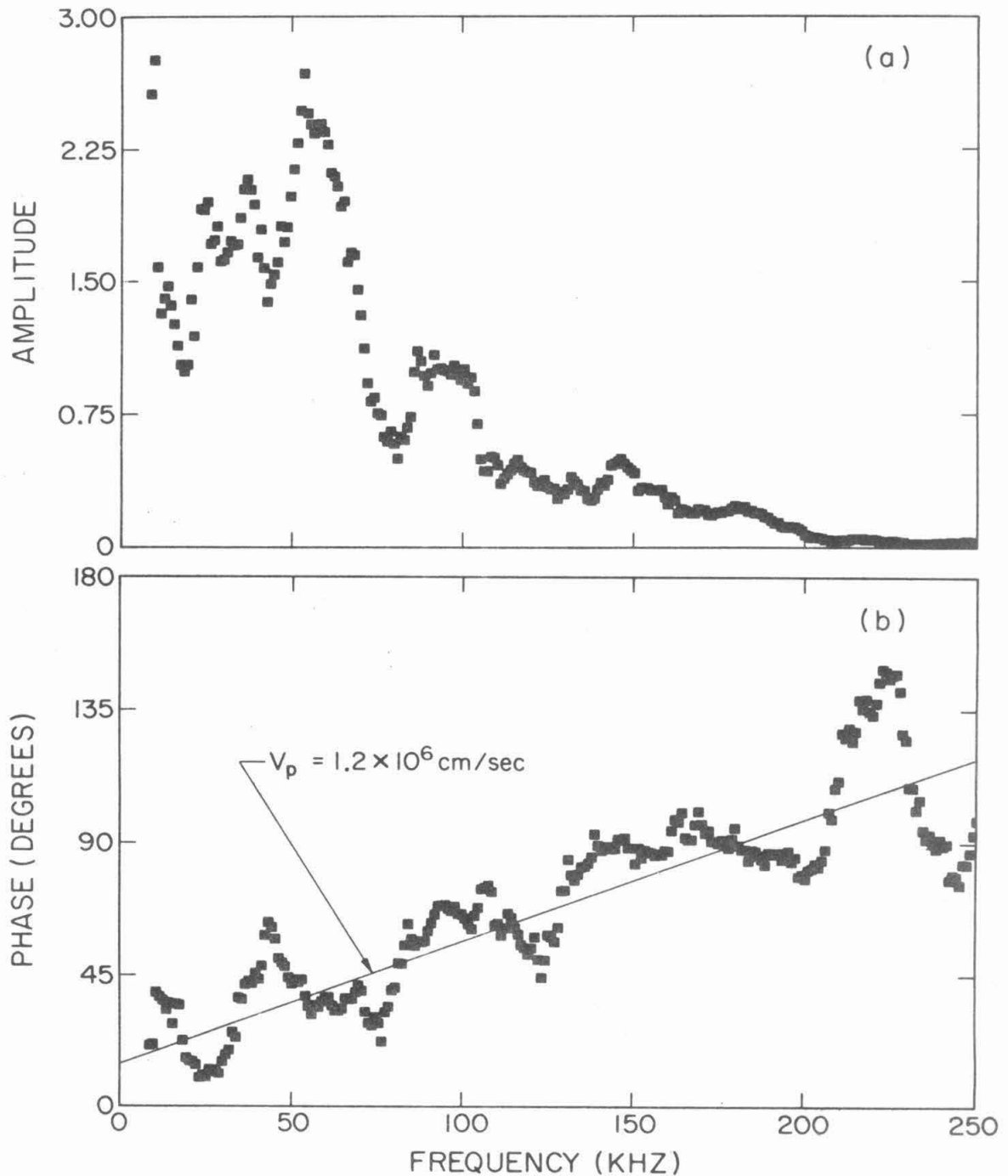
Figure 15. The running averaged amplitude (a) and phase (b) of the cross spectral density function for the signals seen in Figure 13. A least squares fit line is drawn through the phase points and from the slope of the line $V_p = 1.2 \times 10^6$ cm/sec was calculated.

In Figures 16a,b,c a series of spectra is shown for the same plasma shot in which $\overline{A}$ and $\overline{B}$ were calculated using (a) 20 equally weighted A(k)'s and B(k)'s, (b) 21 Gaussian weighted A(k)'s and B(k)'s with the Gaussian weighting function falling to e^{-1} at the end points $(G(10) = G(-10) = e^{-1})$, and (c) 21 Gaussian weighted A(k)'s and B(k)'s with the Gaussian weighting function falling to e^{-2} at the end points $(G(10) = G(-10) = e^{-2})$. It can be seen that the effect of Gaussian averaging is to smooth, but not to drastically alter, the main features of the amplitude spectrum.

If any type of perturbation with a poloidal dependence $e^{i(m\theta-\omega t)}$ were present in the plasma, then one would expect to observe peaks in the spectra at frequencies $f = mV_p/2\pi r$; where V_p is the azimuthal phase velocity of the fluctuations, m is the azimuthal mode number, and r is the radial distance from the center of the plasma. From the plot of the phase difference between the probe signals versus frequency, the average azimuthal phase velocity can be computed, and since r is known, the expected azimuthal mode frequencies can be calculated. The results of these calculations and the amplitude of the cross power spectral density function for two different plasma shots are shown in Figure 17. The frequencies of the observed peaks and certain calculated mode frequencies can be seen to correspond. This agreement was observed for all plasma shots recorded in which the probes were separated in the azimuthal direction (roughly four hundred shots) and was not affected by the type of spectral averaging performed. Thus, the observed peaks seemed to be related to specific azimuthal modes of the plasma.
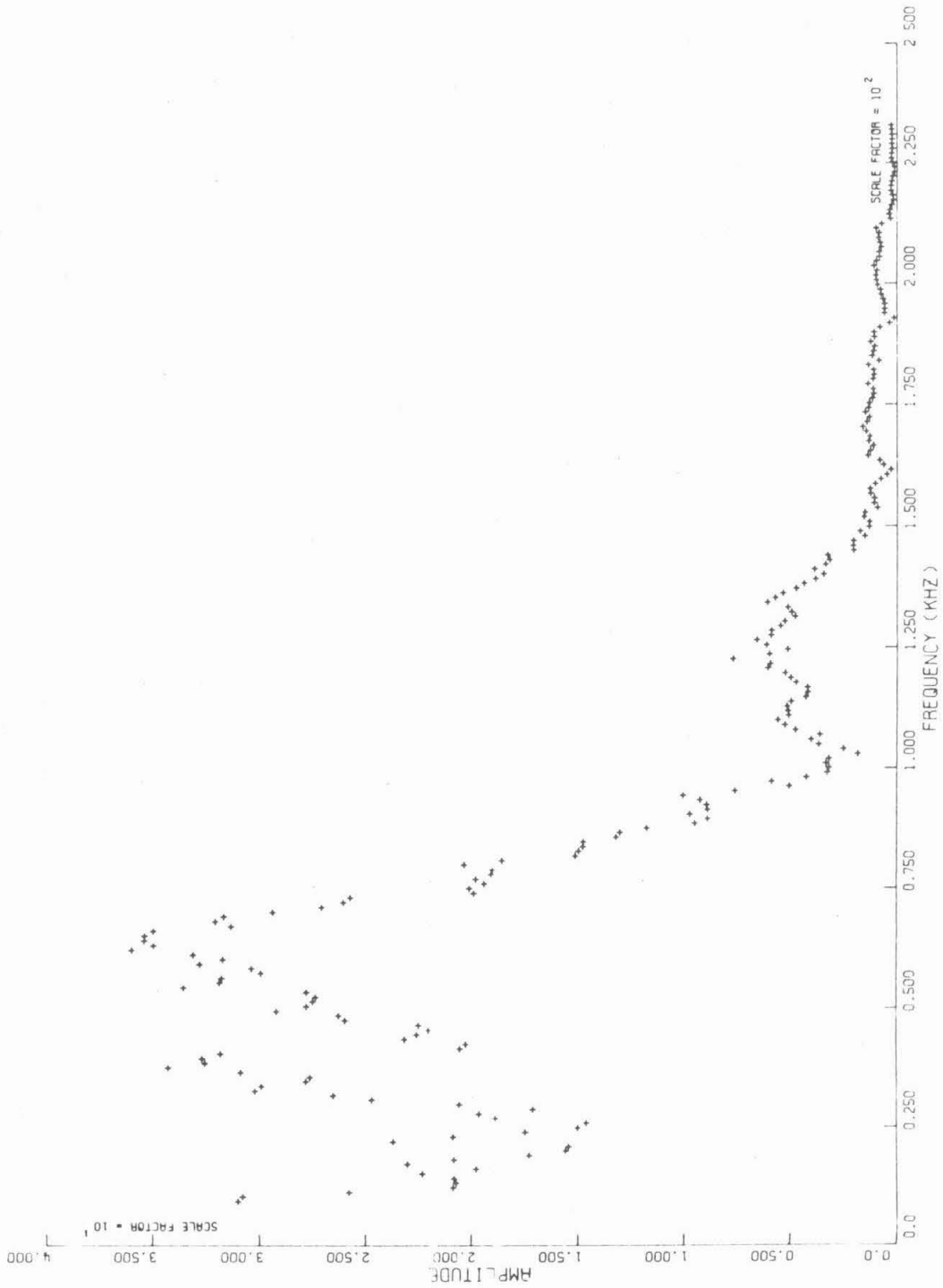
Figure 16a. The running averaged amplitude of the cross spectral density function when 20 adjacent A(k)'s and B(k)'s were averaged with equal weight.
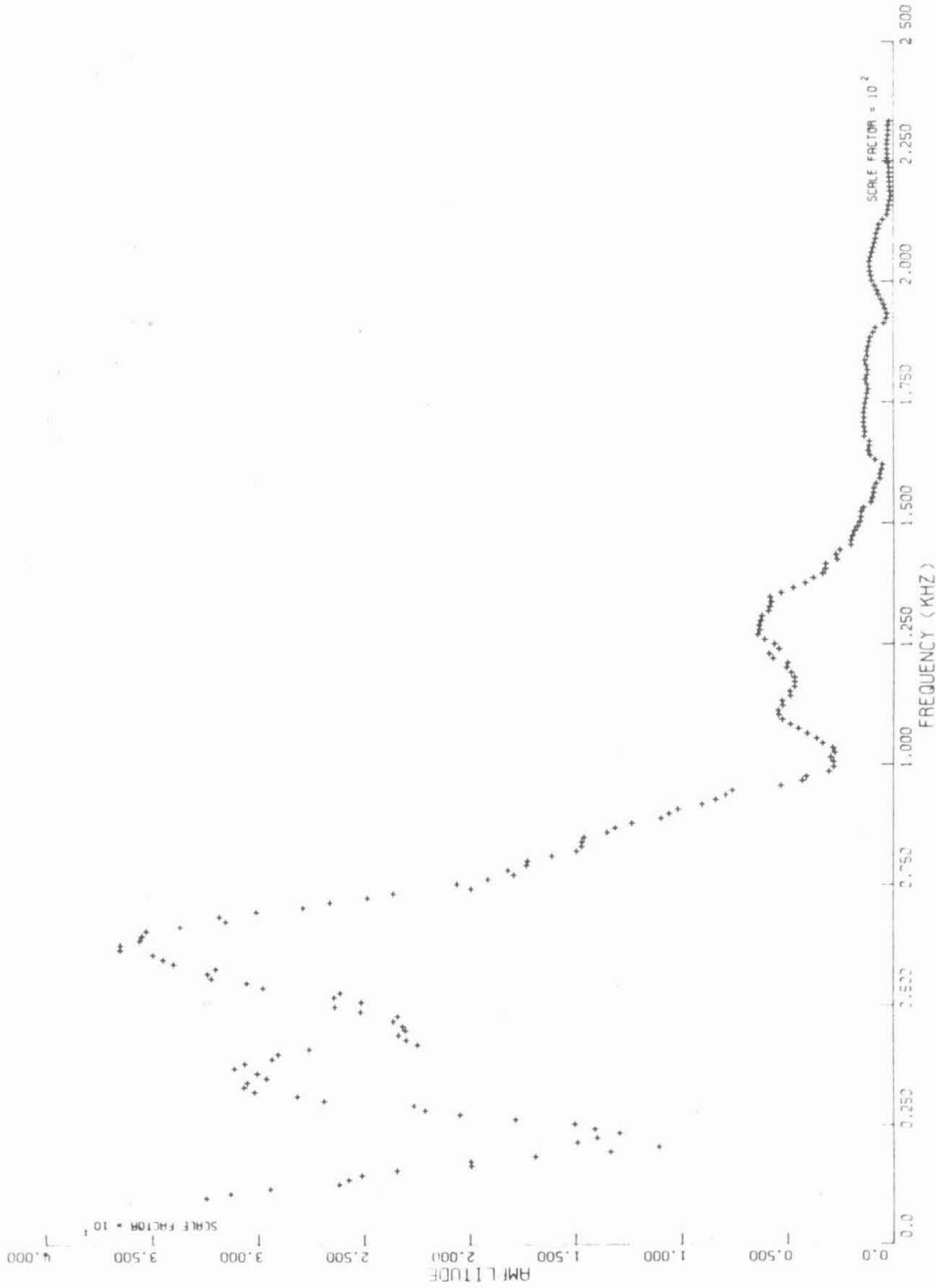
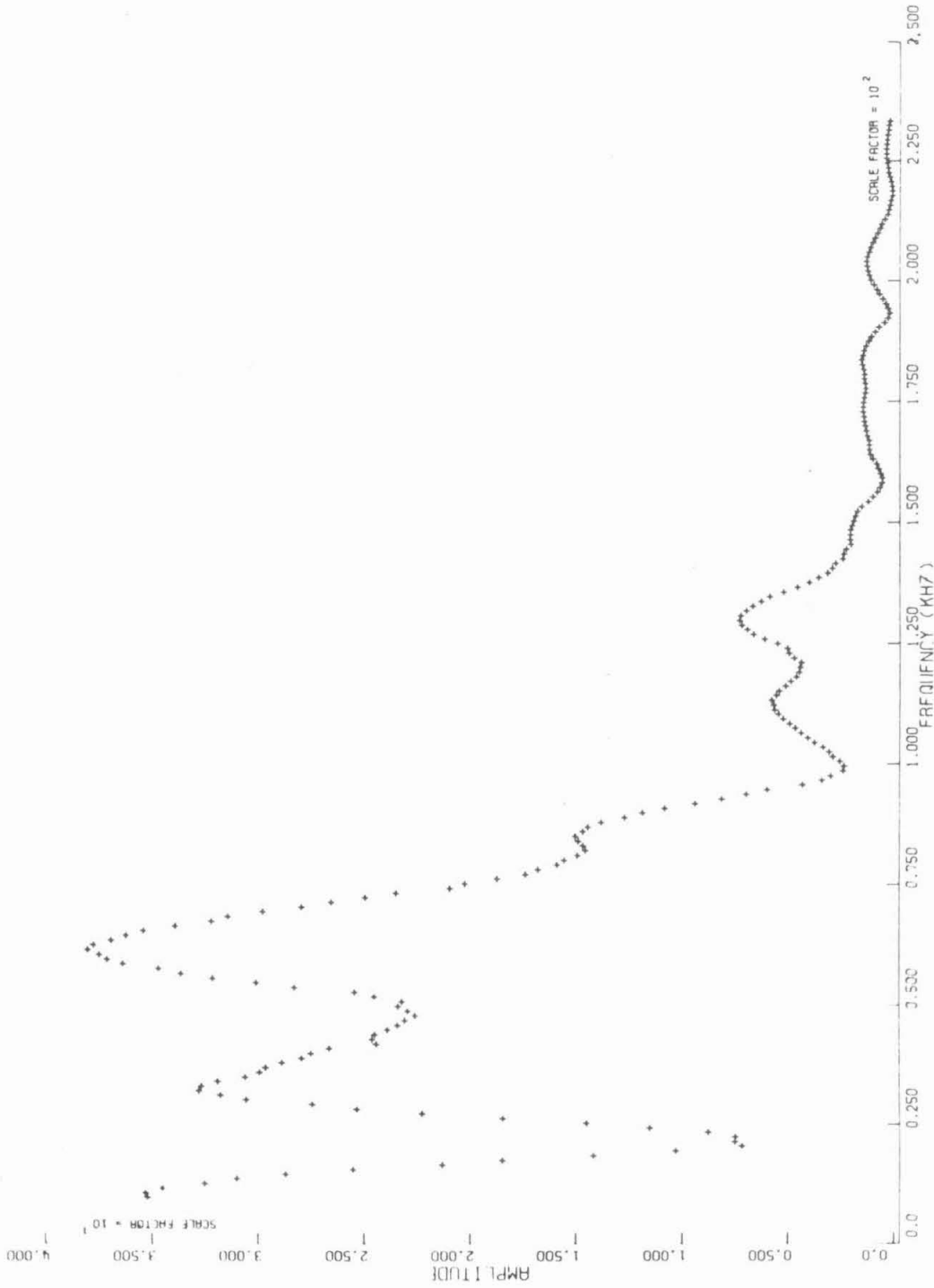Figure 16b. The running averaged amplitude of the cross spectral density function when 21 adjacent A(k)'s and B(k)'s were Gaussian averaged with G(10) = e⁻¹.

Figure 16c. The running averaged amplitude of the cross spectral density function when 21 adjacent A(k)'s and B(k)'s were Gaussian averaged with G(10) = e⁻².
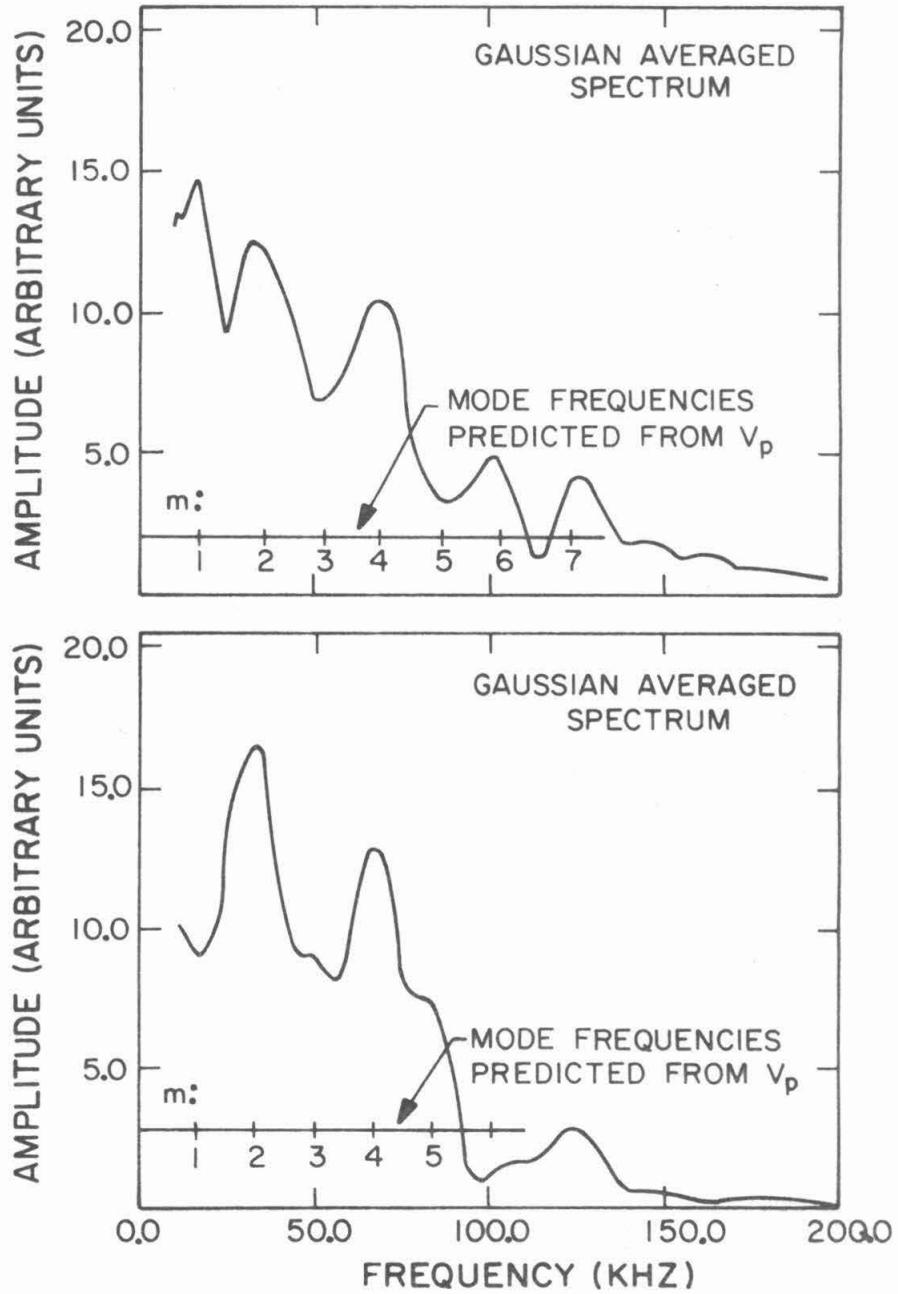
Figure 17. The Gaussian averaged amplitude spectrum for two different plasma shots showing the correspondence between peak frequencies and expected mode frequencies from V_p.

The amplitude and coherence spectra for a typical plasma shot are shown in Figures 18a,b. The coherence at the amplitude peaks was roughly 0.75, and this value indicates that the two probe signals were fairly coherent at the frequencies corresponding to amplitude maxima. Moreover, it is well known that coherence values are affected by the amount of averaging performed,[35] and slightly larger values (around 0.80 - 0.85 at amplitude peaks) were obtained if fewer points were used in the Gaussian averaging process. However, since the spectrum becomes somewhat "noisier" as fewer points are averaged, the amount of averaging used in Figure 18 was found to be appropriate for the study of the fluctuation spectra.

6.2 Correlation Function

By varying the azimuthal spacing between the probes, the azimuthal correlation length of the fluctuations was determined. The normalized correlation function for several azimuthal probe separations, x, is shown in Figure 19. The correlation dropped to roughly 0.25 for a probe separation of 4.0 cm, and the shift of the peak relative to the zero time delay point indicated that the azimuthal phase velocity was in the ion diamagnetic drift direction. The magnitude of the phase velocity determined from the correlation function $(V_p \simeq 1.1 \times 10^6 \text{cm/sec})$ was in good agreement with that obtained from the phase, see Figure 15, of the cross power spectral density function, as expected, based on the convolution theorem. Since the correlation length was short compared with the circumference of the plasma at the probe tips, some dispersion in the phase velocities of the different azimuthal modes may have existed.
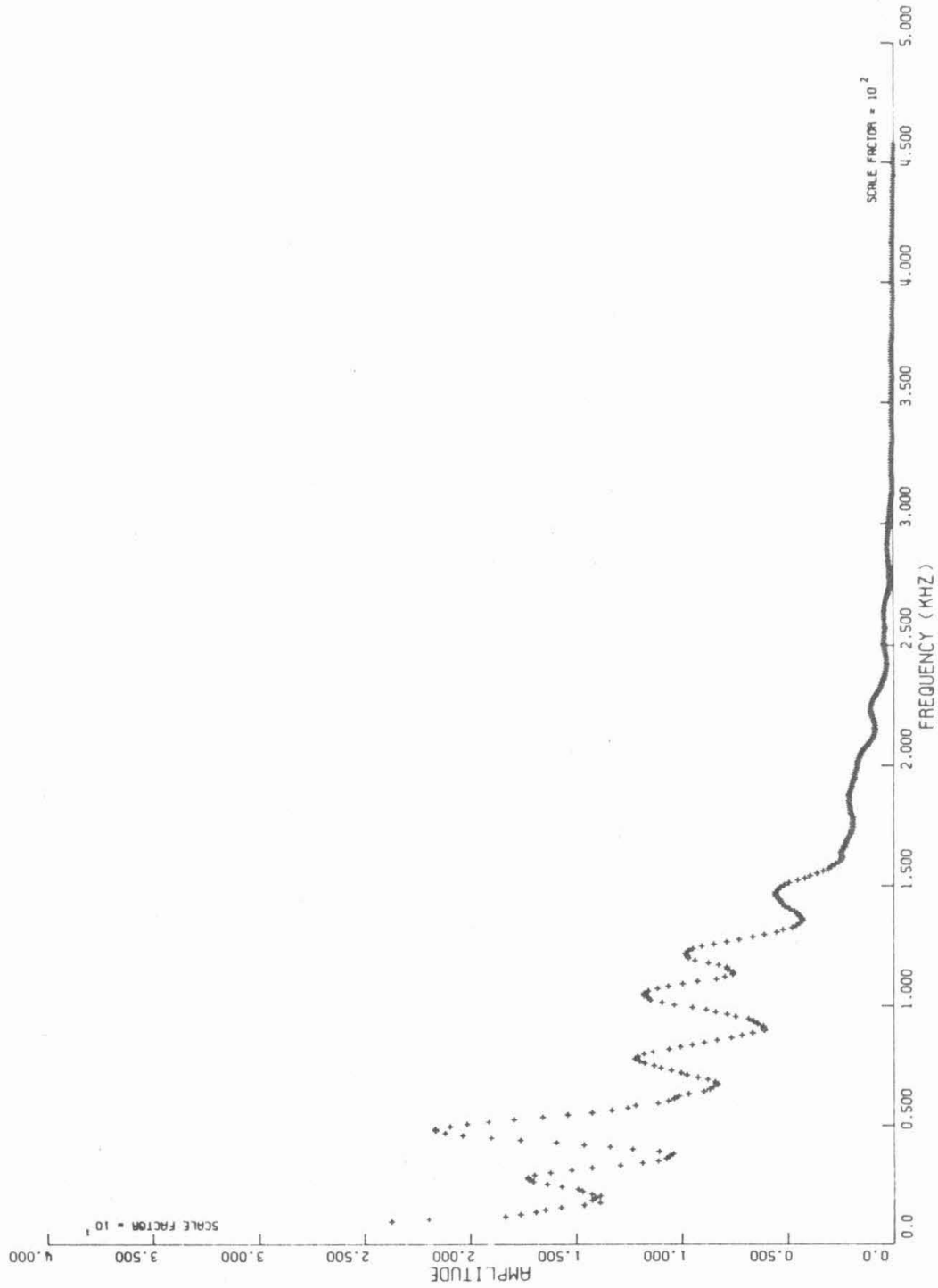
Figure 18a. A typical amplitude spectrum for which the coherence spectrum in Figure 18b was calculated. The running averaged spectrum was calculated using 21 Gaussian weighted $A(k)$'s and $B(k)$'s with $G(10) = e^{-2}$.
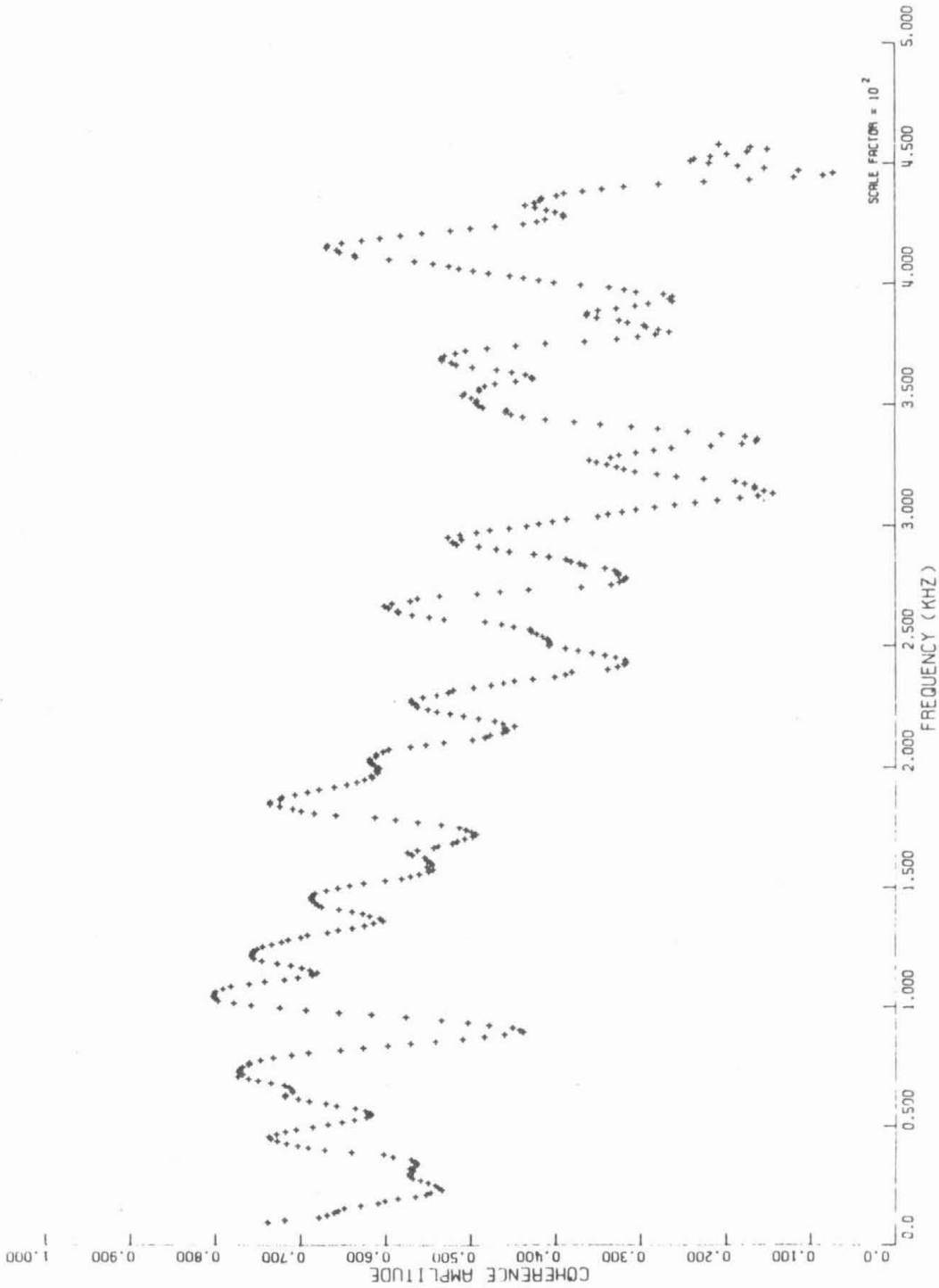
Figure 18b. The coherence spectrum for the same plasma shot as in Figure 18a, x (azimuthal probe separation) = 3.0 cm.
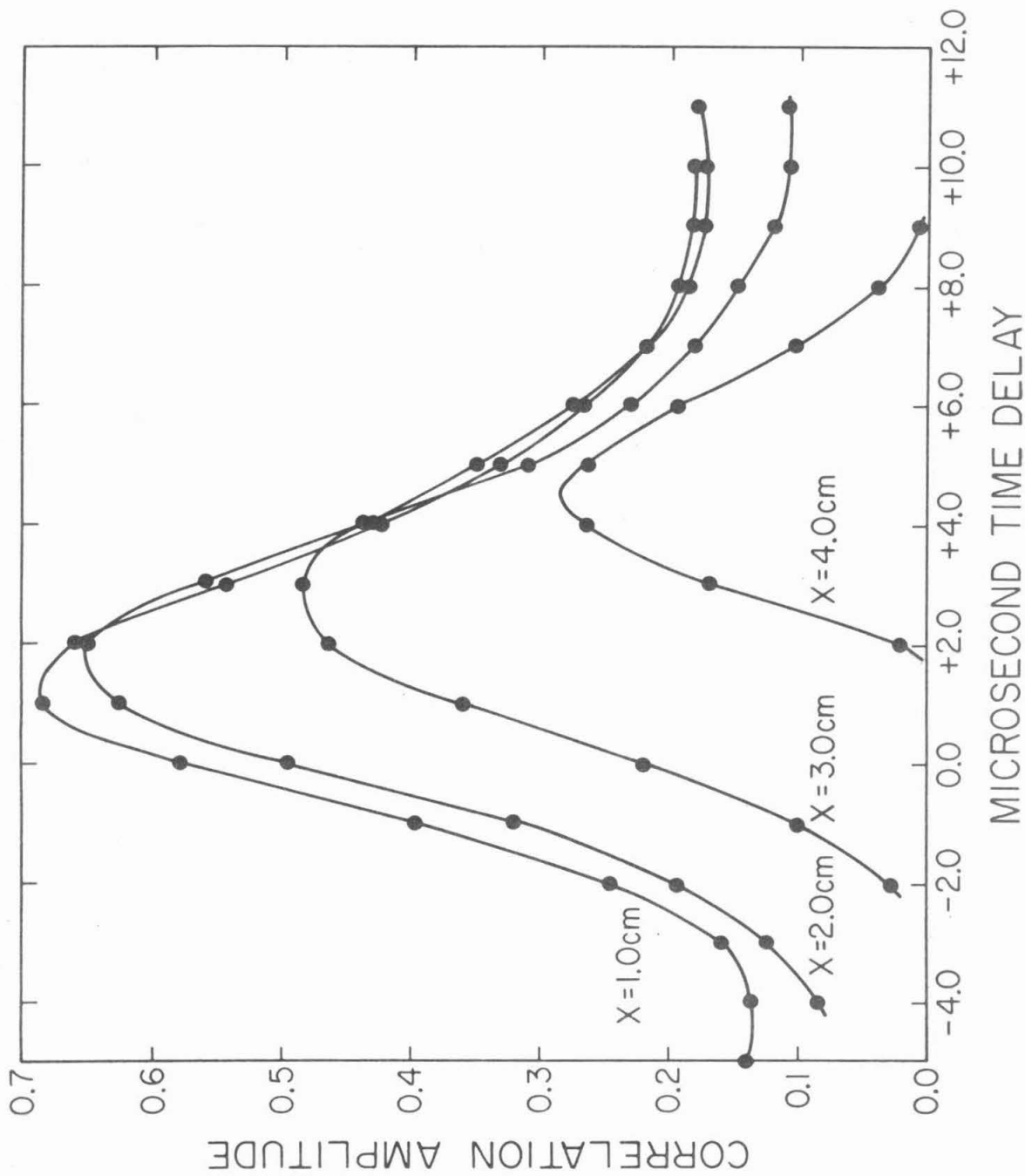
Figure 19. The normalized azimuthal correlation function for several azimuthal probe separations, x. I_p = 12 kA, B_t = 4.2 kG, r = 12.5 cm, t = 2.0-3.0 msec. Data averaged over 5 plasma shots.

The probes were also positioned so that the tips were separated radially, and the correlation function was again determined. In Figure 20 the normalized correlation function is shown for various radial probe separations in which the outer probe was kept at a fixed radius, r = 13.8 cm. The rate of decrease of the radial correlation was larger than that of the azimuthal correlation as the probes were moved apart; however, at probe separations of roughly 4.0 cm both the radial and azimuthal correlation was 0.25.

From the shift of the correlation peaks relative to the zero time delay point, the radial phase velocity was found to be directed outward-- toward the vacuum liner. The magnitude of the radial phase velocity varied considerably as machine parameters were changed, and the results will be discussed in Chapter VII. The outer probe radius was also decreased while keeping the inner probe tip at $r \simeq 11.0$ cm. The phase velocities calculated in this manner agreed with the results obtained by keeping the outer probe fixed. Thus, for the outer regions of the plasma, the radial phase velocity was not found to be a function of the radius.

The precision port aligner allowed one probe to be twisted relative to the other so that the vector connecting the two probe tips could have a large axial component. A little geometry then allowed the phase velocity in the axial direction to be calculated once the azimuthal phase velocity was measured. The axial phase velocity was found to be in the direction of electron current flow with a magnitude ($V_p \simeq 1.4 \times 10^6$ cm/sec) of the order of the azimuthal phase velocity for a variety of machine parameters (plasma current, toroidal magnetic field, and time in the discharge were
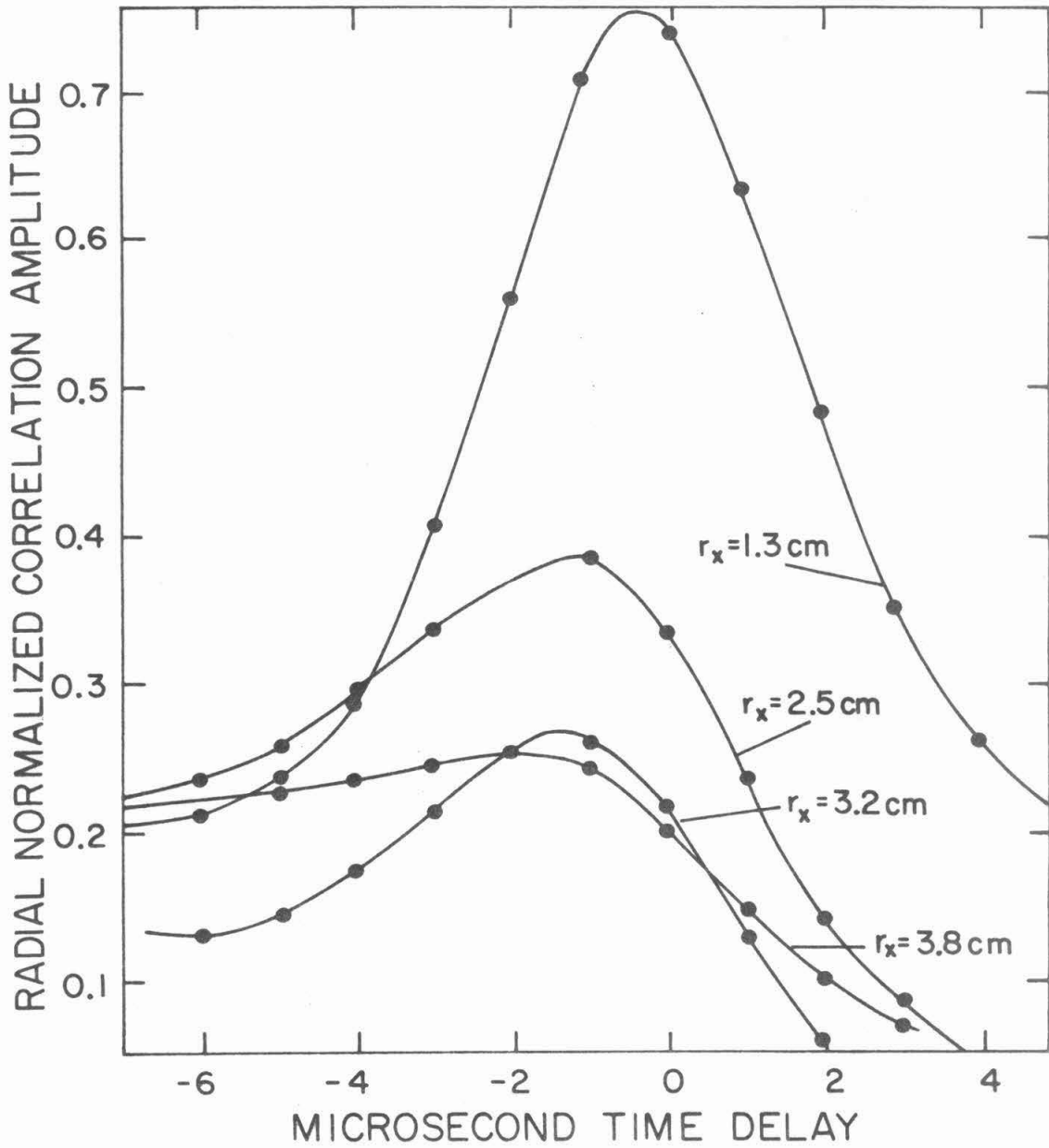
Figure 20. The normalized radial correlation function for several radial probe separations, r_x. The outer probe was kept at a fixed radius r = 13.8 cm. I_p = 12 kA, B_t = 4.2 kG, t = 2.0 - 3.0 msec. Data averaged over five plasma shots.

varied.) For a current driven collisional drift wave of the type dis-
cussed by Ellis and Motley,[14] theory predicts that the axial phase
velocity should be in the direction of electron flow with $\omega/k_z \gg \omega/k_y$.

6.3 Temporal and Radial Dependences of the Fluctuation Characteristics

As discussed previously, the plasma duration was approximately
twelve milliseconds, and the line averaged electron density rose to a
peak value of roughly $1.0 \times 10^{13} \text{cm}^{-3}$ 1 msec after the plasma was formed,
and fell to $2.0 \times 10^{12} \text{cm}^{-3}$ 1 msec later. Most of the data in this thesis
were taken after the density had become approximately constant and while
the plasma current was near its maximum. However, during the high density
phase of the plasma shot, strong sawtooth type oscillations at frequencies
between 8 and 13 kHz were observed on both probe signals.

The sawtooth oscillations had amplitudes which were typically five
times larger than the higher frequency fluctuations which were predominant
at later times in the discharge and propagated azimuthally in the electron
diamagnetic drift direction. Typical sawtooth signals, their spectrum,
and their correlation function are shown in Figures 21a,b,c. The correla-
tion length for the sawtooth oscillations was a few centimeters longer
than for the higher frequency fluctuations; and the axial phase velocity
of the sawtooth signals was in the direction of electron flow with a
magnitude of the order of their azimuthal velocity. Between 1.5 and 2.0
milliseconds after the plasma was formed, when the two types of signals
had approximately the same amplitudes, the correlation function developed
two distinct peaks on each side of the zero time delay point. Thus, a
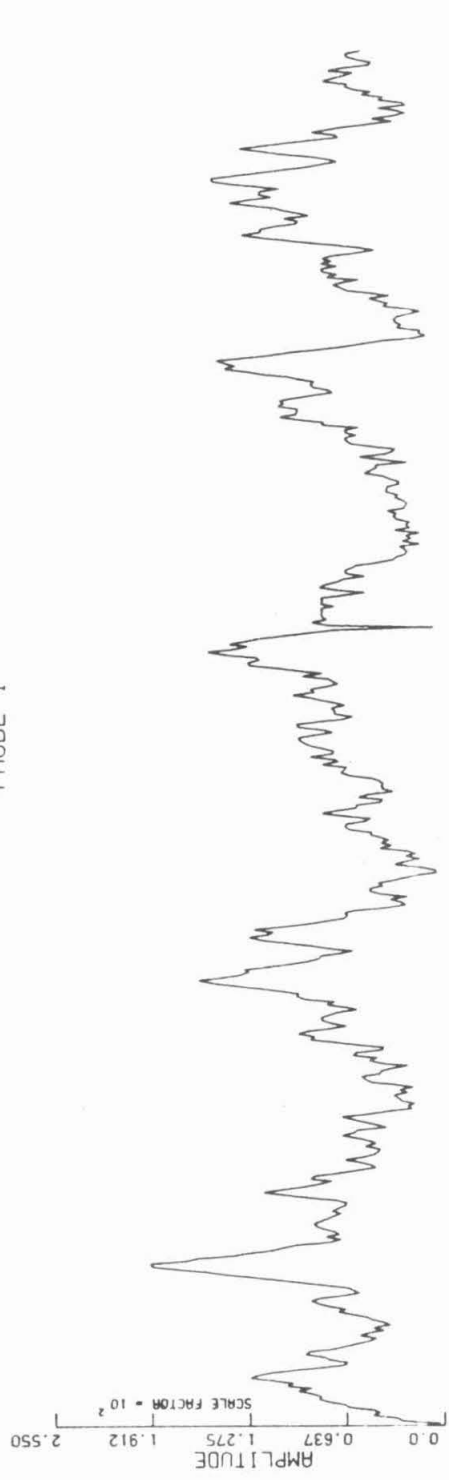
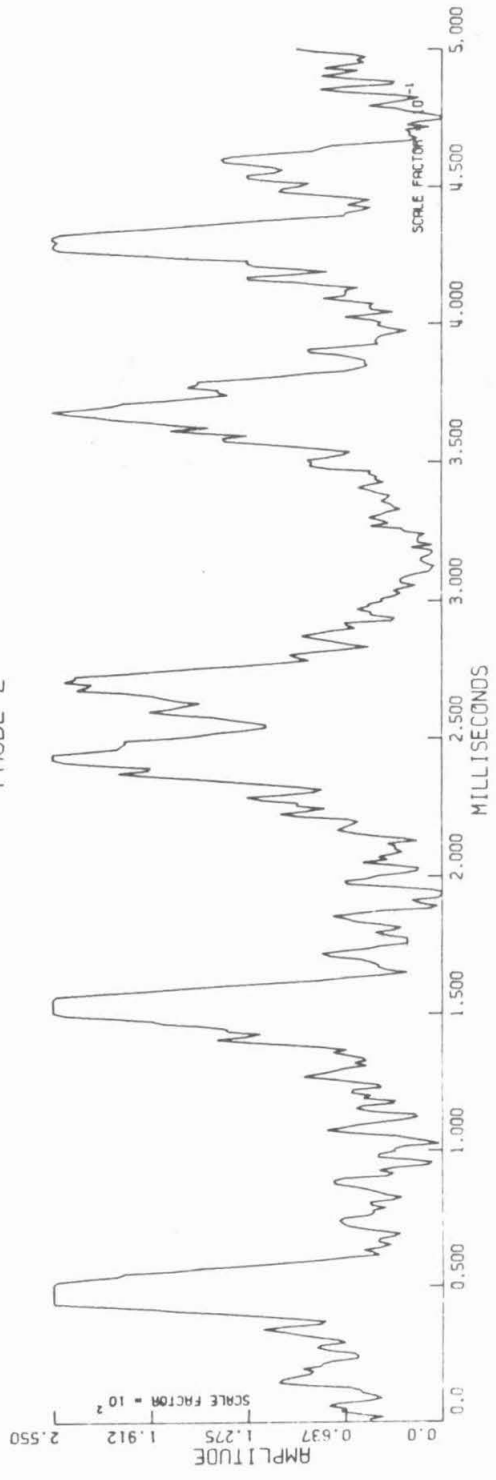Figure 21a. Typical sawtooth type signals seen during the first two milliseconds of the plasma lifetime when the electron density was at its maximum ($n_e \simeq 8.0 \times 10^{12}$ cm^{-3}). $x = 3.0$ cm, $r = 12.5$ cm, and $B_t = 4.2$ kG.
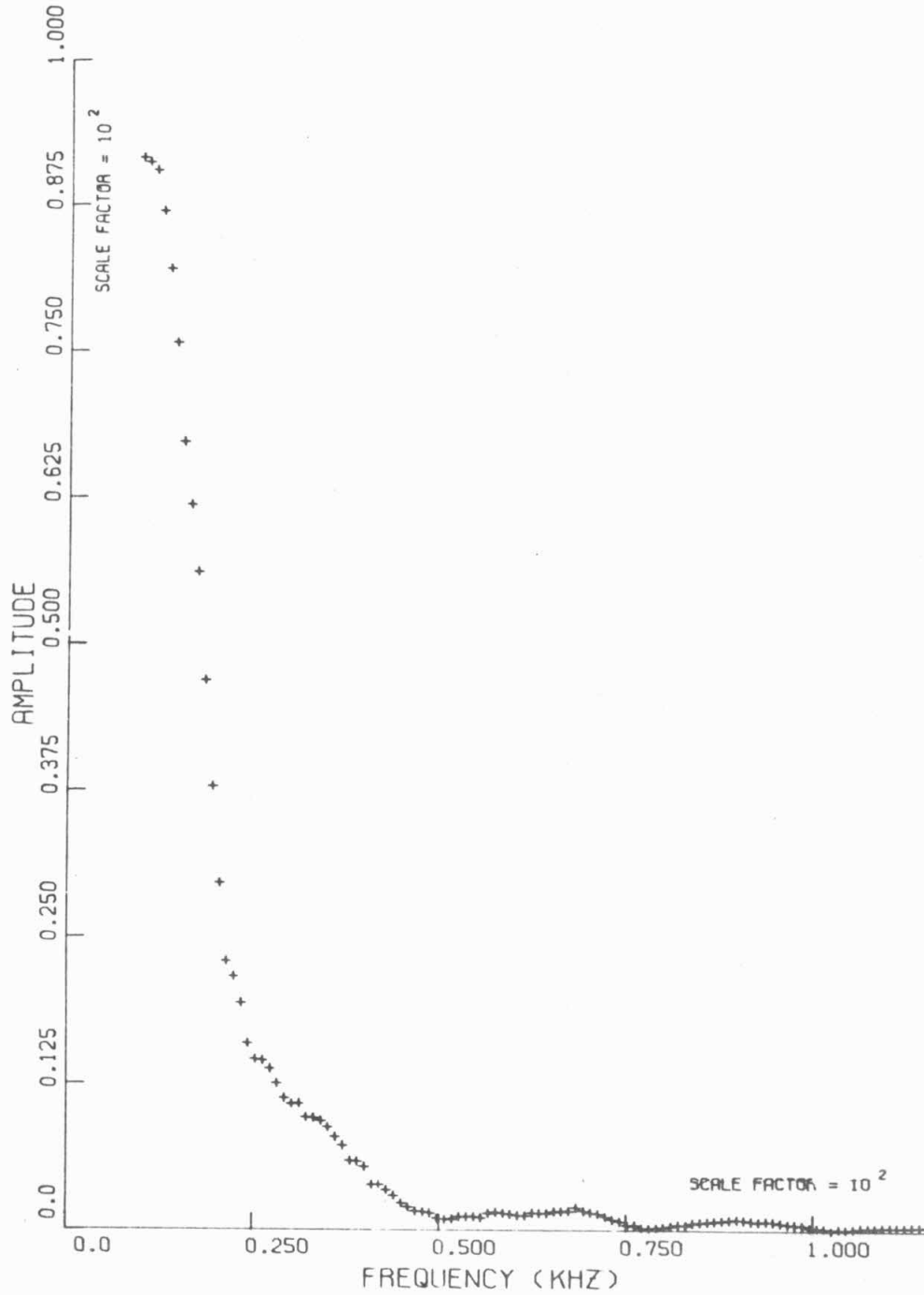
Figure 21b. The Gaussian averaged amplitude spectrum of the sawtooth signals seen in Figure 21a.
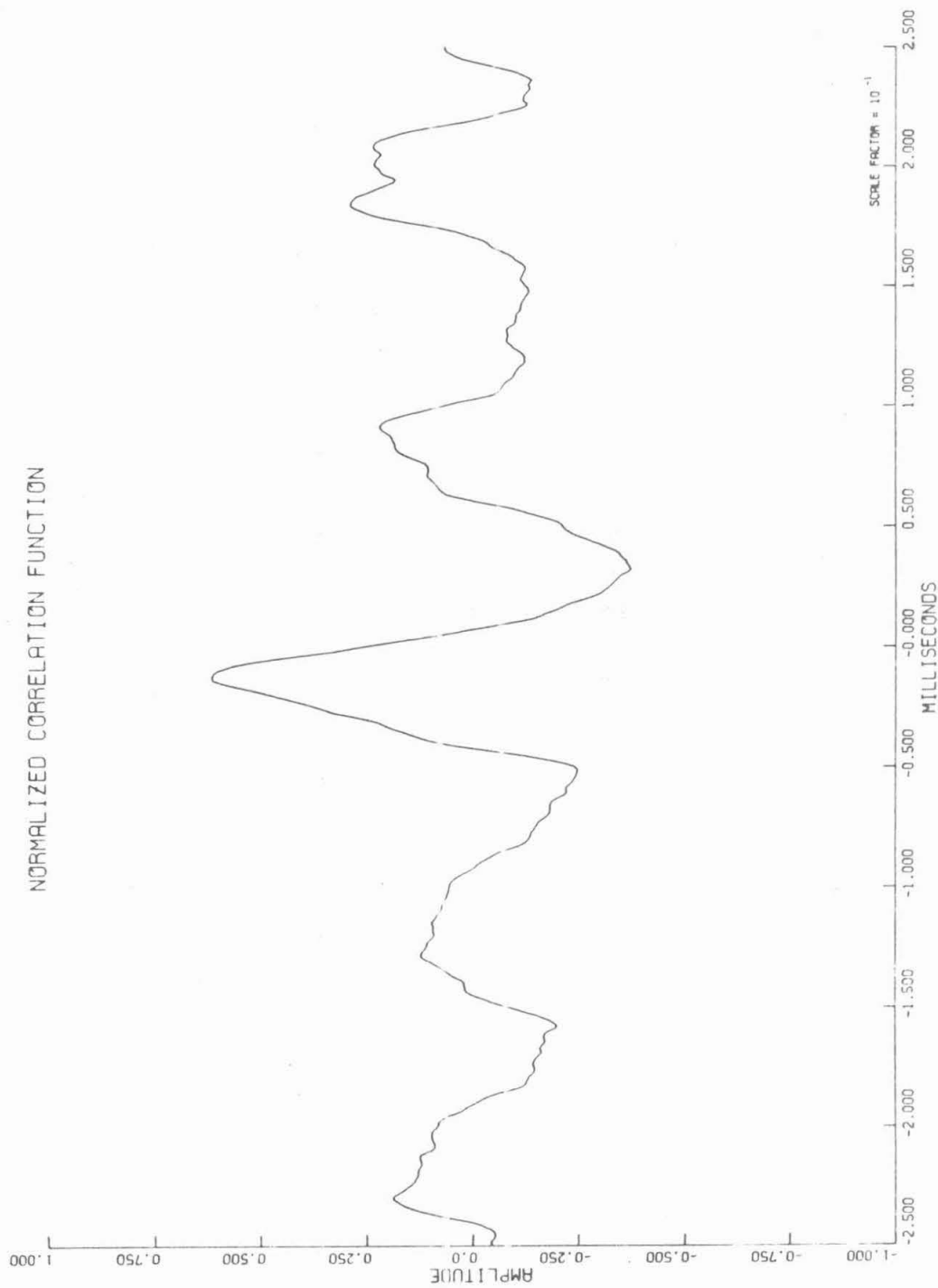
Figure 21c. The normalized correlation function of the sawtooth signals seen in Figure 21a.

"transition period" existed for roughly 0.5 millisecond during which neither type of signal was dominant.

The complete time evolution of the azimuthal modes is summarized in Figure 22. The top two traces show the plasma current and electron density. The third section describes the time evolution of the azimuthal mode numbers m as observed from the spectra. The average azimuthal mode number <m> was calculated by multiplying the amplitude of each major peak in the cross power spectral density function by its corresponding mode number, adding the products, and then dividing by the sum of the amplitudes. Although the value of <m> does not represent the most predominant mode in the plasma at the probe positions, the variations in <m> provided a means of studying the effects on the overall mode structure at the probe locations when plasma conditions varied. The fourth section contains a plot of the average azimuthal phase velocity, $\overline{V}_\theta$, as a function of time in the discharge.

As can be seen from Figure 22, the average azimuthal mode number <m> increased with time during the discharge, while the phase velocity decreased after the first 2 msec. The $\vec{E} \times \vec{B}$ velocity remained fairly constant between 2.0 and 6.0 msec and was approximately five times smaller than the measured phase velocity at 2.0 msec. Thus, the observed fluctuations propagated in the ion diamagnetic drift direction even after the $\vec{E} \times \vec{B}$ velocity was taken into account. (In the calculation for the radial electric field which was used to compute the $\vec{E} \times \vec{B}$ velocity, the effect of the large electron temperature gradient at $r = 11.5$ cm was included. See Appendix A.)
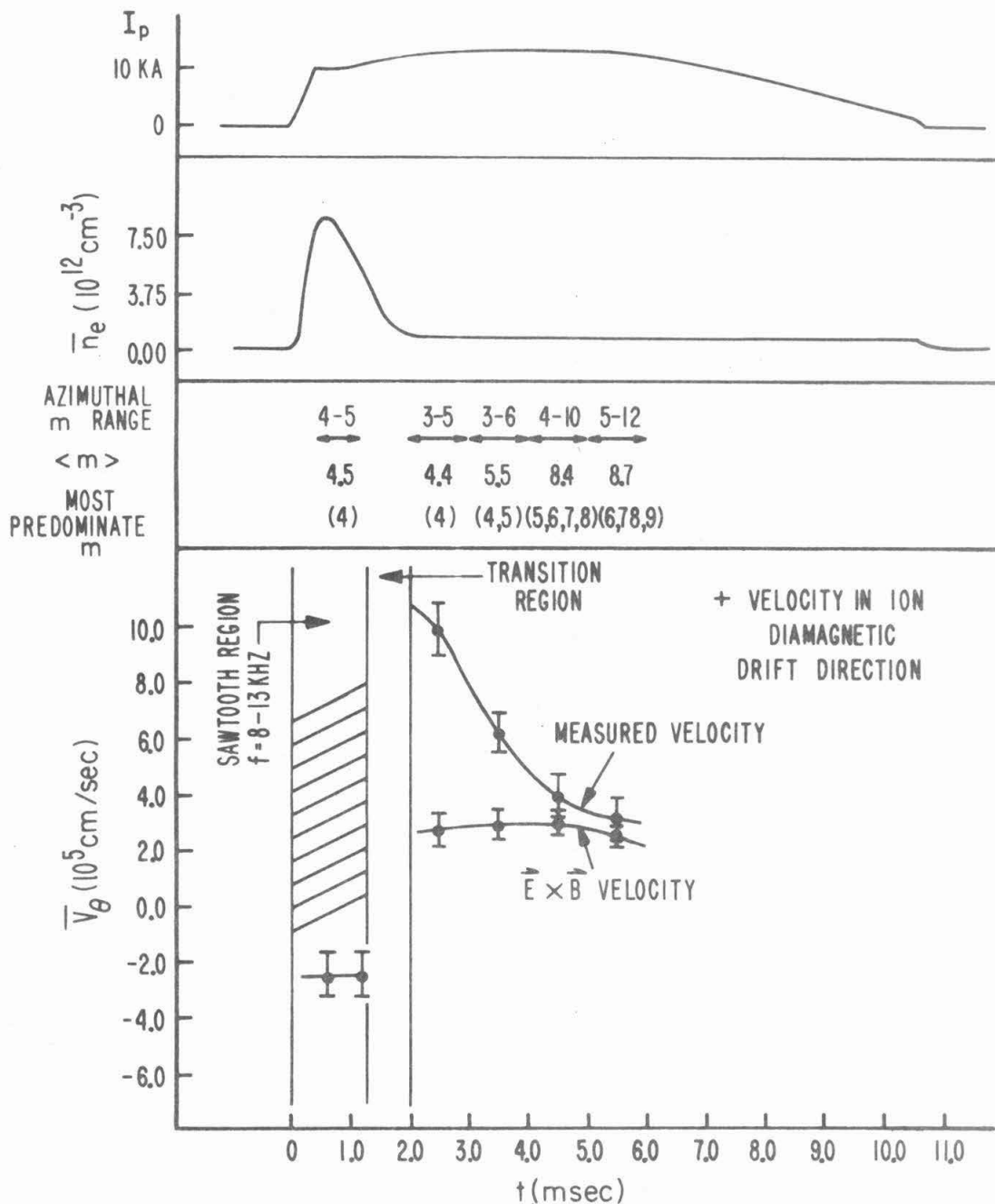
Figure 22. Time evolution of the azimuthal fluctuation characteristics for B_t = 4.2 kG, r = 12.5 cm, x = 3.0 cm, vertical field slow bank voltage = 26 volts. Data were averaged over five plasma shots.

In Figure 23 the radial phase velocity and correlation amplitude are plotted as a function of time in the discharge. The radial phase velocity exhibited a decrease with time which was similar to that of the azimuthal velocity and was almost zero during the high density phase when the sawtooth oscillations were present. The correlation amplitude was also low when the density was at its peak.

The radial dependence of the azimuthal characteristics is shown in Figure 24. The most predominant modes and <m> increased as the radial position of the probes was increased. This dependence would be expected if the fluctuations were related to drift-tearing type modes, since $q(r)$ is an increasing function of the radius. The azimuthal phase velocity and the maximum value of the normalized correlation function both de-creased as the radial position increased. The hump in the $\vec{E} \times \vec{B}$ velocity was due to the large temperature gradient at $r = 11.5$ cm; however, the $\vec{E} \times \vec{B}$ velocity was always smaller than the measured phase velocity.

Finally, values of $\delta n/n$ (which were calculated numerically by dividing the root mean square of the fluctuations of the ion saturation current by the average ion current) are plotted in Figures 25 and 26 for various radial positions and times in the discharge. $\delta n/n$ had a minimum value at $r \simeq 12.5$ cm and increased slightly on either side of this point. Also, there was a small increase in $\delta n/n$ during the high density phase of the plasma shot, but once the density reached a steady value, the fluctua-tion level was relatively constant in time.
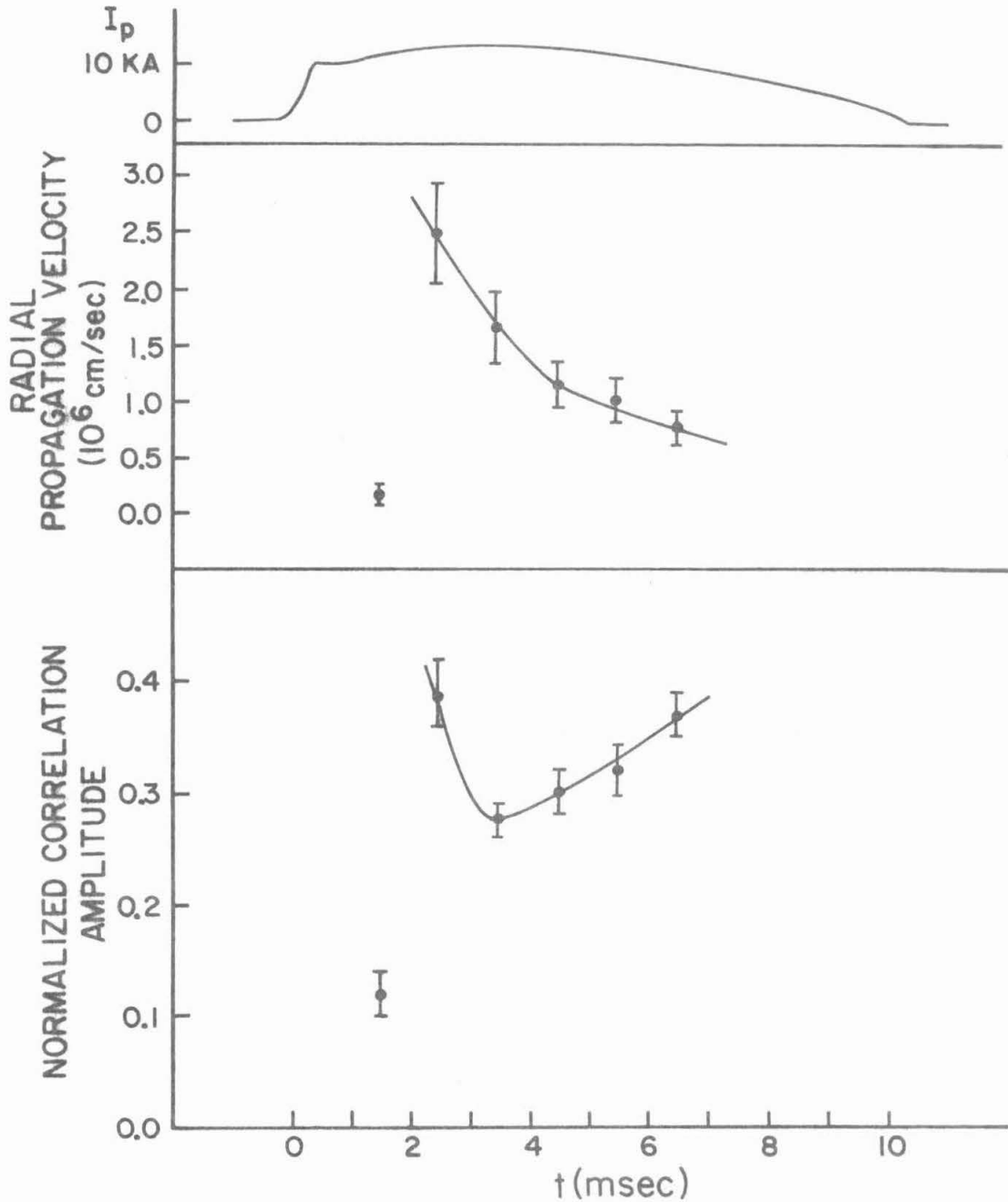
Figure 23. Time evolution of the radial phase velocity and normalized
correlation amplitude for B_t = 4.2 kG, r_1(first probe) =
13.8 cm, r_2(second probe) = 11.2 cm. Data were averaged
over eight plasma shots.
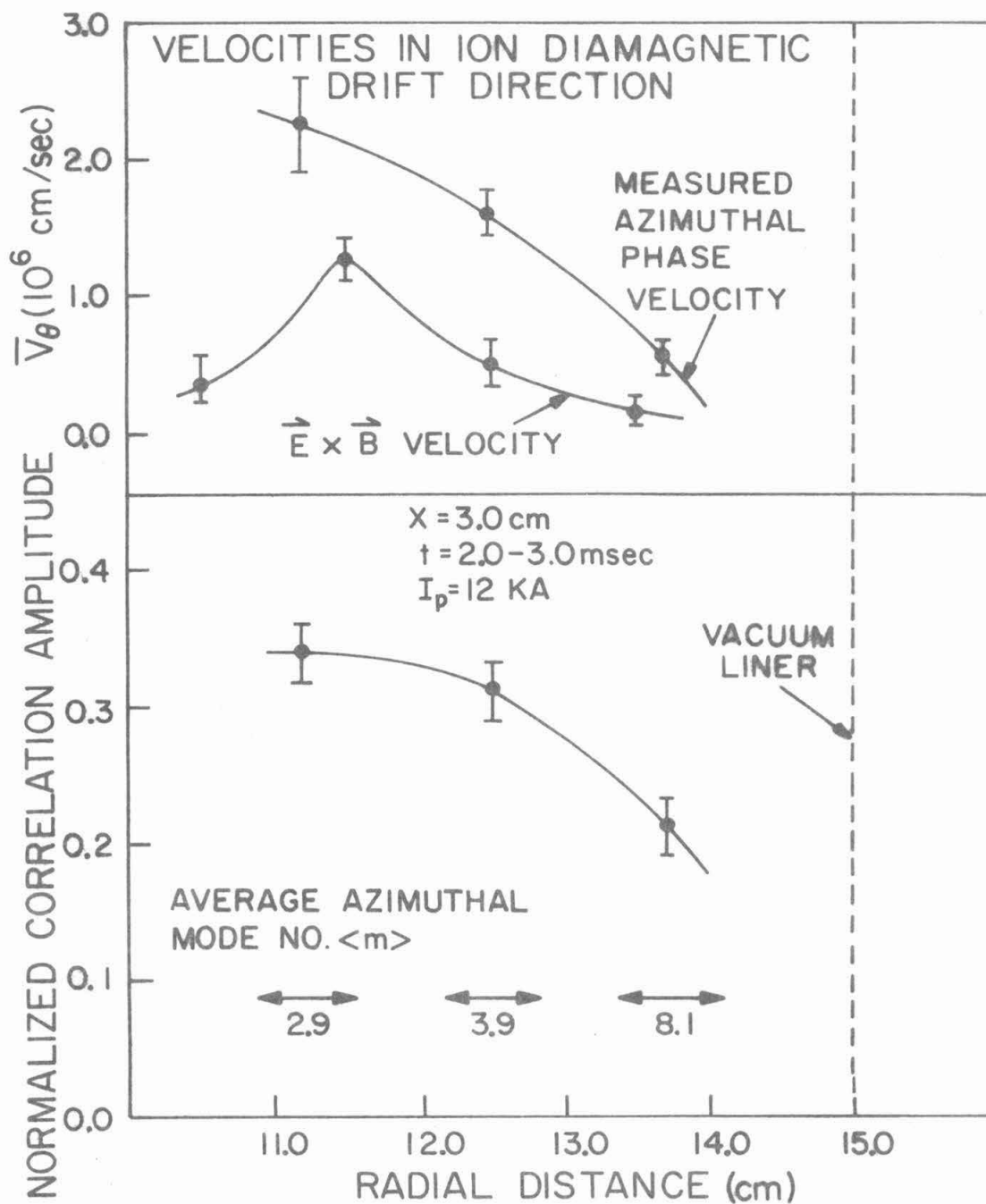
Figure 24. Radial dependence of the azimuthal fluctuation characteristics. B_t = 4.2 kG and vertical field slow bank voltage = 24 volts. Data were averaged over eight plasma shots.
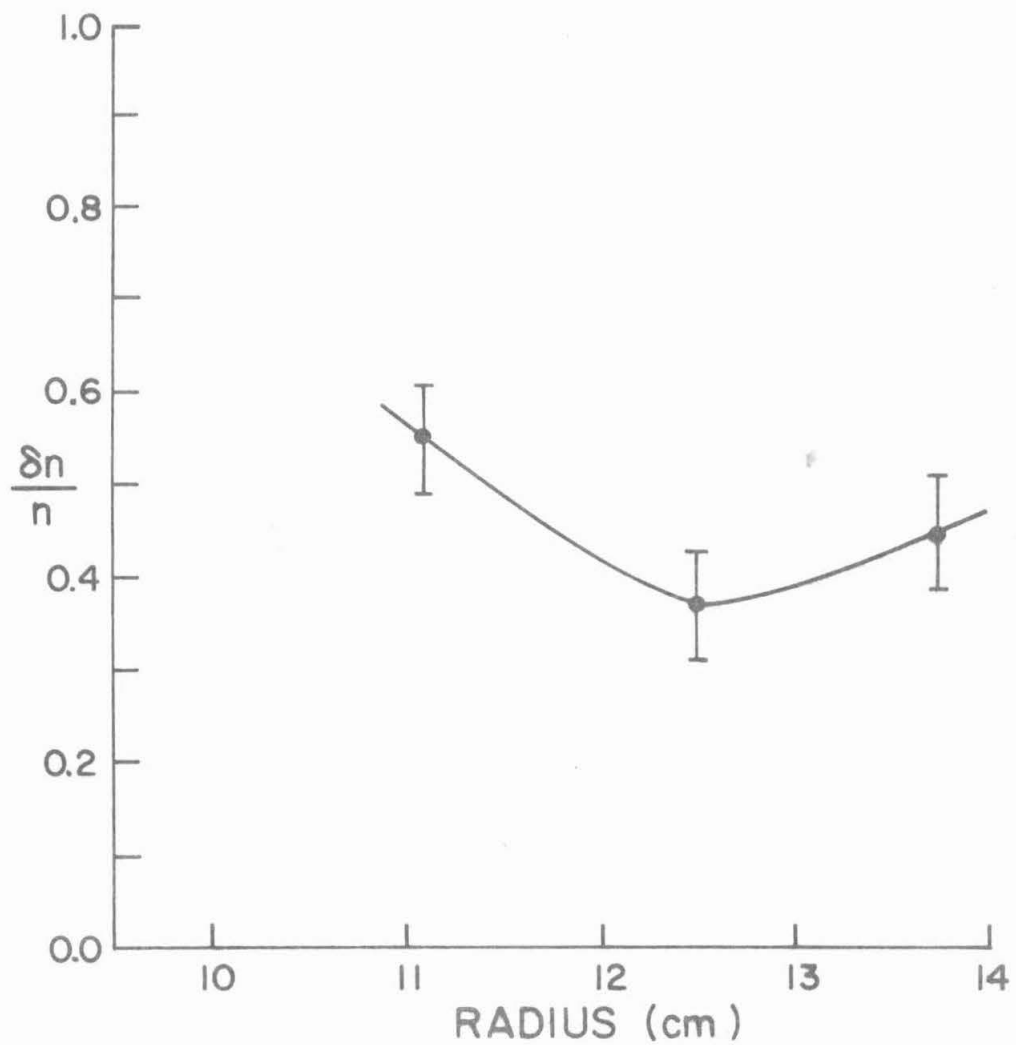
Figure 25. Electron density fluctuation level ($\delta n /n$) versus radial position. t = 2.0-2.25 msec, B_t = 4.2 kG, I_p = 12 kA. Data were averaged over six plasma shots.
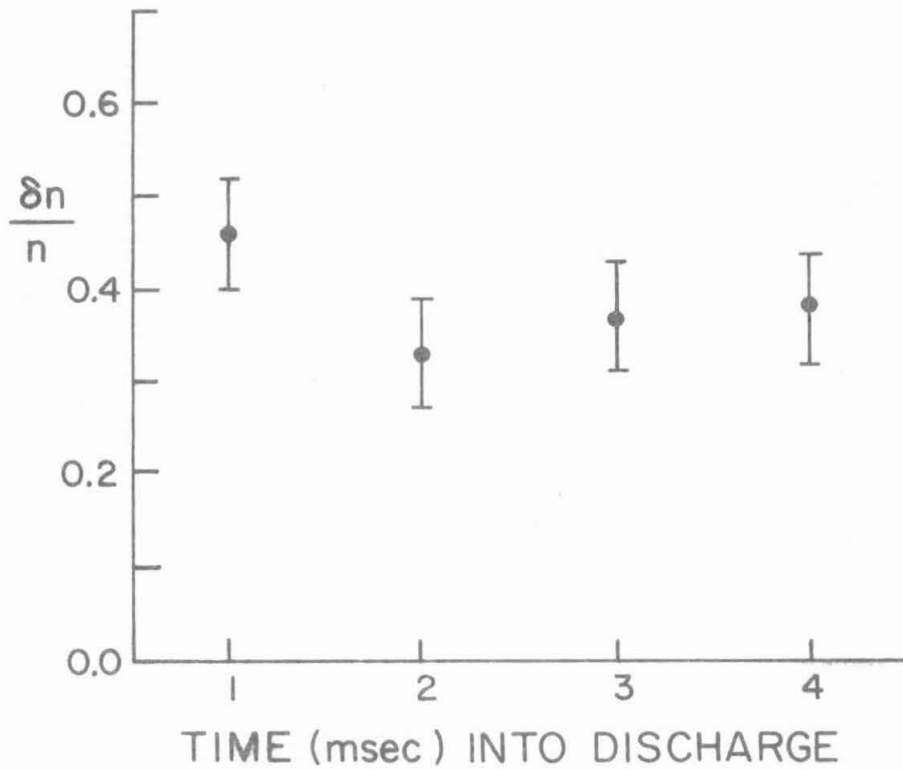
Figure 26. Electron density fluctuation level ($\delta n/n$) versus time in the discharge.   r = 12.5 cm, B_t = 4.2 kG, I_p = 12 kA. Data were averaged over four plasma shots.

VII. EFFECTS ON THE FLUCTUATIONS DUE TO CHANGES OF MACHINE PARAMETERS

In this chapter the changes in the fluctuation characteristics will be described when the tokamak parameters were varied. Since similar studies have been performed on the ST tokamak[25] with magnetic loops placed outside the limiter, it is useful to compare some of the results in this chapter with the ST observations. This comparison will be made in Section 8.2.

7.1 Effects of Filling Pressure

Normally, plasmas were created in the Caltech tokamak using a H_2 filling pressure of 1.05×10^{-4} Torr. If the filling pressure was lowered, the electron density was also lowered. When the filling pressure was raised, the electron density was larger, but due to a lack of sufficient ohmic heating power, the plasma duration τ_d dropped. Hence, when plasma lifetimes of at least 5 msec were required for experiments, the maximum H_2 filling pressure which could be used was about 1.8×10^{-4} Torr. Typical plasma current and density traces are shown in Figure 27 for a filling pressure of 1.6×10^{-4} Torr. At this pressure the conductivity temperature (assuming $Z_{eff} = 1.5$) was roughly a factor of 2 smaller than for plasmas produced at 1.05×10^{-4} Torr (see Figure 9).

The azimuthal propagation characteristics using a H_2 filling pressure of 1.6×10^{-4} Torr are also summarized in Figure 27. Several comparisons can be made between Figures 22 and 27, in which H_2 pressures of 1.05×10^{-4} Torr and 1.6×10^{-4} Torr were used, respectively. First, at the same time in the discharge, the average azimuthal mode number was
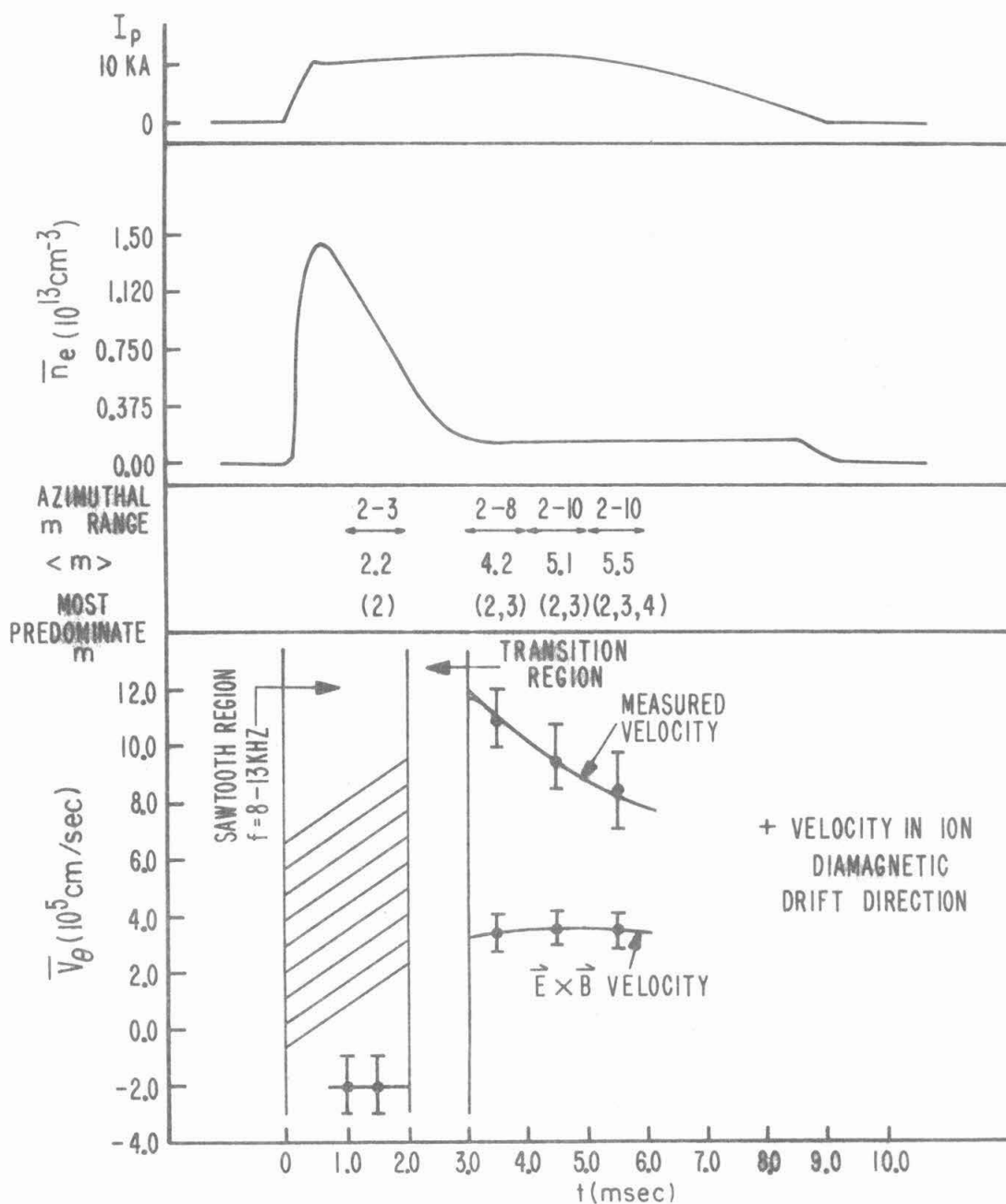
Figure 27. Time evolution of the azimuthal fluctuation characteristics for B_t = 4.2 kG, r = 12.5 cm, x = 3.0 cm, H_2 filling pressure = 1.6 x 10^{-4} Torr, vertical field slow bank voltage = 28 volts. Data were averaged over five plasma shots.

lower for the higher pressure plasma. Second, at the higher pressure <m> did not become as large in the later part of the discharge as it did at the lower pressure. Third, increasing the pressure increased both the length of time the low frequency oscillations were dominant and the width of the transition region, but had no effect on the sawtooth frequency. (The broadening of the sawtooth region was most likely due to the wider density peak at the beginning of the plasma shot at higher pressures.) Finally, the pressure did not affect either the magnitude of the azimuthal phase velocity or its characteristic decrease as a function of time during the discharge. At 1.6×10^{-4} Torr the $\vec{E} \times \vec{B}$ velocity was again much smaller than the observed phase velocity.

The maximum value of the normalized correlation function of the azimuthal fluctuations for plasma shots using H_2 filling pressures of 1.05×10^{-4} Torr and 1.6×10^{-4} Torr are graphed in Figure 28. In both cases the maximum value of the correlation function was highest during the sawtooth activity and decreased after approximately 2.0 msec; however, the maximum value of the correlation function was higher during the entire shot for the higher pressure plasma. This increase in correlation with pressure may have been due (although there was no conclusive evidence) to the fact that at higher pressures the lower order modes were enhanced. Thus, the spectrum tended to be more peaked around a single dominant frequency.

7.2 Effects of Toroidal Magnetic Field

The toroidal magnetic field was varied to ascertain what effect it had on the fluctuations. Data were taken at $B_t = 2.7$ kG and $B_t = 4.7$ kG,
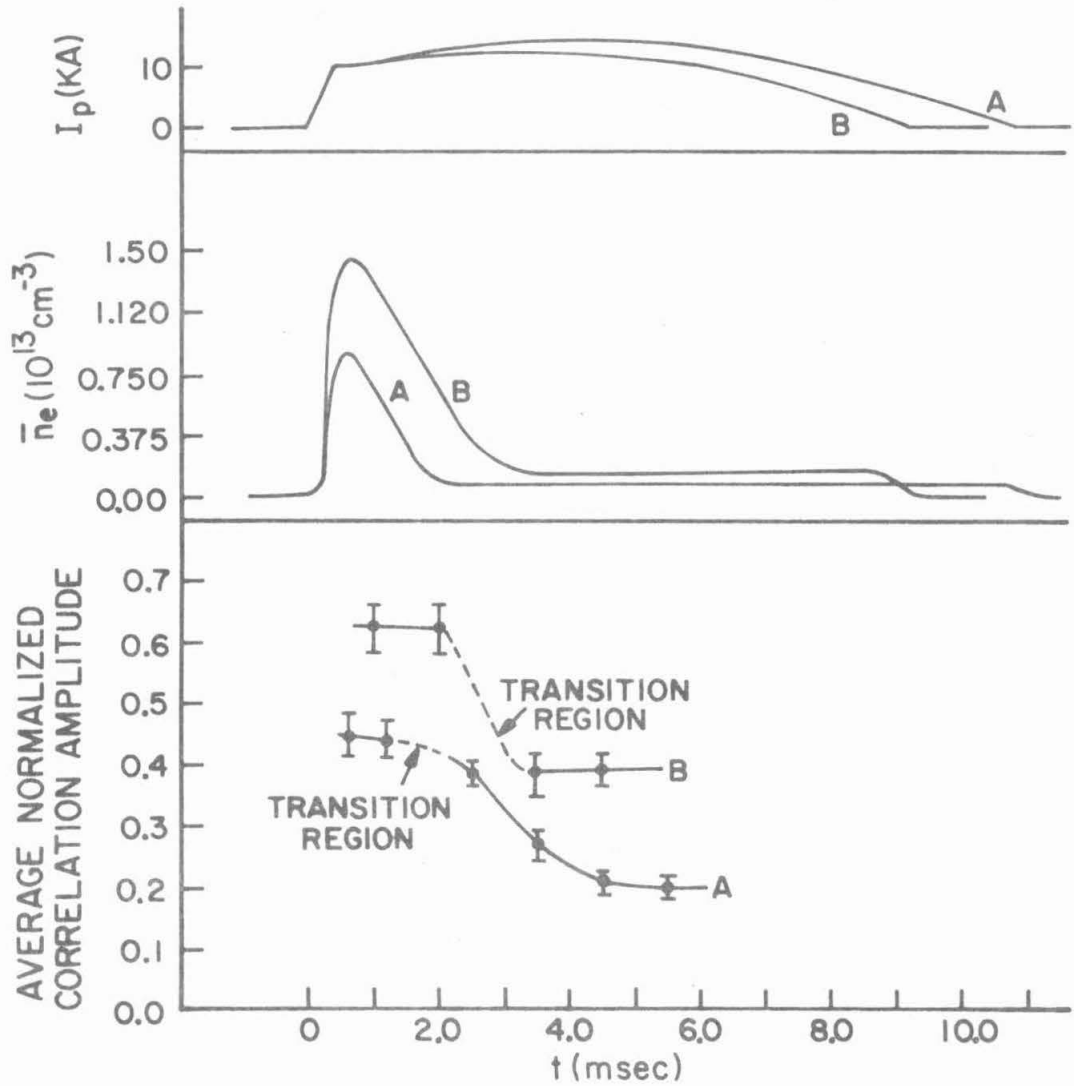
Figure 28. Time evolution of the maximum value of the normalized azimuthal correlation function using H_2 filling pressures of 1.05×10^{-4} Torr (A curves) and 1.6×10^{-4} Torr (B curves). Data were averaged over five plasma shots; $x = 3.0$ cm, $r = 12.5$ cm, and $B_t = 4.2$ kG.

and the results for the azimuthal propagation characteristics are sum-
marized in Figure 29. The correlation amplitude peak for B_t = 4.7 kG
was smaller and occurred at a larger time delay than the correlation peak
for B_t = 2.7 kG. The phase velocity and average azimuthal mode number <m>
for B_t = 2.76 kG were V_p = 1.3 x 10^6 cm/sec and <m> = 3.6, respectively. For
B_t = 4.7 kG, the phase velocity was V_p = 7.5 x 10^5 cm/sec, and the average
azimuthal mode number was <m> = 5.8. Thus, the average azimuthal mode
number was proportional to B_t while the phase velocity was inversely pro-
portional to B_t. (E_r was determined to be constant as B_t was varied.)

Since the $\vec{E} \times \vec{B}$ velocity varies as $1/B_t$ for tearing modes which
are carried by the $\vec{E} \times \vec{B}$ drift, one would expect the phase velocity to
vary inversely with the magnetic field. Moreover, since $q(r) = \frac{r}{R} \frac{B_t}{B_p(r)}$,
as B_t is increased, $q(r)$ is increased. So for tearing modes, the azi-
muthal mode number should increase linearly with B_t. However, the two-
fluid theory of Ellis and Motley[14] predicts the same dependence of the
azimuthal mode number on B_t for current driven collisional drift waves,
although at much shorter wavelengths than observed in the Caltech tokamak.
Thus, the observed dependence of the average azimuthal mode number on B_t
supports either a drift or tearing mode interpretation for the fluctua-
tions.

The radial propagation characteristics as a function of B_t are
shown in Figure 30. Both the radial phase velocity and the maximum
value of the normalized correlation function were found to drop linearly
with increasing magnetic field. Moreover, $\delta n/n$ did not change at
$r \simeq 12.5$ cm as B_t was varied.

Finally, as the magnetic field was lowered below $B_t \simeq 2.7$ kG

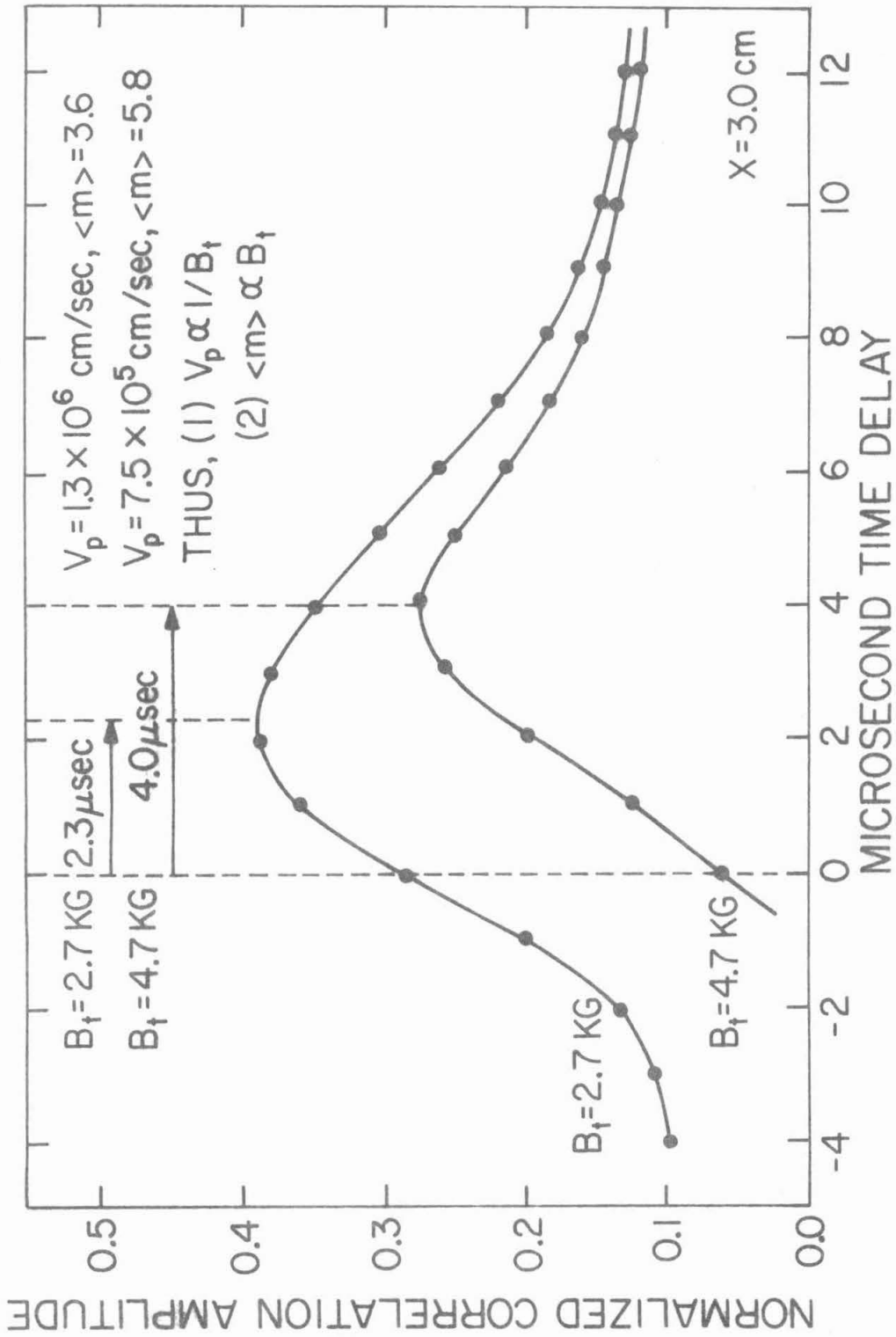Figure 29. Effect of B_t on the normalized azimuthal correlation function. $I_p = 12$ kA, r = 12.5 cm, and t = 2.0-3.0 msec. Data were averaged over fifteen plasma shots.

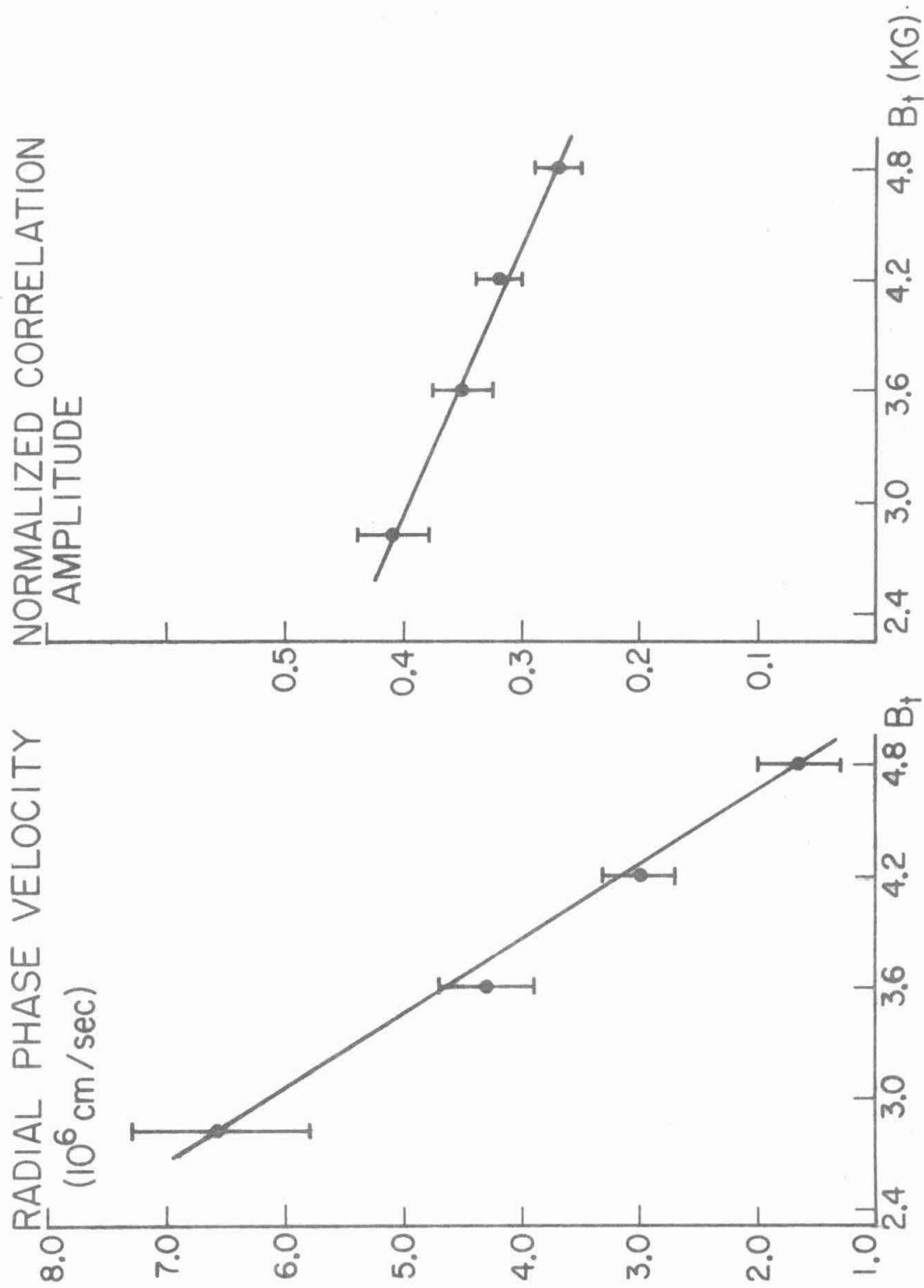Figure 30. Radial phase velocity and the maximum value of the normalized radial correlation function versus B_t. I_p = 12 kA, t = 2.0-3.0 msec, r_1 = 10.0 cm, r_2 = 12.5 cm. Data were averaged over fifteen plasma shots.

(with the ohmic heating fixed) the plasma became grossly unstable, and
the current abruptly dropped to zero after approximately 6 msec. In
Figures 31a,b the spectrum is shown when such a disruption did and did
not occur for $B_t = 2.7$ kG. The $m = 2$ mode was always predominant before a
gross instability developed. This result supports a drift-tearing mode
interruption of the fluctuations, since the $m = 2$ tearing mode is thought
to play a major role in the disruptive instability.[36]

7.3 Effects of Plasma Current

When the ohmic heating slow bank voltage was increased, a larger
plasma current was produced. The conductivity and Langmuir probe temper-
atures also increased as seen in Figure 7. Several values for Z_{eff} were
assumed in the conductivity calculations. Since the electron diamag-
netic drift velocity is proportional to the electron temperature, it was
of interest to determine what effect the value of the plasma current had
on the azimuthal phase velocity. The maximum value of the normalized
correlation function and the azimuthal phase velocity are plotted in
Figure 32 as a function of the plasma current for the 1.0 msec interval
in which data were taken (between 2 and 3 msec). As can be seen, the
phase velocity did not increase linearly with the plasma current as would
be expected for a diamagnetic drift, and the correlation amplitude re-
mained relatively constant. (When varying the plasma current, the verti-
cal field was adjusted so as to keep the plasma column located in the same
position. This was accomplished by observing the in-out signal and the
electron density at the probe tips.)

The average azimuthal mode number <m> was determined for the dif-
ferent plasma currents at several different radii and several different
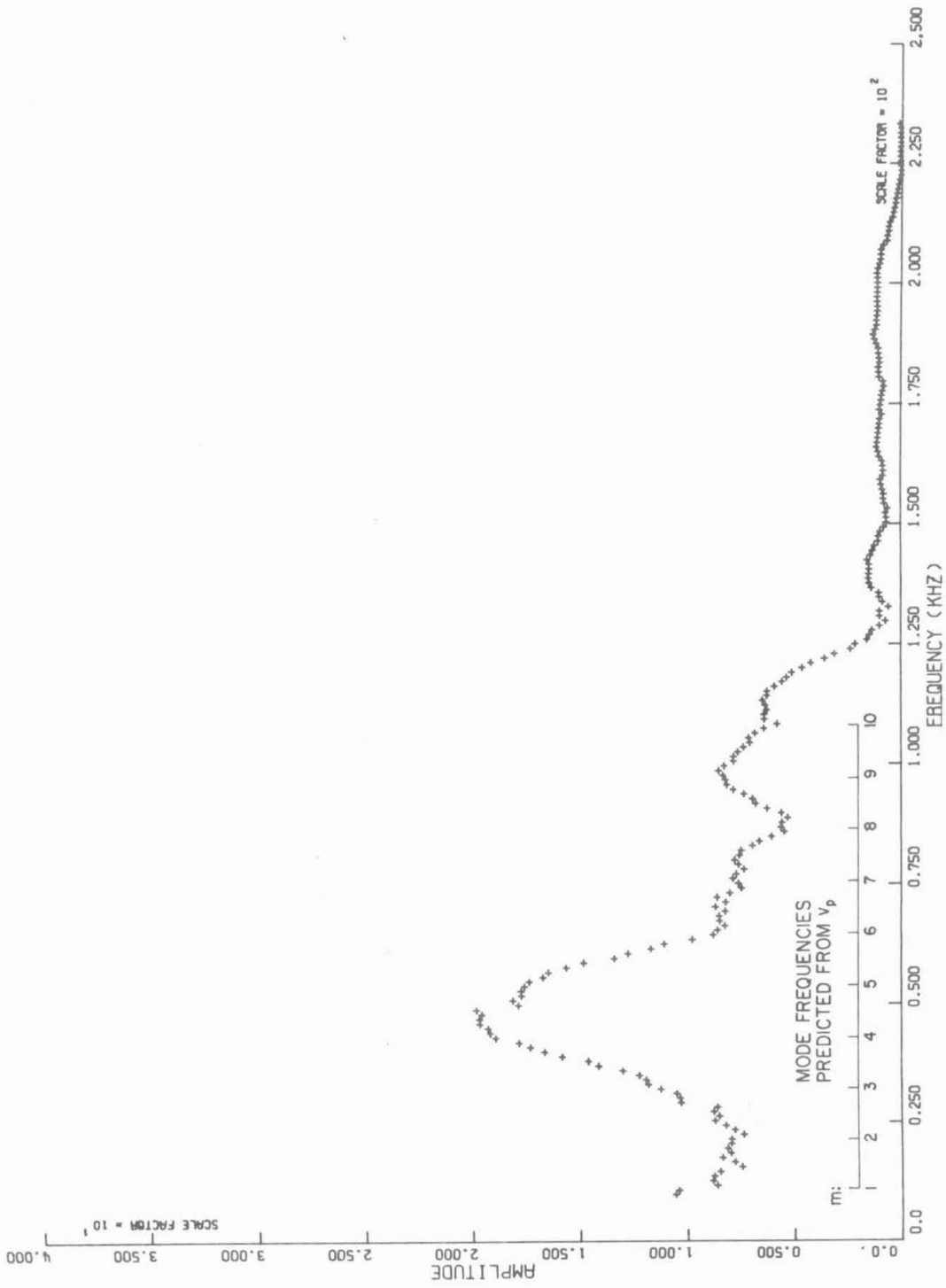
Figure 31a. A typical Gaussian averaged amplitude spectrum when <u>no</u> disruption occurred with $B_t = 2.7$ kG.
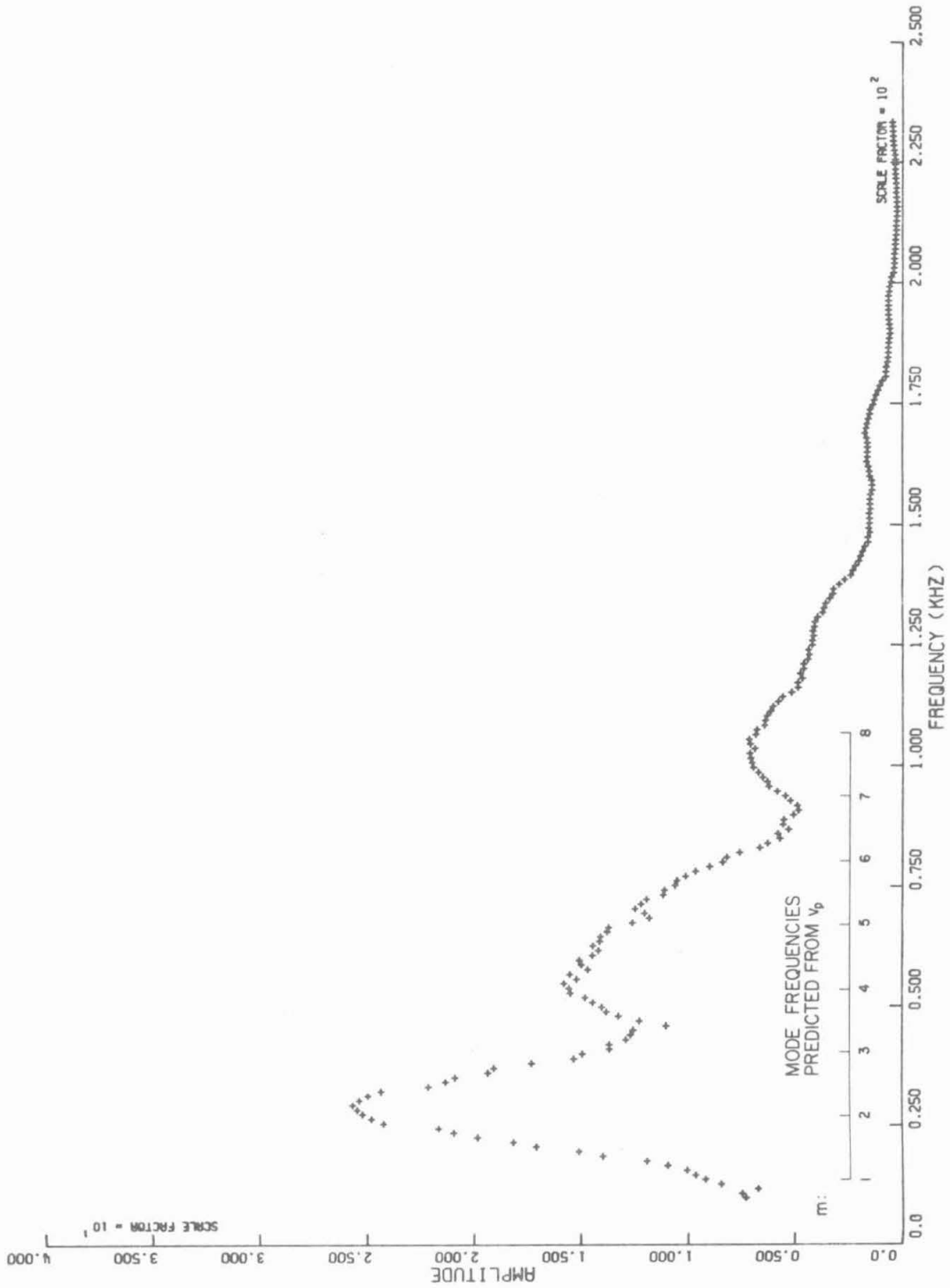
Figure 31b. A typical Gaussian averaged amplitude spectrum when a disruption occurred with B_t = 2.7 kG. All machine parameters were the same as in Figure 31a.
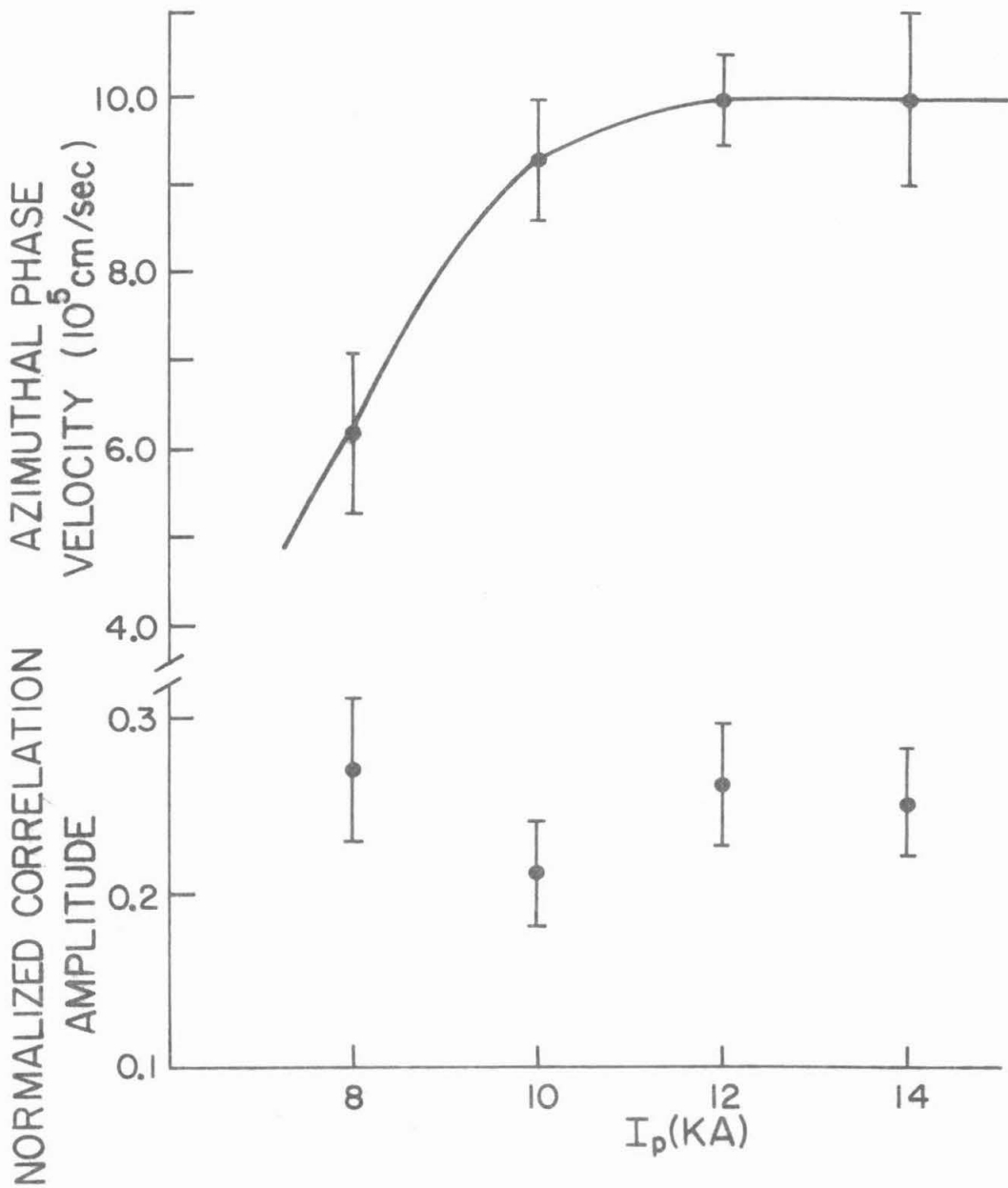
Figure 32. The azimuthal phase velocity and the maximum value of the
normalized azimuthal correlation function versus I_p.
B_t = 4.2 kG, r = 12.5 cm, t = 2.0-3.0 msec, and x = 3.0 cm.
Data were averaged over ten plasma shots.

times during the discharge. The results are given in Figure 33. The average azimuthal mode number <m> exhibited a somewhat striking $1/I_p$ dependence when the radius and time were fixed. As would be anticipated from the results already presented, the curves shifted to larger <m> values as both the radius and the time in the discharge in which data were taken were increased. All curves, however, showed the same <m> dependence on I_p. This dependence would be expected for a tearing-type mode[17] since q(r) is inversely proportional to the plasma current.

In Figure 34 the radial phase velocity and the maximum value of the normalized radial correlation function are plotted as a function of I_p. The radial phase velocity showed a strong dependence on I_p, but the radial correlation amplitude was nearly constant as I_p was changed. Again, the vertical field was adjusted so as to keep the plasma column located in the same position as the current was varied. The density fluctuation level was found to be independent of the plasma current; see Figure 35.

7.4 Gas Puffing Results

Since one of the major problems in controlled thermonuclear research has been to obtain an extremely high density plasma, various methods have been employed to try to increase the electron density in tokamaks. In earlier toroidal devices, discharge cleaning procedures were not employed; and therefore the walls recycled hydrogen and impurities into the vacuum chamber and kept the densities fairly constant during the discharge. However, in the Caltech tokamak, discharge cleaning provided a relatively low Z_{eff} plasma, since particles which hit the vacuum chamber were not readily replaced by hydrogen or higher Z mate-
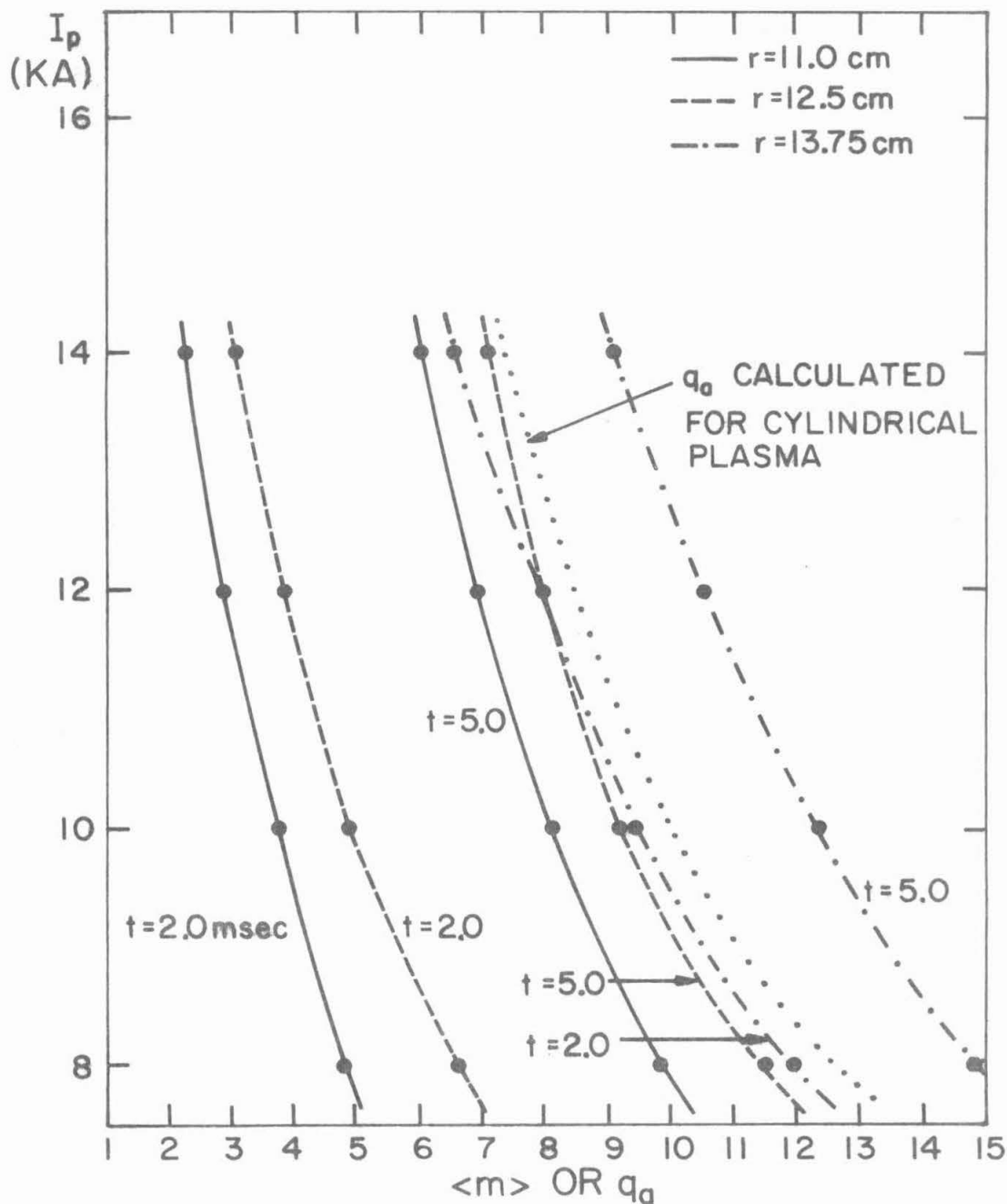
Figure 33. The average azimuthal mode number <m> versus I_p at differ-
ent radii and times during the discharge. B_t = 4.2 kG and
data were averaged over six to ten plasma shots.
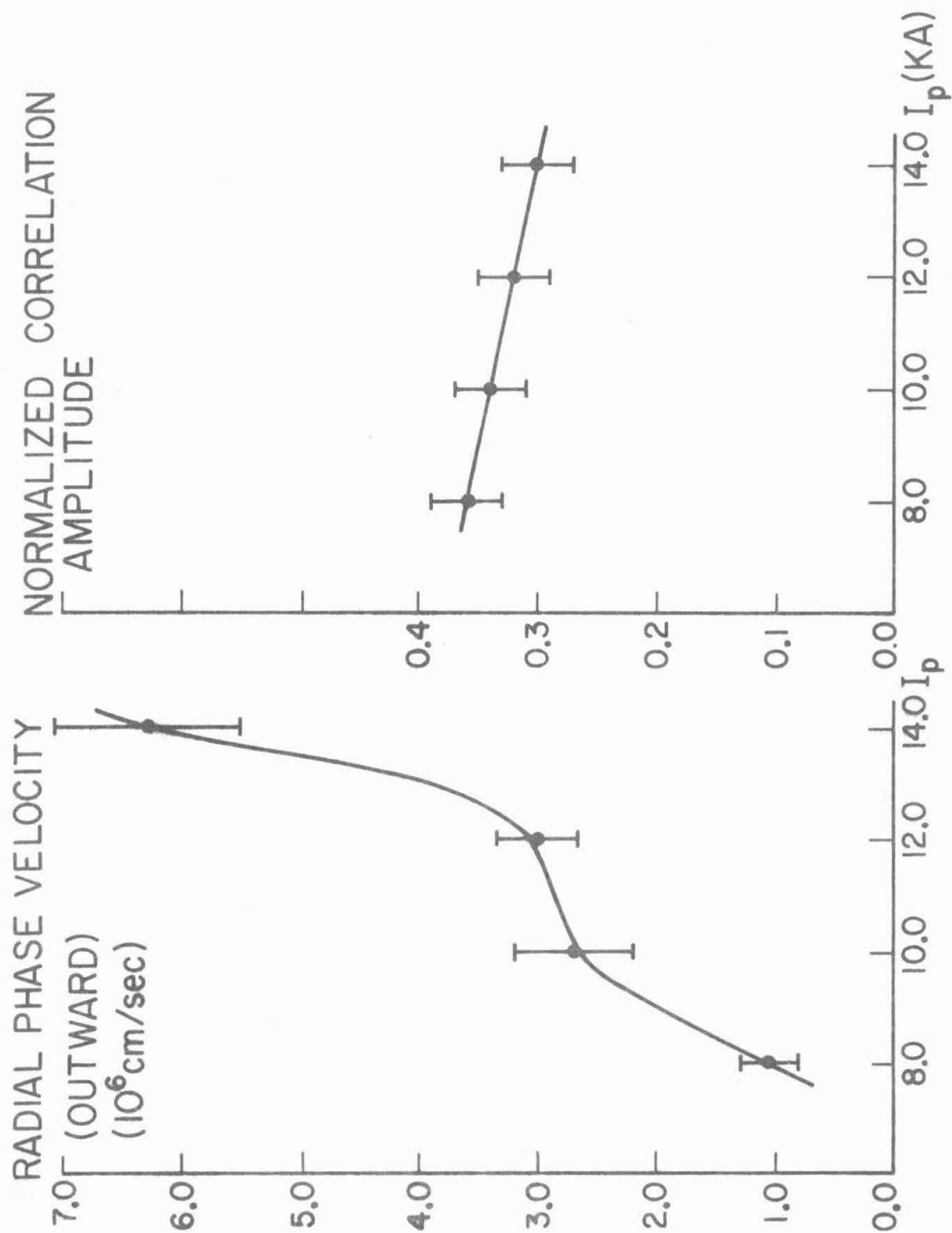
Figure 34. The radial phase velocity and the maximum value of the normalized radial correlation function versus I_p. B_t = 4.2 kG, t = 2.0-3.0 msec, r_1 = 11.2 cm, r_2 = 13.7 cm. Data were averaged over ten plasma shots.
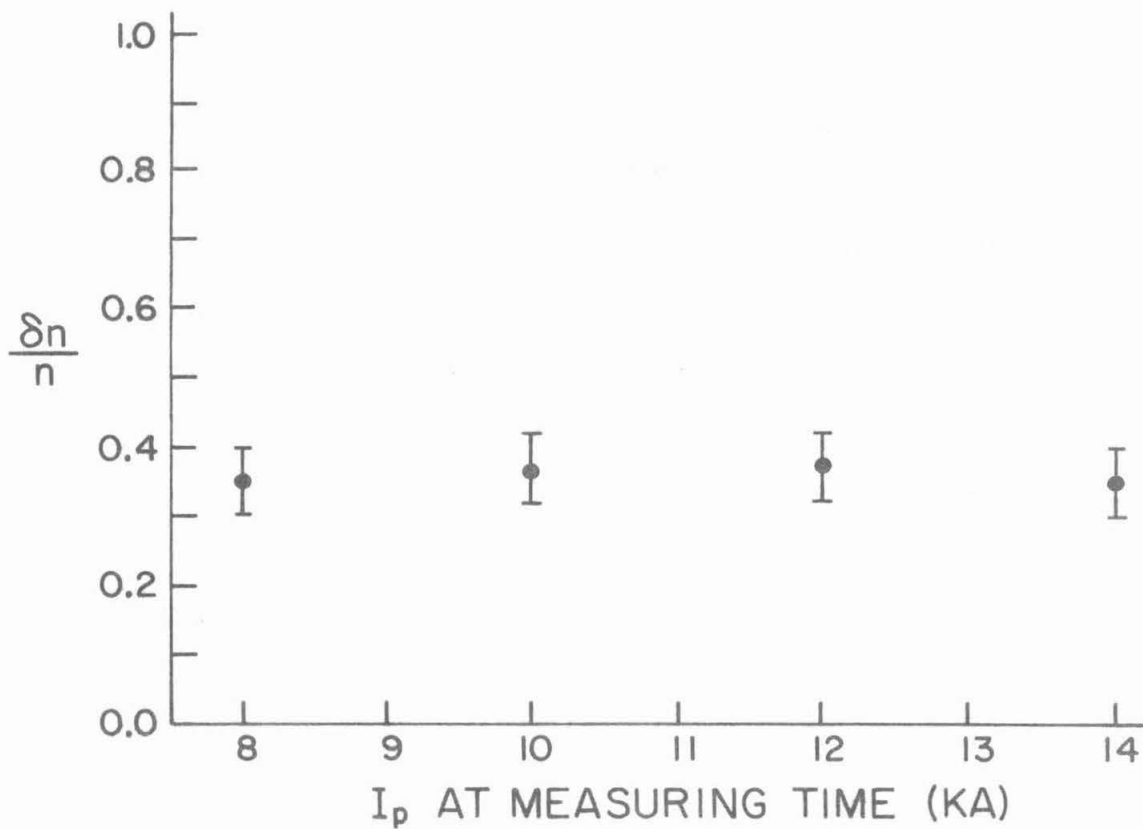
Figure 35. Density fluctuation level ($\partial n/n$) versus I_p. t = 2.0-3.0 msec, B_t = 4.2 kG, r = 12.5 cm. Data were averaged over five plasma shots.

rials. Hence, the density fell after the first few milliseconds, and neutral gas injection was required to prevent this decay. The method used to add H_2 during the discharge is called "gas puffing".

The fast acting piezoelectric valve which was used to gas puff was mounted in one port of the tokamak; a Granville-Phillips leak valve was employed to allow small amounts of H_2 to flow to the backside of the piezoelectric valve. The piezoelectric valve required a minimum applied voltage of about 38 volts to begin opening but needed 100 volts to open completely. Moreover, the speed at which it opened was drastically affected by the initial bias voltage which was applied and the degree to which it was "overvoltaged." If the voltage on the valve was programmed to rise from zero to 125 volts in roughly 0.2 milliseconds, the valve required many milliseconds to open completely. If, however, an initial 35 volt bias was applied and then the voltage was raised to 125 volts in 0.2 millisecond, the valve opened completely in one millisecond. The electronic switching circuit used for gas puffing was partially designed and constructed by Bruce S. Levine.

Some of the effects of gas puffing on the azimuthal propagation characteristics are compiled in Figure 36. The top three sections show the plasma current, electron density, and fluctuation characteristics during the fourth millisecond when no gas puffing was used. The bottom three sections show the same information when a small amount of gas was added to double the density during the fourth millisecond of the plasma lifetime. As can be seen, the azimuthal propagation velocity was unchanged by gas puffing; but both the normalized correlation amplitude and the average azimuthal mode number decreased when the extra gas was added.
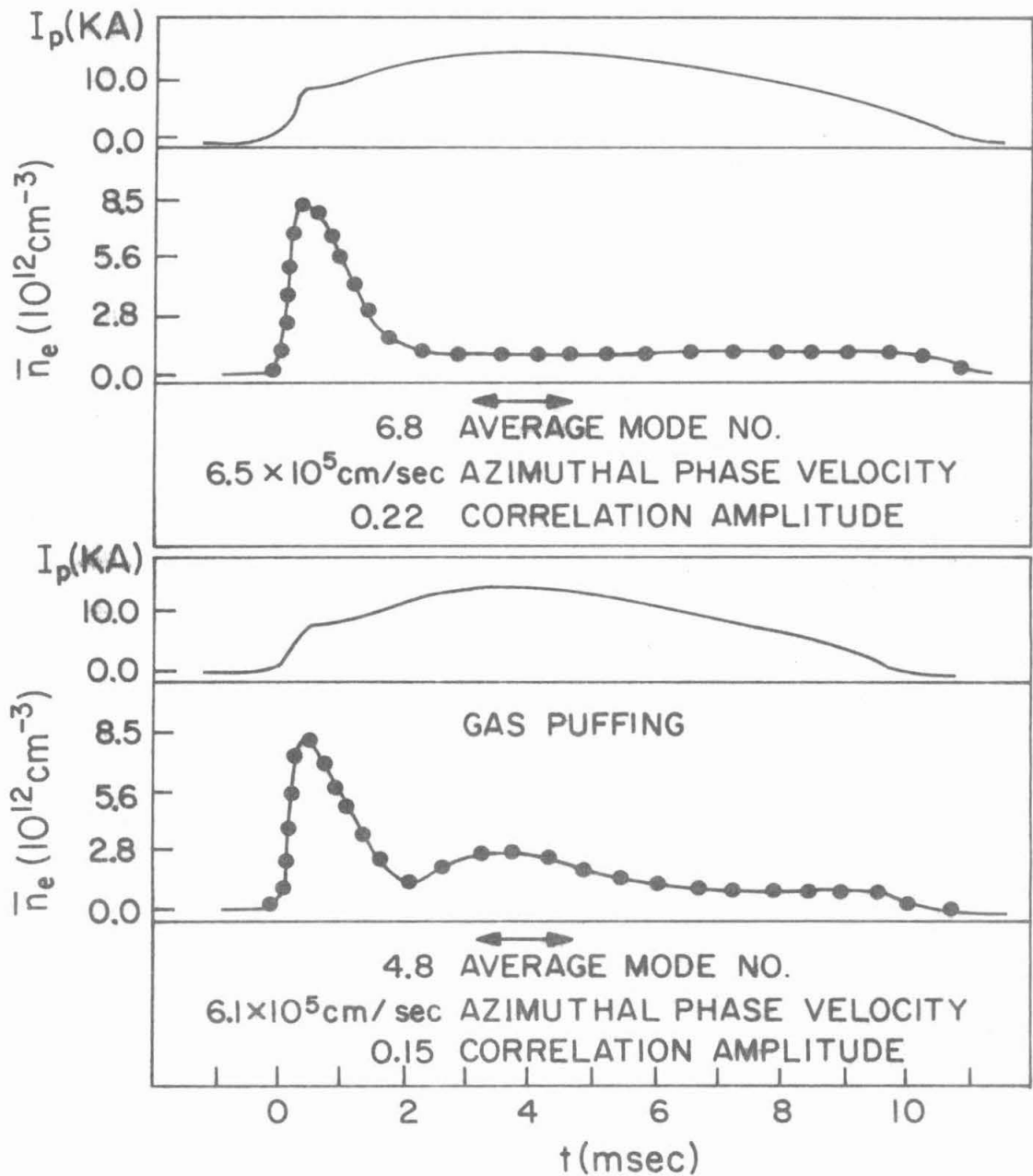
Figure 36. Effects of gas puffing on the azimuthal **propagation** characteristics. The top three sections are for no gas puffing, and the bottom three sections show the effects of a small puff at t = 4.0 msec. Data were averaged over ten plasma shots; x = 3.0 cm, r = 12.5 cm, and B_t = 4.2 kG.

As more neutral gas was puffed during the discharge, the plasma became progressively more unstable (as partially indicated by large glitches on the plasma current traces), and the lower order modes with frequencies $f \simeq 10$ kHz became predominant. Figure 37 shows the plasma conditions when enough gas was added to eliminate most of the density decay at $t = 1.0$-2.0 msec. The voltage applied to the piezoelectric Veeco valve is shown on the bottom trace, and the ohmic heating slow bank voltage was set to its maximum value ($V \simeq 500$ volts) in order to sustain the plasma for as long as possible. The spectrum for this case is presented in Figure 38.

The large peak at $f = 13$ kHz in Figure 38 is reminiscent of the spectra of the sawtooth oscillations described earlier. However, the correlation function was not reproducible when enough gas was added to eliminate most of the density decay; the correlation peaks did not consistently lay on one side of the zero time delay point, and the correlation amplitudes varied considerably from shot to shot. Thus, no phase velocity information could be obtained for the 13 kHz fluctuations.

Finally, a series of progressively longer gas puffs were used to study the fluctuation level as a function of the plasma density. The results of the calculations for $\delta n/n$ for different densities, as represented by the number of extra fringes seen on the microwave interferometer signal, are presented in Figure 39. No change in the fluctuation level was observed as the density was increased.

In summary, when the plasma density was increased either by raising the filling pressure or by gas puffing, the average azimuthal
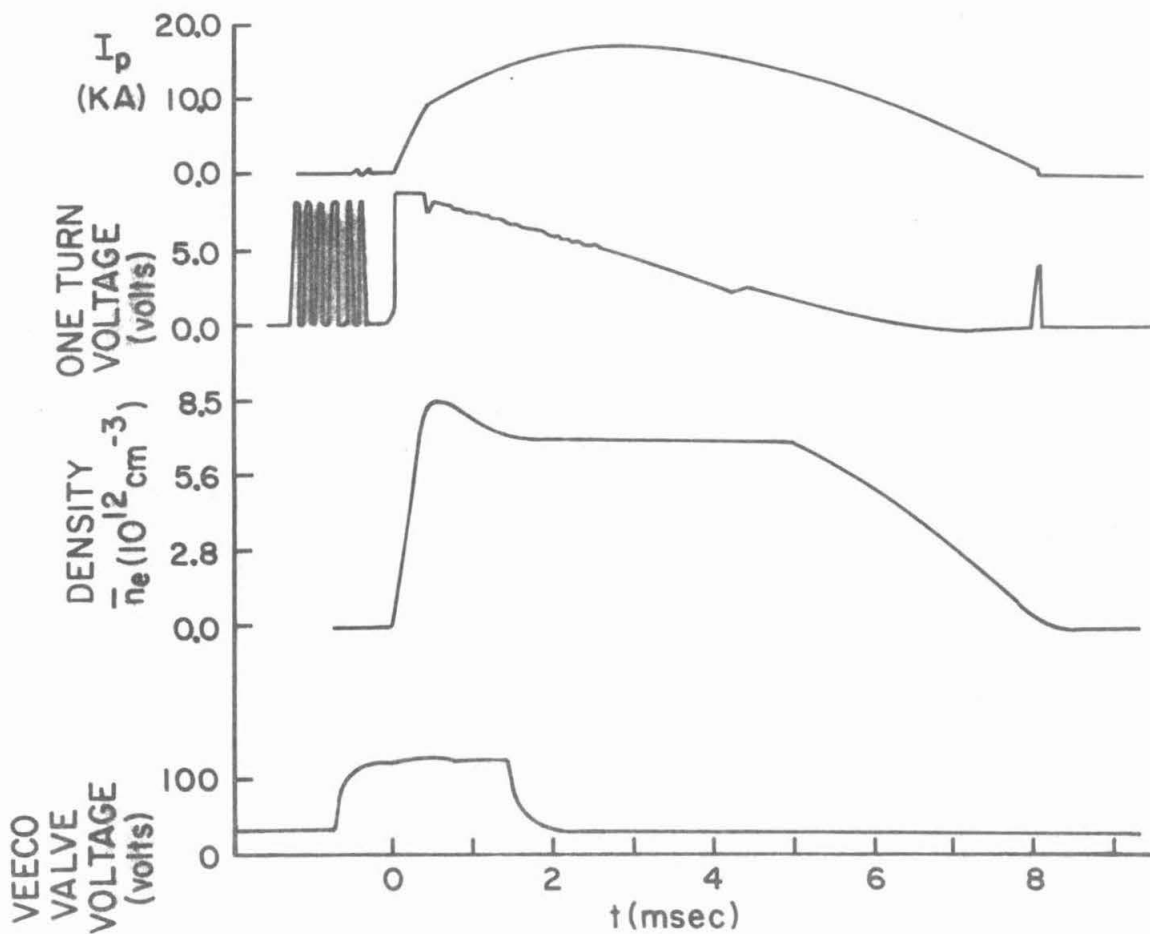
Figure 37. The plasma current, one turn voltage, electron density, and voltage on the Veeco valve when enough gas was puffed to eliminate most of the density decay at t = 1.0-2.0 msec.
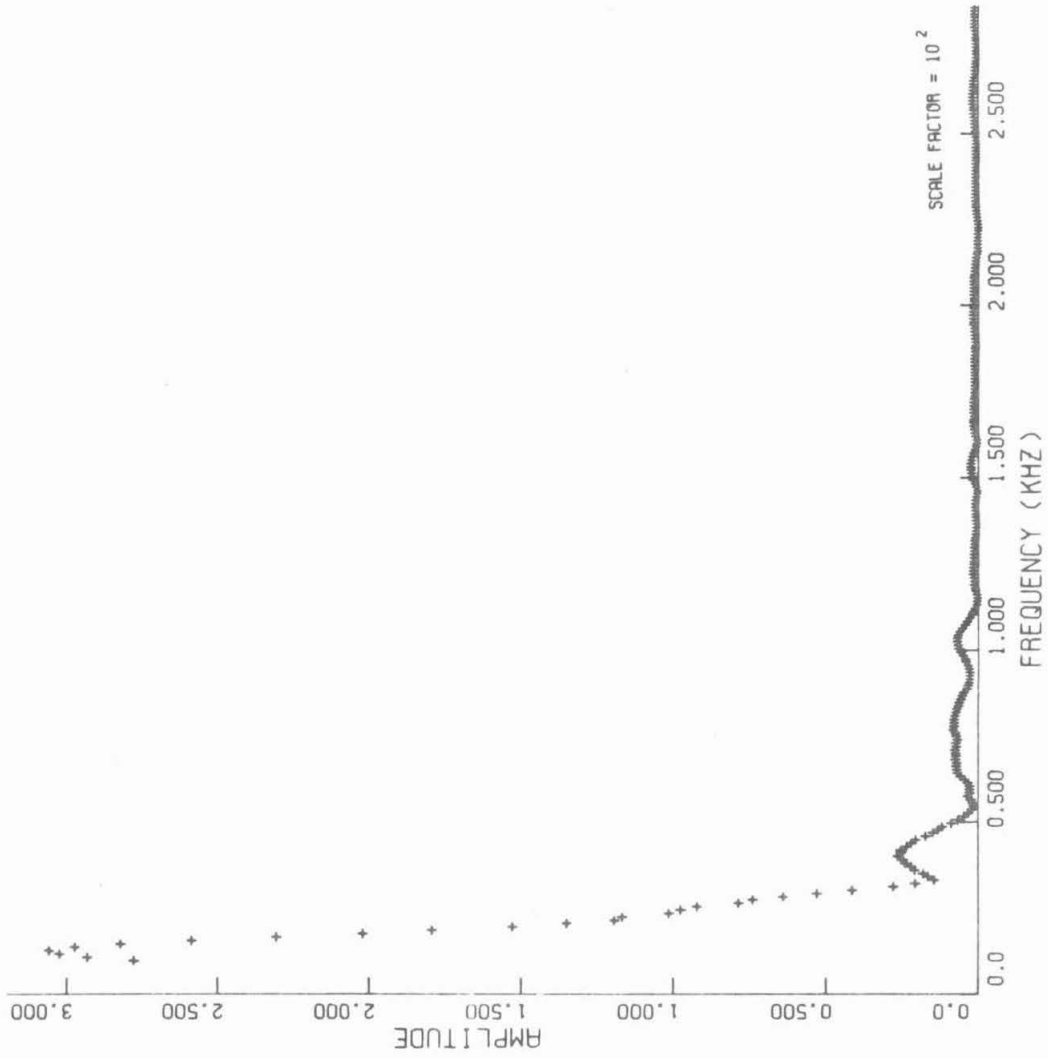
Figure 38. The amplitude spectrum of the azimuthal fluctuations for the plasma conditions of Figure 37.
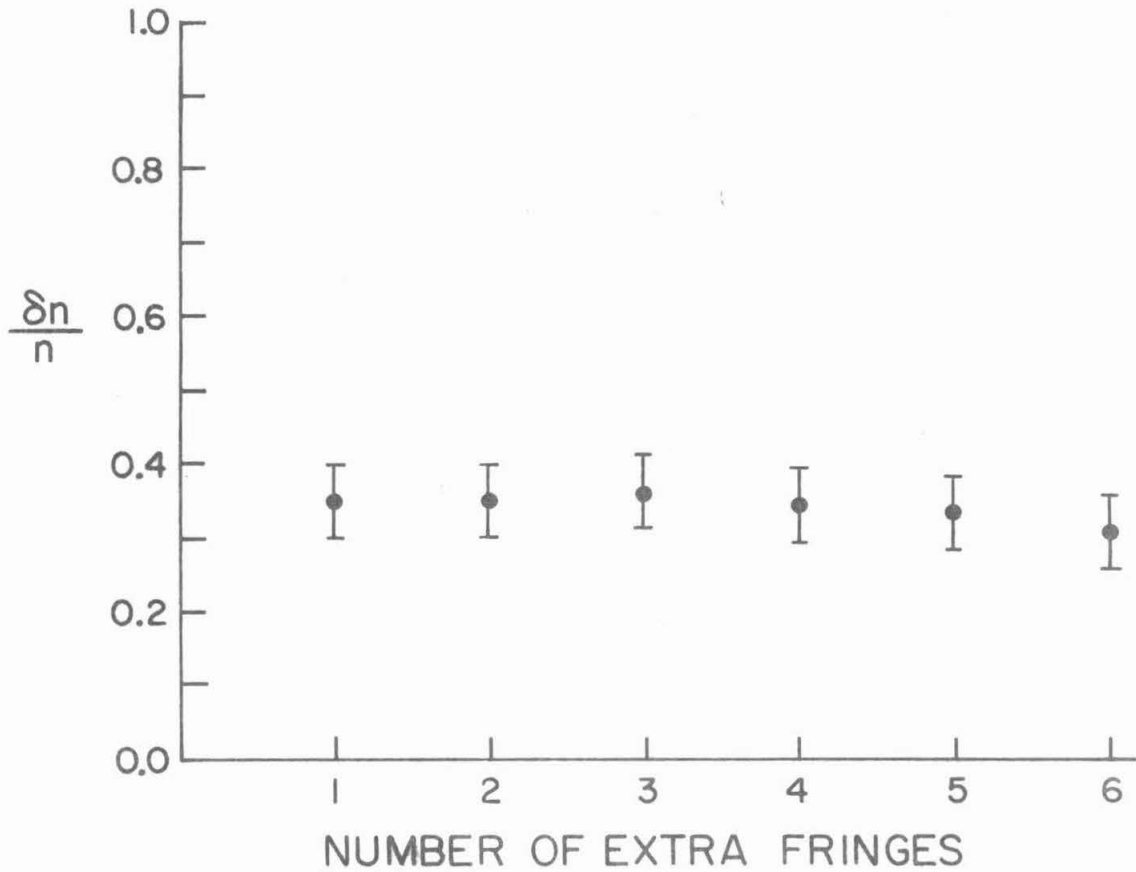
Figure 39. $\delta n/n$ versus the amount of <u>extra</u> H_2 added by puffing. One microwave fringe corresponds roughly to $n_e \simeq 1.5 \times 10^{12}$ cm^{-3}. $B_t = 4.2$ kG, $t = 3.2$-4.2 msec, $r = 12.5$ cm. Data were averaged over five plasma shots.

mode number decreased; similar observations were made on the ST tokamak with magnetic loop probes. Since tokamak plasmas are known to become more unstable as the density is increased,[37] the results indicate that the lower order mode fluctuations are probably more deleterious to gross plasma confinement than are the higher order modes. This conclusion is also supported by the results obtained when the toroidal magnetic field was lowered.

VIII. SUMMARY AND CONCLUSIONS

Due to the diversity of experimental data that have been presented
in this thesis, a summary of the principal characteristics of the fluctu-
ations will be presented in this chapter. Also, some general conclusions
will be stated, and comparisons will be made between recent drift and
tearing mode theories and the observations on both the Caltech and ST
tokamaks. Finally, several ideas for future experiments are given in the
last section.

8.1 Summary of the Fluctuation Characteristics

<u>After the first 2 msec</u> of the plasma lifetime, the fluctuation char-
acteristics were the following

1. Broadband spectra were observed which extended from 1 kHz to
   roughly 200 kHz

2. The aximuthal wavelengths were between 6 and 70 cm

3. The azimuthal phase velocity was in the ion diamagnetic drift
   direction even after local $E \times B$ velocities were taken into
   account

4. The radial phase velocity was directed radially outward and was
   was independent of radius for the outer regions of the plasma

5. Peaks existed in the spectra which seemed to be related to
   specific azimuthal modes

6. Both the radial and azimuthal correlation lengths were roughly
   4 cm, and they decreased slightly as the toroidal magnetic field
   was increased

7. The density fluctuation level $\delta n/n \simeq 0.35$ for $r \geq 12$ cm, and was
   constant as the plasma current, toroidal magnetic field, and
   density were varied. However, $\delta n/n$ increased by approximately
   50% as the radial distance was decreased below $r = 12$ cm.

8. The average azimuthal mode number of the fluctuations $<m>$ scaled roughly with plasma parameters according to the relation

$$<m> \simeq (7.5 \times 10^{-4}) \frac{B_t \, r^2}{I_p \, p^{1/2}} \quad ,$$

for t = 2-3 msec and 13.5 cm > r > 10 cm. B_t is to be expressed in KG, I_p in KA, r in cm, and p (H_2 filling pressure) in torr.

9. The scaling of the azimuthal phase velocity with plasma parameters was given by

$$V_\theta \simeq (2.9 \times 10^9) \frac{I_p}{B_t \, r^3 \, t^{3/2}} \quad ,$$

for $I_p \leq 12$ kA, 13.5 > r > 10 cm, and 7 msec > t > 2 msec. t is to be expressed in msec and V_θ in cm/sec.

10. Magnetic loop probe measurements indicated that the poloidal magnetic field fluctuation spectra were similar to the electrostatic probe spectra.

The radial phase velocity decreased with time at approximately the same rate as the azimuthal phase velocity and scaled according to the relation

$$V_r = (1.3 \times 10^5) \frac{I_p^3}{B_t^2 \, t^{3/2}} \quad ,$$

for p = 1.05 $\times$ 10^{-4} torr, 14 cm > r > 10 cm, and 7 msec > t > 2 msec, where V_r is also expressed in cm/sec. In addition, the axial phase velocity after the first 2 msec was in the direction of electron current flow with a speed of the same order of magnitude as the azimuthal speed (for a range of parameters, time in discharge, B_t, and I_p were varied).

Moreover, it was found that the average azimuthal mode number $<m>$ decreased when extra H_2 was added during the discharge by gas puffing techniques. However, when the density fall-off was nearly eliminated by gas puffing, the spectra possessed a large peak around 10 kHz, and the correlation function was not reproducible for successive plasma shots.

During the first 2 msec of the plasma lifetime when the density rose and fell to its stable value, sawtooth type oscillations were seen with very sharply peaked spectra around 10 kHz. The amplitude of the sawtooth signals was roughly five times larger than the amplitude of the higher frequency fluctuations which were predominant later; and the azimuthal phase velocity of the sawtooth oscillations was in the electron diamagnetic drift direction with a magnitude approximately 0.2 times that of the azimuthal phase velocity observed at t = 2.0-3.0 msec. Finally, during the period in which the sawtooth signals were present, both the radial phase velocity and normalized radial correlation were very small compared with their values later in the discharge, and $\delta n/n$ was approximately 30% larger than at later times.

8.2 Conclusions--Theory versus Experiment

As stated earlier, the two types of instability which are currently thought to play a major role in the anomalous particle transport observed in tokamaks are the drift-type waves and the MHD tearing modes. Unfortunately, in past experiments the results have never conclusively determined which type of oscillation was dominant nor which was most important in enhancing diffusion. Some experimental groups have reported observing drift-type waves, while other groups have explained their results on the basis of MHD theory. The results of this thesis indicate that tearing modes modified by diamagnetic drifts are probably

important in determining the characteristics of the fluctuations seen in the Caltech tokamak; and a theory in toroidal geometry which adequately combines the essential features of both the drift and tearing mode instabilities is most likely needed to accurately describe the results.

The kinetic theory of tearing modes of Drake and Lee[18] was described in Chapter II, and the predictions of their theory appear to be in better agreement with the results of the present experimental work than the conclusions from older theories. However, several discrepancies still remain between their predictions and the present observations. Moreover, many other attempts[38] have recently been made to try to unify drift wave analysis with the usual MHD stability theory. In fact, at the time of writing, the number of theories approximately equals the number of groups working in the field, and thus more effort is needed to reconcile the differing approaches to the problem.

To conclude this section, three groups of experimental results from the Caltech tokamak will be outlined. The <u>results given below will pertain to the fluctuations seen after the first 2 msec of the plasma lifetime,</u> since the sawtooth type oscillations are thought to be related to a gross internal disruption[39] and were of secondary interest in this thesis. The first group is composed of results which are not consistent with a classical drift wave theory; the second group summarizes results which seem to support the newer drift-tearing mode analyses; and the third group consists of results which are not fully explained by current theory.

I. Results which do not support a classical drift wave interpretation

A. The azimuthal wavelengths were longer than predicted by the two-fluid theory of Ellis and Motley[14] for current-driven collisional drift waves.

B. The azimuthal phase velocity was in the ion diamagnetic drift direction.

C. No sharp increase in the azimuthal propagation velocity was observed at $r \simeq 11.5$ cm where T_e and n_e had large gradients.

D. The azimuthal propagation velocity decreased as the time at which data were taken was increased; however, $1/n\, dn/dr$, B_t, and T_e were relatively constant during the period in which the velocity decreased; T_e actually increased slightly.

E. The axial phase velocity was in the direction of electron current flow which is opposite to that expected for drift waves (see Ellis and Motley, 1974).

F. No change in the azimuthal phase velocity was observed when small puffs of neutral gas were added to the discharge. One would expect a local change in T_e and $1/n\, dn/dr$.

G. The density fluctuations were not strongly localized in the region of maximum density gradient as observed for drift waves in Q-machines[14] and the FM-1 spherator.[40]

II. Results which support a drift-tearing mode interpretation

A. Long azimuthal wavelengths (6-70 cm) were observed.

B. The spectra were broad and contained several regularly spaced peaks. This may indicate that the disturbances are not strongly

localized around the $\vec{k} \cdot \vec{B} = 0$ singular layers. Several modes would be expected to be present at the same radius if the region of B field line tearing were sufficiently wide. The effect of including density and temperature gradients in the tearing mode analysis has been shown[18] to broaden the disturbance layers.

      C. The average mode number decreased, as would be expected if $q(r) \propto <m>$, when:

      1. the radial position r was decreased;

      2. the toroidal magnetic field was decreased;

      3. the plasma current was increased.

      D. The same parametric dependencies of the average azimuthal mode number (on filling pressure, B_t, I_p, and density variations due to gas puffing) that were observed in the Caltech tokamak were also seen for the unstable modes in the ST tokamak.[25] On ST, magnetic loop probes placed outside the limiter were used to observe the fluctuations, and hence strong MHD activity was probably present.

      E. The azimuthal phase velocity had a $1/B_t$ dependence as would be expected if kink-tearing type modes were being carried around the torus by the $\vec{E} \times \vec{B}$ drift. (However, for drift waves the azimuthal phase velocity is also proportional to $1/B_t$.)

      F. The m = 2 mode was predominant when a disruption of the plasma occurred (i.e., when B_t was too low to stabilize the plasma current produced by ohmic heating). The m = 2 tearing mode is thought to be a precursor for the disruptive instability.[36]

      G. The electrostatic and magnetic loop probe signals had similar spectra.

III. Experimental results which remain unexplained

A. The spectrum indicated that several azimuthal modes may have been present at the same radius; and thus, the disturbance layers may have had widths of several centimeters. This is broader than predicted by recent drift-tearing theory.

B. The observed azimuthal propagation velocity was in the same direction as the $\vec{E} \times \vec{B}$ velocity but was larger in magnitude. Theory cannot fully account for the discrepancy.

C. Most of the parametric dependences of the radial propagation characteristics are not explained by present theories.

D. No theoretical explanation is available for the observed azimuthal or radial correlation lengths.

E. In the ST tokamak, the magnetic fluctuations had narrow spectra, and the azimuthal mode number decreased with time. These observations do not agree with the results of the present study.

Hence, the results of this thesis favorably support the concept of unifying the theories for drift and tearing modes, but quantitative agreement between theory and experiment is still lacking.

8.3 Suggestions for Future Work

The results of this thesis suggest that poloidal magnetic field fluctuations with characteristics similar to those observed for the floating potential oscillations may have been present. A complete description of the fluctuations and their relation to particle transport therefore requires a study of the related magnetic field oscillations.

The correlation lengths and propagation characteristics of the poloidal magnetic field fluctuations could be studied with magnetic loop probes, and the results could be compared with the floating potential oscillation characteristics. Moreover, the effects of R.F. heating on plasma stability are not well known, and thus a study of the changes in the fluctuation characteristics when R.F. power is applied would be extremely important.

Since the sawtooth oscillations seen in tokamak plasmas are thought to be related to internal disruptions and have been studied by x-ray techniques,[39] it would be of interest to try to correlate line averaged soft x-ray signals and probe signals during the high density phase of the plasma. Also, since it is known that as the particle density is increased in tokamaks the plasma becomes more unstable,[37] this study could concurrently be performed when large amounts of neutral gas are added during the discharge. Obviously, information regarding the physical mechanisms and the spatial extent of the sawtooth oscillations might be obtained.

Finally, the theory for the observed oscillations is still in a rudimentary stage, and much analytical and numerical work remains to be done before a complete understanding of turbulence in tokamak plasmas is achieved.

Appendix A

THE RELATION BETWEEN THE FLOATING AND SPACE POTENTIAL IN THE
PRESENCE OF AN ELECTRON TEMPERATURE GRADIENT

The following elementary derivation for the relationship between the floating and space potential was derived by P. Vandenplas[41] during his visit at Caltech in the summer of 1977.

The floating potential V_f of a plasma is defined to be the potential of a Langmuir probe when the probe draws no net current from the plasma. Thus, at the floating potential the electron and ion particle flux, Γ_e and Γ_i, respectively, are equal. Now in the sheath surrounding the probe $\Gamma_e = n_o V_e\, e^{+e(V-V_p)/KT_e}$ and $\Gamma_i \simeq n_o V_s$, where V_p is the potential of the plasma, V is the voltage of the probe, and V_s is the ion sound speed. Thus, at $V = V_f$

$$n_o \sqrt{\frac{KT_e}{m_i}} \simeq n_o\, e^{+e(V_f-V_p)/KT_e} \sqrt{\frac{KT_e}{m_e}} \quad , \quad (1)$$

or

$$\frac{KT_e}{m_i} \simeq e^{+2e(V_f-V_p)/KT_e}\, \frac{KT_e}{m_e} \quad , \quad (2)$$

so

$$V_f - V_p \simeq \frac{KT_e}{2e} \ln(\frac{m_e}{m_i}) \quad , \quad (3)$$

hence

$$\vec{\nabla}_r V_p \simeq \vec{\nabla}_r V_f + \frac{K\vec{\nabla}_r T_e}{2e} \ln(\frac{m_i}{m_e}) \quad : \quad (4)$$

In order to determine the radial electric field E_r, $\vec{\nabla}_r V_p$ must be known. However, V_p is difficult to measure experimentally, and moreover,

in a magnetized plasma F. Chen[42] has noted that the Langmuir curve may
not have a distinct electron saturation region. Thus, one must measure
the radial profiles of both the floating potential and the electron
temperature to determine E_r.

A more sophisticated derivation of the space potential taking
into account the modification of the ion density in the sheath region
can be found in Ref. 43. The results for Γ_e and Γ_i are

$$\Gamma_e = n_0 \, e^{+e(V-V_p)/KT_e} \sqrt{\frac{KT_e}{2\pi m_e}} \quad , \tag{5}$$

and

$$\Gamma_i = \chi \, n_0 \sqrt{\frac{KT_e}{m_i}} \quad , \tag{6}$$

so

$$\vec{\nabla}_r V_p = \vec{\nabla}_r V_f + \frac{K\vec{\nabla}_r T_e}{2e} \ln\left(\frac{1}{2\pi x^2} \frac{m_i}{m_e}\right) \quad , \tag{7}$$

where $\chi \simeq 0.6$ for $T_e \gg T_i$. Since $1/2 \ln(m_i/m_e) = 3.76$ and
$1/2 \ln[1/(2\pi x^2)(m_i/m_e)] = 3.35$ for hydrogen, the third terms in equations
(4) and (7) differ by only ten percent. Equation (7) was used to cal-
culate the radial electric fields in this thesis.

Appendix B

COEFFICIENTS OF THE MODIFIED ELLIS AND MOTLEY

DRIFT WAVE DISPERSION EQUATION

The coefficients used in equation (2.20) are

$$a_3 = T_e/T_i \quad b = T_e/T_i \; \frac{1}{2} \, k_\perp^2 \, r_{Li}^2 \tag{1}$$

$$a_2 = (\omega_1^* + i\nu_{\shortparallel})(1 + b) - T_e/T_i(\omega_2^* - i\nu_\perp)$$

$$+ \; T_e/T_i \; b(-2.71\omega_1 + 4i\nu_{\shortparallel}) \tag{2}$$

$$a_1 = (-\omega_2^* + i\nu_\perp)(\omega_1^* + i\nu_{\shortparallel}) - (\omega_1^* + i\nu_{\shortparallel})(2.71\omega_1 - 3_i\nu_{\shortparallel})(1+b)$$

$$-1.14i \; \nu_{\shortparallel} \, (1.71i \; \nu_{\shortparallel} \; - 1.5\omega_1)(1 + b)$$

$$- \; T_e/T_i(\omega_2^* - i\nu_\perp)(-2.71\omega_1 + 4i\nu_{\shortparallel}) - T_e/T_i \; b_i\nu_{\shortparallel}(2.71 \; _1 - 3i\nu_{\shortparallel})$$

$$- \; T_e/T_i \; b(1.71i\nu_{\shortparallel} \; - 1.5\omega_1)(0.67\omega_1 + 1.14i \; \nu_{\shortparallel}) \tag{3}$$

$$a_0 = (\omega_2^* - i\nu_\perp)[\frac{T_e}{T_i} \, i\nu_{\shortparallel}(2.71\omega_1 - 3i\nu_{\shortparallel}) + \frac{T_e}{T_i} \, (1.71i \; \nu_{\shortparallel} - 1.5\omega_1)$$

$$\times \; (0.67\omega_1 + 1.14i\nu_{\shortparallel})] + (\omega_2^* - i\nu_\perp)[(\omega_1^* + i\nu_{\shortparallel})$$

$$\times \; (2.71\omega_1 - 3i\nu_{\shortparallel}) + 1.14i\nu_{\shortparallel} \, (1.71i\nu_{\shortparallel} \; - 1.5\omega_1)] \quad , \tag{4}$$

where $\omega_1^* = -k_y \; \dfrac{cKT_e}{eB} \; \dfrac{1}{n} \; \dfrac{\partial n}{\partial x}$

$\omega_2^* = -k_y \; \dfrac{cKT_i}{eB} \; \dfrac{1}{n} \; \dfrac{\partial n}{\partial x}$

$$\omega_i = -k_z \frac{eE_{zo}}{m_e} \tau_{ei} \equiv k_z \mu_o$$

$$\nu_{\shortparallel} = (k_z^2 KT_e / 0.51 \, m_e) \, \tau_{ei}$$

$$\nu_{\perp} = \frac{3}{10} \, b^2 \nu_{ii} \qquad , \qquad \nu_{ii} = (m_e/2m_i)^{1/2} / \tau_{ei}$$

and

$$\tau_{ei} = \frac{3}{4} (m_3/2\pi)^{1/2} (KT_e)^{3/2} / \ell n \, \Lambda \, e^4 n \qquad .$$

REFERENCES

1. Rose, David J. and Clark, Melville, Plasmas and Controlled Fusion, MIT Press, 1961, pp. 431-432.

2. Chen, Francis F., Introduction to Plasma Physics, Plenum Press, New York and London, 1974, p. 166.

3. Pfirsch, P. and Schlüter, A., Garching Report MPI-PA-7-62 (1962); Cap, Ferdinand F., Handbook of Plasma Instabilities, vol. I, Academic Press, New York, 1976, p. 336.

4. Furth, H. P. and Rosenbluth, M. N., Plasma Physics and Controlled Nuclear Fusion Research (Proc. Conf. Novisibirsk, 1968) 1, IAEA, Vienna, 1969, p. 821.

5. Rosenbluth, M. N., Hazeltine, R. D., and Hinton, F. L., "Plasma Transport in Toroidal Confinement Systems", Phys. Fluids 15, 116 (1972).

6. Bolton, R.A.E. et al., "Plasma Containment in the Proto-Cleo-Stellarator", Plasma Physics and Controlled Nuclear Fusion Research (Proc. Madison Conference, June 17-23, 1971) (IAEA, Vienna, 1972), vol. III, p. 79.

7. Ohkawa, T., Gilleland, J. R., and Tamano, T., "Observation of Neo-classical, Intermediate, and Pfirsch-Schlüter Diffusion in the d.c. Octopole", Phys. Rev. Lett. 28, 1107 (1972).

8. Artsimovich, L. A., Glukhov, A. V., and Petrov, M. P., JETP Letters 11, 304 (1970).

9. Kelley, G. G., et al., Garching/Munich Conference, paper B3-I; Berry, L. A., Clarke, J. F., and Hogan, J. T., "Ion Energy Containment in the Oak Ridge Tokamak", Phys. Rev. Lett. 32, 362 (1974).

10. Hendel, H. and Chu, T., "Collisional Drift Instabilities" in Methods of Experimental Physics, 9A, L. Griem, ed., Plasma Physics, Academic Press, New York, 1970.

11. Yoshikura, S. and Christofilos, N. C., "Amplification of Pseudo-Classical Diffusion for Toroidal Confinement Devices", Plasma Physics and Controlled Nuclear Fusion Research (Proc. Madison Conference, June 17-23, 1971)(IAEA, Vienna, 1972), vol. II, p. 357.

12. Boyd, T.J.M. and Sanderson, J. J., Plasma Dynamics, Barnes and Noble, Inc., New York, 1969, p. 42.

13. Chen, Francis F., Introduction to Plasma Physics, Plenum Press, New York and London, 1974, pp. 194-197.

14. Ellis, R. F. and Motley, R. W., "Current-Driven Collisional Drift Instability", Phys. Fluids 17, 582 (1974).

15. Kruskal, M. D. et al., "Hydromagnetic Instability in a Stellarator", Phys. Fluids 1, 421 (1958).

16. Kruskal, M. D., U.S. Atomic Energy Commission Report No. NYO-6045 (PM-S-12) (1954).

17. Furth, H. P., Rutherford, P. H., and Selberg, H., "Tearing Mode in the Cylindrical Tokamak", Phys. Fluids 16, 1054 (1973).

18. Drake, J. F. and Lee, Y. C., "Kinetic Theory of Tearing Instabilities", UCLA report PP6-282 (1976).

19. Hazeltine, R. D., Dobrott, D., and Wang, T. S., "Kinetic Theory of Tearing Instability", Phys. Fluids 18, 1778 (1975).

20. Bol, K., "Density Fluctuations in the Etude Stellarator", Phys. Fluids 7, 1855 (1964).

21. Young, K. M., "Fluctuations in the Plasma of the Model Stellarator", Phys. Fluids 10, 213 (1967).

22. Makishima, K. et al., "Simultaneous Measurements of the Plasma Current Profile and Instabilities in a Tokamak", Phys. Rev. Lett. 36, 142 (1976).

23. Mirnov, S. V., Semenov, I. B., "Investigation of the Instabilities of the Plasma String in the Tokamak-3 System by Means of a Correlation Method", Atomnaya Energiya 30, 20 (1971).

24. Prater, R. et al., "Observation of the Dissipative Trapped Electron Instability in Toroidal Geometry", G.A. report A14220 (1977).

25. Hosea, J. C. Bobeldyk, C., Grove, D. J., "Stability Experiments on the ST Tokamak", Plasma Physics and Controlled Nuclear Fusion Research (Proc. Madison Conference, June 17-23, 1971) (IAEA, Vienna, 1972), vol. II, p. 425.

26. Hamberger, S. M. et al., "Experimental Study of Enhanced Diffusion by Electrostatic Fluctuations in an Ohmically Heated Toroidal Plasma", Phys. Rev. Lett. 37, 1345 (1976).

27. Surko, C. M. and Slusher, R. E., "Study of the Density Fluctuations in the Adiabatic Toroidal Compressor Tokamak Using CO_2 Laser Scattering", Phys. Rev. Lett. 37, 1747 (1976).

28. Mazzucato, E., "Small-Scale Density Fluctuations in the Adiabatic Toroidal Compressor", Phys. Rev. Lett. 36, 792 (1976).

29. Cross, R. C., "Construction of Diagnostic Equipment for the Texas Tech Tokamak", Texas Tech University, Plasma Laboratory Report NSF-ENG-7303941-2 (1977).

30. Gould, R. W., Professor of Applied Physics, California Institute of Technology, private communication.

31. DFT/Discrete Fourier Transform (RHARM, FORT, FOUR2), Caltech Computer Center Report C268-239-370.

32. Barber, N. F., Experimental Correlograms of Fourier Transforms Pergamon Press, Inc., New York, 1961, Chapters 7 and 8.

33. Smith, D. E., Powers, E. J., Caldwell, G. S., "Fast-Fourier-Transform Spectral-Analysis Techniques as a Plasma Fluctuation Diagnostic Tool", IEEE Transactions on Plasma Science, PS-2 (1974).

34. Constructed by David Q. Hwang.

35. Kim, Y. C., Powers, E. J., "Effects of Frequency Averaging on Estimates of Plasma Wave Coherence Spectra", IEEE Transactions on Plasma Science, PS-5 (1977).

36. Rutherford, P. H., Furth, H. P., Rosenbluth, M. N., "Nonlinear Kink and Tearing Mode Effects in Tokamaks", Plasma Physics and Controlled Nuclear Fusion Research (International Atomic Energy Agency, Vienna, 1971), vol. II, p. 553.

37. Callen, J. D. and Dory, R. A., "Magnetohydrodynamic Equilibria in Sharply Curved Axisymmetric Devices", Phys. Fluids 15, 1523 (1972).

38. Bulletin of the American Physical Society, vol. II, October 1977, pp. 1142, 1143, 1152, 1153, 1154; Kaw, P. "Some Nonlinear Effects in Tearing Mode Instability", Princeton University Plasma Physics Laboratory report MATT-1264 (1976); Chen, Liu, Rutherford, P. H., T Tang, W. M., "Drift-Tearing Instabilities Due to Trapped Electrons", Princeton University Plasma Physics Laboratory Report PPPL-1338 (1977).

39. Waddell, B. V., et al., "Internal Disruptions in Tokamaks", Oak Ridge National Laboratory report ORNL/TM-5840 (1977).

40. Okabayashi, M. and Arunasalam, V., "Study of Drift Wave Turbulence by Microwave Scattering in a Toroidal Plasma", Princeton University Plasma Physics Laboratory Report PPPL-1310 (1977).

41. Vandenplas, P. E., Laboratoire de Physique des Plasmas, Ecole Royale Militaire, Brussels, Belgium, private communication.

42. Chen, Francis F., "Electric Probes", Plasma Diagnostic Techniques, R. H. Huddlestone and S. L. Leonard, eds., Academic Press, New York, 1965, pp. 113-200.

43. Swift, J. D., Schwar, M.J.R., Electrical Probes for Plasma Diagnostics, London Iliffe Books Ltd., pp. 11-15.

44. Finn, John M., "The Coupling of Tearing Modes in Tokamaks", Princeton University Plasma Physics Laboratory Report PPPL-1322 (1977).

45. Drake, J. F., "The Coupling of Tearing Modes by Toroidal Effects", UCLA Report PPG-309 (1977).

46. Martel, Hardy C., Assoc. Professor of Electrical Engineering, California Institute of Technology, private communication.

47. Taylor, R. J., Bull. A.P.S. (Series II) 19, 421 (1974), and private communication.